POLYMER-DRUG CONJUGATES AND HYBRID NANO-STRUCTURES FOR ANTICANCER DRUG DELIVERY AND LABEL-FREE CELLULAR IMAGING

SOMA DEY

Ph.D. THESIS
2015

SREE CHITRA TIRUNAL INSTITUTE FOR MEDICAL SCIENCES AND TECHNOLOGY, TRIVANDRUM
Thiruvananthapuram - 695012

POLYMER-DRUG CONJUGATES AND HYBRID NANO-STRUCTURES FOR ANTICANCER DRUG DELIVERY AND LABEL-FREE CELLULAR IMAGING

A THESIS PRESENTED BY

SOMA DEY

TO

SREE CHITRA TIRUNAL INSTITUTE FOR MEDICAL SCIENCES AND TECHNOLOGY, TRIVANDRUM
Thiruvananthapuram

IN PARTIAL FULFILMENT OF THE REQUIREMENTS FOR THE AWARD OF DOCTOR OF PHILOSOPHY

2015

To my beloved father……

who has made me what I am

CERTIFICATE

I, **Soma Dey**, hereby certify that I have personally carried out the work depicted in the thesis entitled, "**Polymer-Drug Conjugates and Hybrid Nano-Structures for Anticancer Drug Delivery and Label-Free Cellular Imaging"**, except where due acknowledgement has been made in the text. No part of the thesis has been submitted for the award of any other degree or diploma prior to this date.

Date:

Signature:
Name of the candidate: **SOMA DEY**

Dr. K. Sreenivasan
Laboratory for Polymer Analysis,
BMT Wing, SCTIMST

This is to certify that **Mrs. Soma Dey** in the department/division of **Laboratory for Polymer Analysis** of this institute has fulfilled the requirements prescribed for the Ph.D. degree of the Sree Chitra Tirunal Institute for Medical Sciences and Technology, Trivandrum.

The thesis entitled **"Polymer-Drug Conjugates and Hybrid Nano-Structures for Anticancer Drug Delivery and Label-Free Cellular Imaging"** was carried out under my direct supervision. No part of the thesis was submitted for the award of any degree or diploma prior to this date.

Date: Signature:

The thesis entitled

POLYMER-DRUG CONJUGATES AND HYBRID NANO-STRUCTURES FOR ANTICANCER DRUG DELIVERY AND LABEL-FREE CELLULAR IMAGING

Submitted by

Soma Dey

For the degree of
Doctor of Philosophy

Of

SREE CHITRA TIRUNAL INSTITUTE FOR MEDICAL SCIENCES AND TECHNOLOGY, TRIVANDRUM
Thiruvananthapuram

is evaluated and approved by

(Name of the guide)	(Name of thesis examiner)

Acknowledgement

I am indebted to many people for their kind help and support for the last five years which made this thesis possible.

At first I would like to express my sincere gratitude to my guide Dr. K. Sreenivasan for introducing me into the exciting field of biomaterials. I earnestly thank him for his sincere guidance, constant encouragement, inspiration and creative & scientific ideas that helped me to enhance my knowledge in this field. I express my sincere gratitude to the Director, SCTIMST and the Head of BMT wing, SCTIMST for providing with all the facilities needed for my research work. I also thank the Registrar and the Deputy Registrar for their academic assistance.

I express my sincere gratitude to my "Doctoral Advisory Committee" members, Dr. Roy Joseph and Dr. P. Ramesh, for their precious suggestions and critical comments. I also gratefully acknowledge the Council of Scientific and Industrial Research (CSIR) for the financial assistance during the entire period of my doctoral study.

I express my sincere thanks to Dr. C. Radhakumary, Mr. Rowsen Moses, Mr. P. R. Hari and Dr. C. L. Gopu for their kind supports, understanding and friendly behavior that helped me a lot throughout my study.

I express my sincere gratitude to Dr. Rekha M. R. for giving me permission to use the cell culture facilities in her lab and also for her kind support, encouragement and valuable suggestions during cell culture studies. I gratefully acknowledge Dr. T.V. Kumary and all staff of Tissue Culture Lab for cytotoxicity evaluation of one of my systems. I am grateful to Dr. Prabha D. Nair for her kind permission for using her lab facilities such as spectrofluorometer and deep freezer for my studies. I thank Dr. Annie John and Ms. Susan Mani for TEM analyses. I am grateful to Dr. Chandra. P. Sharma and Mr. Willi Paul for their support in particle size distribution and zeta potential measurements. I thank Dr. Lissy K. Krishnan and Dr. Anugya Bhat for evaluation of in vitro hemolysis of my samples. I thank Dr. H. K. Verma and all staff of Bioceramics Lab, especially Mr. Vijayan S. for XRD analyses. I express my hearty thanks to Dr. Luxmi Verma and Mrs. Soumini Mathew from NIIST, Trivandrum for helping in NMR (^{1}H and ^{13}C) analyses.

I am grateful to all the former and present lab mates Dr. Vidya Raj, Dr. Manju S., Mr. Durgadas, Ms. Shantikrishna A., Dr. Priya A. Nair of Laboratory for Polymer

Analysis for their friendship, help and timely support. My sincere thank goes to Ms. Lizebona August, Ms. Caroline and Ms. Priya from Biosurface Technology Lab for their kind help and friendly supports during my cell culture studies. I also thank all staff of BMT Wing, who directly or indirectly helped me for the successful completion of this work.

I express my gratitude and regard to my parents, brother and sister-in-law for their genuine love and prayers for me. I extend my sincere thanks and warm regards to my beloved husband Mr. Ranajit Pal for his unconditional love, understanding, support and sincere prayer which smoothly paved the way to successful completion of the work. I also express thanks and lots of love to my son master Ishan Pal for loving and accepting me in spite of all the negligence towards him during those busy days of my work.

Last but not the least; I express gratitude and regards from the core of my heart to the Almighty God for His blessings which really helped me to concentrate in my work resulting in the successful completion of my thesis.

Soma Dey

Date:

Place: Trivandrum

Table of Contents

List of Figures

List of Tables

List of Schemes

Abbreviations

1-PyCHO	1-pyrenecarboxaldehyde
A	Absorbance
Alg	Alginate
AuNPs	Gold Nanoparticles
BPLP	Aliphatic biodegradable photoluminescent polymer
CA	Citric acid
Ccm	Curcumin
CMC	Critical micelle concentration
Cryo-TEM	Transmission electron microscopy at cryogenic condition
DCC	1,3-dicyclohexyl carbodiimide
DDS	Drug delivery systems
DLS	Dynamic light scattering
DMAP	4-dimethyl amino pyridine
DMEM	Dulbecco's Modified Eagle's Medium
DMSO	Dimethyl sulfoxide
EDC	N-(3-dimethylaminopropyl)N-ethylcarbodiimide
EPR	Enhanced permeation and retention
F	Fluorescence intensity
FA	Folic Acid
FBS	Fetal bovine serum
FCC	Face centered cubic
FITC	Fluorescein isothiocyanate
FTIR	Fourier transform infrared spectroscopy
GPC	Gel permeation chromatography
GSH	Glutathione
GSHBP	GSH containing biodegradable fluorescent polymer
LC	Liquid chromatography
L-Cys	L-Cysteine
MDR	Multi drug resistance
MEM	Minimum essential medium

MTT	3-(4,5-Dimethylthiazol-2-yl)-2,5-diphenyl tetrazolium bromide
MTX	Methotrexate hydrate
NHS	N-hydroxysuccinimide
NMR	Nuclear magnetic resonance
NR	Nile Red
PBS	Phosphate buffered saline
PEG	Poly(ethylene glycol)
Q.Y.	Quantum yield
RES	Reticuloendothelial system
SA	Succinic anhydride
SPR	Surface plasmon resonance
TEA	Triethylamine
TEM	Transmission electron microscopy
UV-Vis	Ultraviolet-Visible
XRD	X-ray diffraction

SYNOPSIS

Cancer is a killer disease that caused 8.2 million cancer deaths worldwide in 2012 alone. There are several strategies for cancer treatment such as surgery, radiation therapy, chemotherapy, hormonal therapy etc. and among these approaches chemotherapy is the widely followed therapeutic approach. The nature of chemotherapeutic agent and the way of delivering the drug to the desired site are the imperative factors for the success of chemotherapy. However, one intrinsic limitation of chemotherapeutics is the incapability of distinguishing normal and cancer cells and hence they exert toxic response to the normal tissues also, leading to several side effects like nausea, vomiting, hair loss etc. Therefore, suitable drug delivery system (DDS) for carrying chemotherapeutics specifically to the desired site is essential. Cancer is generally a disease of old age and studies have shown that only 5 – 10% of all human cancers are caused by genetic factors. Lifestyle, for example, food habit is responsible for most of the cancers in human beings. Research has indicated that Southeast Asia is a continent with low incidence of cancers and people from this continent very often consume turmeric (*curcuma longa*) as one of the spices. Curcumin (Ccm) is one of the active components of turmeric possessing chemo-preventive and chemotherapeutic activity. Application of Ccm in cancer treatment is, however, restricted due to its low aqueous solubility, instability and consequent poor bioavailability. Considering these facts, in this study, various nano-vectors were designed based on polymer-drug conjugates and polymer stabilized gold nanoparticles (AuNPs) for enhancing aqueous solubility and stability of Ccm along with safer Ccm delivery to cancer cells. In this

study, a polymer based fluorescent material was also designed for simultaneous drug delivery and label-free cellular imaging. Resistance to chemotherapy shown by cancer cells is a major impediment to successful cancer therapy. However, reports reflect that simultaneous application of two anticancer drugs can be a rational approach to redress the problem of chemoresistance in cancer cells. In the present work, Ccm and methotrexate (MTX) conjugated DDS based on biopolymer stabilized AuNPs was designed *via* a completely "green" synthetic route.

Polymer-drug conjugates are one of the most useful polymer therapeutics as they can circumvent poor aqueous solubility of hydrophobic drugs and improve drug stability. So far different types of natural and synthetic polymers have been used to design polymer-Ccm conjugates. Herein, alginate was chosen to develop Alginate-Ccm (Alg-Ccm) conjugate since it is non-immunogenic bio-polymer. Alg-Ccm conjugate was synthesized by direct covalent conjugation of Ccm to C-6 carboxylate groups in alginate through ester linkage using DCC/DMAP in Water/DMSO (1:1 v/v) mixture. FTIR, ^{1}H NMR, UV-Vis absorption and fluorescence emission spectroscopic analyses confirmed the covalent conjugation. Self-assembly of Alg-Ccm conjugate into micelle like structure in aqueous medium was characterized by DLS analysis and the critical micelle concentration (CMC) was determined using 1-pyrene carboxaldehyde as the probe. Spherical Alg-Ccm conjugate micelles were visualized by TEM analysis. Total Ccm content and stability of the drug in the conjugate was determined by UV-Vis spectroscopy. Cytotoxicity of Ccm in conjugate was evaluated by both test on extract method (for qualitative assessment) and MTT assay (for quantitative assessment) against

L-929 mouse fibroblast cells and compared with that of free Ccm. Suitably functionalized AuNPs are excellent vectors for drug delivery. In this work, Ccm conjugated water soluble polymer (P1) stabilized AuNPs (Ccm-SA-P1-AuNPs) was fabricated. In order to design Ccm-SA-P1-AuNPs, at first P1 with free thiol group was generated *via* melt-polycondensation reaction between poly (ethylene glycol) (PEG), citric acid (CA) and L-Cysteine. P1 stabilized AuNPs was prepared from citrate reduced AuNPs via ligand replacement reaction. P1-AuNPs was succinylated followed by the conjugation with Ccm *via* succinate ester linkage to get Ccm-SA-P1-AuNPs. FTIR spectra and DLS analyses were used to characterize each stage of modification. ^{1}H NMR spectra confirmed the Ccm conjugation. XRD pattern of Ccm-SA-P1-AuNPs confirmed the face centered cubic (FCC) crystal lattice of the AuNPs as well as ascertained amorphous/disordered crystalline phase of Ccm in conjugated condition. The cytotoxicity of Ccm-SA-P1-AuNPs was assessed by MTT assay against C6 cancer cell line (glioma cells from rat brain tumor) and the facile uptake of Ccm-SA-P1-AuNPs by C6 cancer cells was confirmed by fluorescence microscopy. With the aim to develop DDS for the simultaneous delivery of two chemotherapeutics, MP@Alg-Ccm AuNPs was fabricated *via* "green" synthetic route following two simple reaction steps. In the first step, AuNPs were generated and stabilized by Alg-Ccm conjugate in aqueous medium. Here alginate acted as both reducing and stabilizing agent. A MTX conjugate of bis(aminopropyl) terminated PEG (MP conjugate) was also developed in aqueous buffer solution (pH 7.4). Finally this MP conjugate was covalently conjugated onto the surface of Alg-Ccm AuNPs using EDC chemistry in aqueous buffer solution to generate

MP@Alg-Ccm AuNPs. XRD analysis confirmed FCC crystal lattice of the Alg-Ccm AuNPs. Each stage of modification of AuNPs was confirmed by FTIR, ^{1}H NMR and UV-Vis spectroscopy; DLS and TEM analyses. Cytotoxic activity (*in vitro*) of MP@Alg-Ccm AuNPs was determined by MTT assay against C6 and MCF-7 (human breast cancer cells) cancer cell lines. Cellular uptake was visualized by fluorescence microscopy. Hemolytic potential of MP@Alg-Ccm AuNPs was also assessed. Materials with intrinsic fluorescence are of prime importance in biomedical field. With the intention to design a nano-structured material with theranostic potential, here a low molecular weight, water soluble, biodegradable fluorescent polymer (GSHBP) was developed by melt-polycondensation reaction between PEG, CA and natural tripeptide glutathione (GSH). GSH, an important anti-oxidant, was chosen because of its usefulness in cancer regression and to obtain few reactive functional groups (like –S-H, -COOH, -O-H) to essentially modify the polymer. Free –COOH functional group in GSHBP, was utilized to fabricate nano-sized micelle forming fluorescent Ccm conjugate (GSHBP-Ccm) *via* esterification reaction. FTIR, ^{13}C and ^{1}H NMR spectra confirmed the formation of GSHBP and the formation of GSHBP-Ccm was confirmed by FTIR, ^{1}H NMR, UV-Vis absorption and fluorescence emission spectra. The characteristic “blue” fluorescence of GSHBP was retained in the conjugate. Nano-sized GSHBP-Ccm micelles were visualized by cryo-TEM analysis in aqueous dispersion. GSHBP-Ccm micelles were also characterized by DLS study and the CMC value was determined using Nile-Red dye as the probe. The conjugate micelle exhibited a slow Ccm release profile under physiological condition. The *in vitro* cytotoxicity of both GSHBP and

GSHBP-Ccm conjugate was studied by MTT assay against C6 cancer cell. For both of the material, hemolytic toxicity was assessed. Facile uptake of the nano-sized fluorescent conjugate micelles was visualized by exploiting the inherent blue fluorescence of GSHBP in conjugate and using the typical green fluorescence of Ccm.

The major findings of this study are as follows: In Alg-Ccm, 100 mg conjugate contained 1.09 ± 0.053 mg of Ccm. Alg-Ccm also showed water solubility more than 10 mg/mL. Thus, conjugation of Ccm to alginate augmented the aqueous solubility of Ccm significantly. In addition, we observed only minimum change in the absorption maxima of Ccm in conjugated state upon incubation in PBS (pH = 7.4) for 6 h, indicating the potential stability of the drug in Alg-Ccm conjugate. Alg-Ccm self-assembled in aqueous medium forming micelle like structure with Ccm occupying the inner hydrophobic core of the micelles. The outer shell of the micelle being made of hydrophilic alginate, Ccm was well protected from hydrolytic degradation in Alg-Ccm conjugate. Ccm in the conjugate showed improved cytotoxicity than that of the free drug against L-929 cells. This observation may be due to augmented aqueous solubility of Ccm upon conjugation to alginate. Thus Alg-Ccm enhanced aqueous solubility and stability of Ccm along with improved toxicity of hydrophobic drug Ccm. In Ccm-SA-P1-AuNPs, Ccm was covalently attached to polymer stabilized AuNPs *via* a succinate ester linkage. 10 mg of Ccm-SA-P1-AuNPs contained 67.5 ± 0.08 μg of Ccm and the water soluble polymer stabilized AuNPs was readily dispersed in water resulting in augmented aqueous solubility of Ccm. Ccm-SA-P1-AuNPs showed faster release at pH 5.3 as the succinate ester linkage is prone to acid catalyzed hydrolysis. However, at

physiological pH (7.4) the release of Ccm was slow ensuring safer delivery of Ccm through blood stream. MTT assay analysis of Ccm-SA-P1-AuNPs against C6 cancer cell line suggested that Ccm in conjuated state showed improved cytotoxic response than that of the free drug. The improved cytotoxicity of Ccm in Ccm-SA-P1-AuNPs may be due to its conjugation to AuNPs *via* hydrophilic polymer P1 resulting in enhanced aqueous solubility of the drug and better internalization of the small sized AuNPs by cancer cells. Ccm-SA-P1-AuNPs thus has the potential to be used as a pH responsive DDS. Herein, the facile synthesis of MP@Alg-Ccm AuNPs using "green chemical" alginate and "green solvent" water is appealing with minimum reaction steps for genarating stable AuNPs. 100 mg of MP@Alg-Ccm AuNPs contained 1.05 ± 0.01 mg of Ccm and 1.26 ± 0.05 mg of MTX. Evaluation of *in vitro* cytotoxicity by MTT assay indicated that MP@Alg-Ccm AuNPs exhibited higher toxicity compared to each free drug (for both C6 and MCF-7 cells) for all concentrations. This improved cytotoxic response may be due to the synergistic effect of both the drugs and the pleiotropic effect of Ccm. Nano-sized MP@Alg-Ccm AuNPs ensured longevity in systemic circulation resulting in improved EPR effect. Facile uptake of the DDS was confirmed by fluorescence microscopy. MP@Alg-Ccm AuNPs was found to be non-hemolytic. Thus MP@Alg-Ccm AuNPs can serve as a potential nano-vector for co-administration of two chemotherapeutics. Water soluble fluorescent GSHBP polymer exhibited almost no or minimum intrinsic toxicity. Upon conjuation with hydrophobic drug Ccm, GSHBP-Ccm conjuate self-assembled in aqueous medium generating nano-sized micelles and Ccm occupied the hydrophobic inner core. GSHBP-Ccm showed high water solubility (30

mg/mL) and 100 mg of the conjuagte contained 178.9 ± 0.01 μg of Ccm. Thus aqueous solubility of Ccm was remarkably increased through its conjugation to GSHBP. GSHBP-Ccm showed improved toxicity towards C6 cancer cells compared to that of the free drug. This observation can be attributed to the augmented water solubility of Ccm in GSHBP-Ccm and enhanced uptake of GSHBP-Ccm micelles by cancer cells (due to small size of micelles). After conjuagtion with Ccm, the conjuate retained the characteristic blue fluorescence of GSHBP. Most interestingly, the C6 cancer cells were imaged by fluorescence microscopy after incubation with GSHBP-Ccm micelles for 3h, utilizing the intrinsic blue fluorescence of GSHBP in the conjugate. Thus the fluorescent polymer GSHBP can be a potential candidate for label-free cellular imaging. Both GSHBP and GSHBP-Ccm conjugate were non-hemolytic in nature. Hence GSHBP-Ccm can be modified to design a multifunctional nano-structured DDS with theranostic potential.

CHAPTER 1

INTRODUCTION

1 Introduction

Cancer, a disease involving dynamic changes in genome (Hanahan et al. 2000), is a severe health hazard. According to the GLOBOCAN report (GLOBOCAN 2012; estimates excluding non-melanoma skin cancer), there were 8.2 million cancer deaths globally along with 14.1 million new cancer cases in 2012. The world wide burden is projected to grow to 27 million of new cancer cases and 17.5 million cancer deaths by 2050 (Jemal et al. 2011). Lifestyle has a high impact on the incidence of this lethal malady (Anand et al. 2008). Fortunately, biomedical science has also progressed to a great extent and cancer research, right from detection to treatment, is on the rise showing some ray of hope. In addition, polymer science has also been satisfactorily advanced and polymers are being used in designing various types of drug delivery systems (DDS). Polymer-anticancer drug conjugates and various other polymeric or hybrid nano-structured DDS have evolved as promising anticancer nanomedicines (Duncan 2006).

1.1 Cancer

Cancer is a class of genetic disorders in which abnormal cells undergo uncontrolled growth. There are more than hundred different types of cancers depending on their origin/cell type. Owing to the mutations or epigenetic alternations affecting genetic coding for protein components, deregulation in growth–controlling pathways of normal cells may take place leading to the development of cancer (Cairns 1975). According to Hanahan and Weinberg, the six distinctive characteristics that all cancer cells share in common include: ability to evade apoptosis, self-sufficiency in growth signal, potential for unlimited replication,

insensitivity to anti-growth signals, sustained angiogenesis and tissue invasion and metastasis (Hanahan et al. 2000) (Feinberg et al. 2006). Two gene classes, namely proto-oncogenes and tumor suppressor gene are found to play key role in development of cancer. When mutated, the proto-oncogenes can turn into cancerous oncogenes and the tumor suppressor genes can get inactivated resulting in excessive multiplication of cells without any crucial breaks in cellular growth. Mutations, in as much as one percent of the total set of genes, in human genome can trigger the formation of different types of cancers (Futreal et al. 2004). According to the cell type of origin there are four types of cancers; (i) carcinoma: arising from the epithelial sheet that covers the surfaces (*e.g.*, skin *etc.*); (ii) sarcoma: these include cancer of the connective tissues (*e.g.*, bone, cartilage, muscle etc.) and fibrous tissues; (iii) leukemia: originates from the blood forming cells and (iv) lymphoma: initiates from the cells of the immune system. Besides, based on the metastatic potential cancers are classified as (i) adenomas: these are benign tumors as the neoplastic growth remains as a single mass without spreading to other parts and (ii) adenocarcinomas: the tumors are malignant in nature invading normal tissues and spreading throughout the body (Ravindran et al. 2009). With the development of medical sciences, diagnoses and treatment of many types of cancer have been improved. At present cancer is treated in various approaches like (i) surgery, (ii) hormonal therapy, (iii) radiation therapy, (iv) chemotherapy (v) immunotherapy etc. Depending on the type of cancer, its stage, aggressiveness and general health condition of the patient, the above mentioned therapeutic approaches can be followed individually or in combination. For example, sometimes after operating the tumor or the entire organ, the patient may be given chemotherapy depending on the

requirements. However, chemotherapy is one of the most useful cancer treatment regimes. In certain cases like undetectable cancer, early stage of cancer, leukemia and obviously for metastatic cancer, chemotherapy is known to be the most effective treatment strategy.

1.1.1 Chemotherapy for effective cancer treatment

In chemotherapy rapidly dividing cancerous cells are killed using various therapeutic agents. The modern era of cancer chemotherapy initiated in 1940s with the first use of alkylating mustard gas analogues for the treatment of lymphomas. Shortly after World War II, the study by Sidney Farber, a pathologist at Harvard Medical School and the father of modern chemotherapy, actively showed that effective pharmacological treatment of cancer was possible. The therapeutic agents used in chemotherapy have the potential to kill tumors *via* different mechanistic pathways. Majority of the chemotherapeutic agents induce cellular apoptosis by affecting nucleic acids (DNA and RNA) either by direct interaction (e.g. alkylating agents like cyclophosphamide and platinum based drugs like cisplatin, carboplatin etc.) and inhibition of DNA/RNA synthesis (e.g. antimetabolites like methotrexate (MTX) and topoisomerase inhibitors like topotecan etc.) or by indirect ways like creating fault in chromosome separation during mitosis *i.e.* mitotic inhibitors (e.g. tubulin active agents like paclitaxel etc.) and by interfering with enzymes involved in DNA replication (e.g. anti-tumor antibiotics like doxorubicin etc.) (Karnofsky 1968) (Espinosa et al. 2003). For the treatment of cancer, chemotherapy can be used either as a primary treatment strategy or in combination with other treatment approaches such as surgery, radiation therapy etc. In chemotherapy, only one therapeutic drug can be used (single chemotherapy) or more than one chemotherapeutic agents can be

used (combination therapy). However, this mode of treatment for cancer possesses certain intrinsic limitations as well. The prime limitation of chemotherapy originates from the intrinsic incapability of the therapeutic agents to discriminate normal and cancerous tissues, leading to the development of drug induced toxicity and severe side effects. The chemotherapeutic agents upsetting the cell division process also affect rapidly dividing normal cells (for instance hair producing cells, bone marrow, mucous lining in the intestinal track etc.) giving rise to side effects such as hair loss, bone marrow depression, nausea etc. Hence the serious toxic effects of anticancer drugs on normal cells urgently call for improved targeted drug delivery vehicles which can release the cytotoxic drugs to the desired cancerous cells leaving the normal cells unscathed. With the advances in the field of cancer research, drug delivery systems (DDS) facilitate carrying chemotherapeutic agents in a safer way to the desired site enhancing the efficiency of chemotherapeutics (Allen & Cullis 2004). Drug delivery system (DDS) can be defined as a systematically engineered vehicle intended to carry the therapeutic molecule to the desired site specifically with enhanced efficacy, reduced side effects and better patient compliance. DDS includes micro/nano sized vehicles such as microcapsules, liposomes, polymeric micelles, polymer-drug/polymer-protein conjugates, inorganic nanoparticles, quantum dots *etc.* along with their allied therapeutics. Utilizing the concept of modern DDS, the pharmacological properties of several conventional free drugs can be improved. Besides, introduction of the concept of nanotherapeutics has made it possible to surmount several limitations of conventional DDS such as poor bioavailability, non-specific biodistribution, lack of targeting, side effects and low therapeutic indices (Moorthi et al. 2011) (Li & Huang 2008). Properly engineered DDS are also able to

provide improved chemotherapeutic regime using existing antineoplastic agents (Farokhzad & Langer 2009).

Multi drug resistance (MDR) is another major concern in successful cancer chemotherapy. In fact it has been found that cancer cells most frequently show reduced response to a chemotherapeutic drug over the course of a chemotreatment. This trait of cancer cells is known as chemoresistance or multi drug resistance (MDR). One of the most important and common causes of MDR in cancer cells include the over expression of ATP-binding cassette (ABC) super family of transporters. These are basically trans-membrane proteins that function as a drug-efflux pump and remove drugs actively from cells. As a result, intracellular drug concentration becomes too scanty to produce any cytotoxic effect. P-glycoprotein (Pgp), breast cancer resistance protein (ABCG2) and multidrug resistance associated protein (MRP-1) are the major transporter proteins in the ABC super family associated with MDR. Modification in glutathione S-transferase activity (GST), changes in topoiosmerase II (Topo IIα) etc. are other factors accountable for the development of MDR (Szakács et al. 2006) (Ejendal & Hrycyna 2002) (Ganta & Amiji 2009). Chemoresistance has been found to be main responsible factor for most of the unsuccessful cases in cancer therapy. Various approaches have been adopted to redress the phenomenon of MDR (Szakács et al. 2006). It has been observed that combination of drugs in chemotherapy (i.e. combination therapy) is a potential strategy in this regard. Combination chemotherapy is highly promising in dealing with MDR because (i) applying multiple drugs working through diverse molecular targets can elevate the genetic barriers that must be overcome for cancer cell mutations, thus impeding the cancer adaptation process (Hu et al. 2010) and (ii)

multiple drugs that target the same cellular pathways can target more selectively with augmented therapeutic efficacy *via* synergistic mechanism (Lehar et al. 2009).

1.2 Targeted Drug Delivery and Nanomedicine for Cancer Treatment

In order to reduce the toxic effects of chemotherapeutic agents to normal healthy tissues, targeted drug delivery is the most useful approach. Using the strategy of targeted drug delivery maximum possible fraction of the drug can be made to interact exclusively with the targeted cancerous tissues. Precise tumor targeting not only reduces the side effects but also leads to augmented internalization, superior release profile of the drug and improved therapeutic efficacy. In addition, use of nanomedicine especially fabrication of multifunctional nano-sized vectors for carrying anticancer therapeutics has revolutionized targeted anticancer drug delivery. Targeted drug delivery, though highly beneficial to chemotherapy, is not an easy task. In addition to the physiological and biochemical hurdles of identification and validation of the molecular targets, drug targeting also faces the pharmaceutical challenges of developing suitable methods for attaching targeting ligands to the DDS. Targeted DDS also demand longer and safer life in systemic circulation (Torchilin 2012). Vascular endothelium, basement membrane and plasma proteins are the three major obstacles for a DDS after its intravenous administration. After intravenous administration when a targeted DDS enters into the blood stream, it interacts with plasma proteins (opsonins) and biodistribution of drugs gets affected (Alexis et al. 2008). Opsonisation and subsequent recognition of the targeted DDS by the reticuloendothelial system (RES) (Maeda et al. 2000) must be avoided. Size and surface characteristics such as surface charge (zeta potential), hydrophilicity/hydrophobicity etc. play the vital role in scheming the *in vivo* bio-

distribution and opsonisation of DDS in blood stream (Mahmoudi et al. 2011). By regulating these physical aspects one can crucially control the extent of opsonisation on the delivery vehicle resulting in enhancement of its longevity in blood to evoke optimum pharmacological action. In order to access the cells of a targeted tissue, DDS need to cross the barrier of extra cellular matrix. For those drugs whose site of action is located in the nucleus of a cell (e.g. plasmid DNA), nuclear membrane is the barrier that the DDS has to cross. Thus an efficient DDS has to overcome all the physiological barriers to release drug to the targeted site. With the aim to drug targeting two basic strategies are followed: passive targeting and active targeting (Danhier et al. 2010).

1.2.1 Passive Targeting

Passive drug targeting is a mechanism by which drug delivery vectors can be preferentially delivered to the desired site of action based on the unique pathophysiological characteristics of tumor tissues compared to the normal tissues. Because of the excessive growth of the tumor cells, there occurs extensive angiogenesis leading to the defective vascular architecture and hypervasculature. In addition, solid tumors possess elevated levels of permeability mediators (e.g. bradykinin, nitric oxide etc.) and they lack functional lymphatic drainage. As a result of these pathophysiological conditions of tumor tissues, suitably engineered DDS can easily permeate inside the abnormal cells and are retained there (Figure 1). This mechanism is known as enhanced permeability and retention (EPR) effect (Matsumura & Maeda 1986) (Maeda et al. 2001). Exploiting the EPR effect, delivery of low molecular weight chemotherapeutics to the tumor site can be improved. As this type of drug targeting relies on the pathophysiological uniqueness of the targeted

tissue, it is called “passive targeting”. However physicochemical properties of the vector such as size, surface charge, surface nature (hydrophilic/hydrophobic) etc.

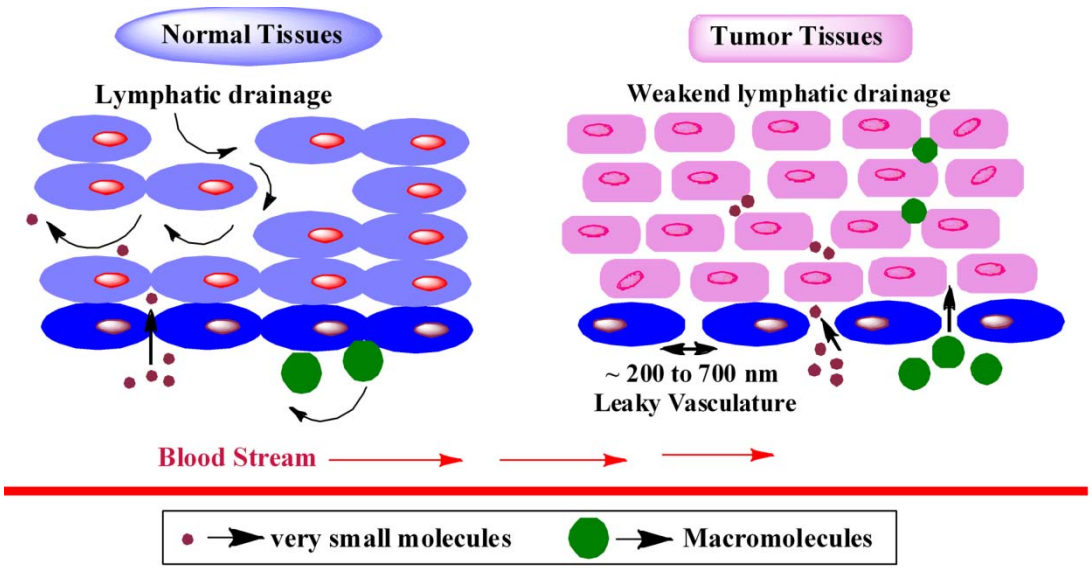

Figure 1: Pathophysiological differences between normal and tumor tissues.

also play significant role in EPR effect assisted passive targeting. Passive targeting through EPR effect can facilitate tumor selective delivery of macromolecular and nano-sized DDS but the delivery vector should be stable enough in the systemic circulation. After intravenous administration, during the journey of the drug delivery vectors through the blood stream, they can undergo opsonisation and hence the propensity to get cleared by the RES also increases. It has been reported that hydrophilic polymers can impart stability to the DDS and help in augmenting their longevity in systemic circulation (Torchilin & Trubrtskoy 1995). Polyethylene glycol is the most widely used hydrophilic polymer with neutral charge for developing engineered drug delivery vectors with less extent of opsonisation and enhanced longevity in systemic circulation. Other hydrophilic polymers (e.g. poly(vinyl

alcohol), poly(vinylpyrrolidone), poly(amino acids), Poly(N-(2-hydroxypropyl) methacrylamide) etc.) have also been conjugated to the drug delivery vectors to impart similar feature to the DDS (Knop et al. 2010).

1.2.2 Active Targeting

Passive targeting exploiting EPR effect is an interesting and simple approach, but it is associated with a major demerit. EPR effect being a highly heterogeneous phenomenon, the extent of passive targeting may be limited (Jain & Stylianopoulos 2010) (Bae & Park 2011). This directs to an alternate approach of drug targeting known as active targeting. In active targeting specific targeting ligands are attached to the surface of DDS through which the vector carrying the therapeutics can actively bind to the receptors over-expressed at the targeted cancer cells (Allen 2002). The mechanism of active targeting is schematically represented in Figure 2. Nevertheless, for actively targeted DDS also EPR-assisted passive extravasation plays the primary role (Lammers et al. 2012) and after coupling with the receptors the actively targeted drug carrier is efficiently internalized inside the cell via receptor mediated endocytosis. Therefore, this approach basically improves target cell recognition by the DDS.

Various types of peptides (e.g. TAT-peptide, RGD peptide), vitamins (e.g. Folic acid), antibodies and growth factors etc. are generally conjugated as the targeting ligands to engineered DDS via esterification or amidation reactions (Byrne et al. 2008). While engineering actively targeted DDS, one must remember and take care of the fact that attaching targeting ligands to a DDS sometimes may enhance the immunogenicity and propensity for opsonisation (Lammers et al. 2012).

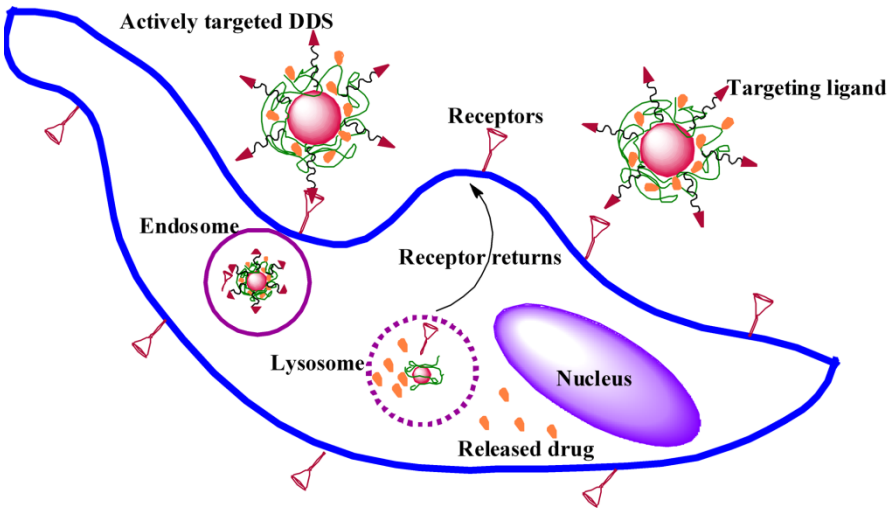

Figure 2: Actively targeted DDS and its intracellular uptake via receptor mediated endocytosis.

1.2.3 Nanomedicines in anticancer drug delivery

From the concept of targeted DDS it is clear that size of the vector is a crucial factor in carrying the chemotherapeutics to the targeted cancer cells. Of late, "nanomedicine" has practically updated cancer management right from diagnosis to treatment stage. Nanomedicine is an umbrella term used to define nano-sized (usually viewed as 1–1,000 nm) drugs and drug delivery vehicles used as medicines (Duncan 2006) and anticancer nanomedicines are intended to improve the biodistribution of chemotherapeutic agents. Nanomedicine has already proved its tremendous potential to improve cancer treatment and management (Ferrari 2005). Various types of nanosystems have so far been used for developing DDS among them metallic nanoparticles (e.g. gold and iron oxide NPs), liposomes, polymeric micelles, polymer-drug conjugates, polymer-protein complex, and carbon based nanomaterials (e.g. carbon nanotubes, carbon dots) etc. are worthy to be mentioned. Specifically engineered nano-sized drug delivery vectors exhibit certain advantages

like enhancement of aqueous solubility of hydrophobic drugs, safe carriage for the toxic drug molecules with minimum loss, enhanced drug loading along with modulating the release and degradation properties of various drugs etc. In addition, properly functionalized nano-vectors can evade opsonisation to a large extent resulting in longer life in systemic circulation and enhanced uptake by the targeted cells *via* EPR effect. Thus these drug vectors can in turn reduce the problem of unwanted toxicity to normal cells. The nano-sized DDS also provide better platform for attaching targeting ligands (for targeted drug delivery) and other relevant moieties (e.g. fluorescent moieties for imaging etc.). Besides, duly engineered nano-vectors carrying multiple chemotherapeutic agents are developed for improving the efficiency of chemotherapeutics by redressing the problems of MDR in cancer. Though the present status of combination therapy needs further improvement, but the merging of two potential research fields *i.e.* combination therapy and nanomedicine has exhibited considerable promise in successful cancer treatment (Hu et al. 2010).

1.3 Polymer Drug Conjugate as Drug Delivery Systems

The concept of targeted polymer-anticancer drug conjugates was born basically from Ringsdorf's vision of utilizing polymer chemistry for drug conjugation (Ringsdorf 1975) and Trouet and De Duve's comprehension that the endocytic pathway might be useful for lysosomotropic drug delivery (Duve et al. 1974). Polymer-Drug conjugates are one of the most important DDS put under the umbrella term "polymer therapeutics" (Duncan 2003).

1.3.1 Fabrication of Polymer drug conjugates

Polymer drug conjugates are developed by direct covalent conjugation of drug molecules to a suitable hydrophilic polymer exploiting the available functional

groups in the polymer. Figure 3 shows the cartoon of a typical polymer-drug conjugate with targeting ligand attached.

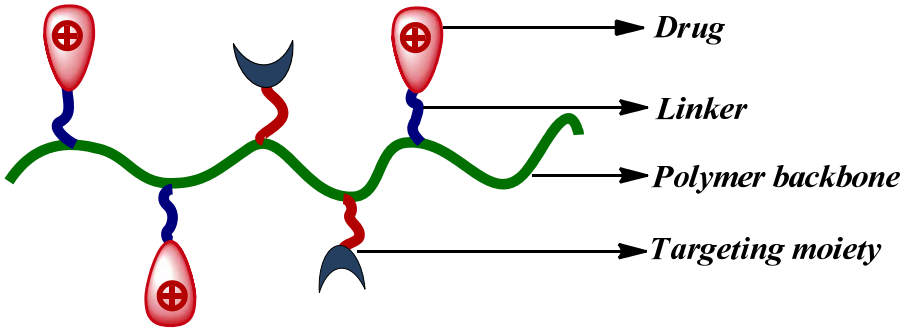

Figure 3: Schematic presentation of an actively targeted polymer-drug conjugate.

For the fabrication of DDS a non-toxic and non-immunogenic polymer with adequate molecular weight should be used. Higher molecular weight of polymer ensures longer time of the conjugate for systemic circulation. Natural/synthetic polymers with admirable biocompatibility and biodegradability are excellent candidates in this regard. However, non-biodegradable polymers should possess adequate molecular weight required for facile renal elimination. The linker bond through which a drug is linked to polymer in a conjugate plays the pivotal role for a DDS. The linker should be stable enough during transportation but should release the payload once the DDS reaches the targeted site of action. Peptidyl and ester linkages are widely used in polymer-anticancer drug conjugates. Other linkages like hydrazone, acetal etc. have also been reported. Some linkages (like ester, hydrazone, amide etc.) are designed to get hydrolyzed under the low pH environment in endosome/lysosome to release the payload. Some peptide linkers may be cleaved by specific enzymes to release the drug in the desired site. In addition, utilizing the large number of diverse functional groups present in a polymer specific targeting ligands

can also be attached to the drug conjugates to make an actively targeted DDS (Duncan 2003).

1.3.2 Polymer Drug conjugates in anticancer drug delivery

Polymer-Drug conjugate is a vital DDS for cancer treatment. For many of the anticancer drugs poor aqueous solubility is the chief limitation. Aqueous solubility of hydrophobic drugs can be augmented dramatically by direct covalent conjugation of the drug to a hydrophilic polymer. Polymer-drug conjugates also have the capability to control the release profile of a drug. Thus drug conjugates can redress the problem of fluctuations in drug release associated with periodic administration and hence can avoid the unwanted side effects, toxicity and organ failure due to high drug concentrations. Conjugation of hydrophobic drugs to suitable polymers offers a chance to alter drug pharmacokinetics and biodistribution which are basically useful for those drugs that exhibit rapid metabolism (e.g. curcumin), faster clearance and/or off target toxicities (anticancer drugs) (Larson & Ghandehari 2012). Low molecular weight anticancer drugs get haphazardly distributed throughout the body giving rise to severe toxic side effects to normal tissues as well. However, upon conjugation to suitable polymeric carriers, the drug conjugates can circulate for a longer time by escaping opsonisation resulting in augmented EPR effect. This can ensure greater accumulation of the DDS to tumor tissues compared to normal ones. Simultaneously, the drug conjugates can limit cellular uptake to endocytic pathway and hence can bypass the mechanisms associated with drug resistance in a cancer cells (Duncan 2006). Thus polymer-anticancer drug conjugates aim to achieve enhanced therapeutic efficacy, reduced side effects and lesser propensity for development of drug resistance.

1.4 Gold Nanoparticles in fabrication of Drug Delivery Systems

Intense research on Gold Nanoparticles (AuNPs) during the past decade has proved AuNPs to be a potential candidate in the field of nanomedicine. To date, various physical and chemical methods have been reported for the synthesis of stable AuNPs (Daniel & Astruc 2004) and among them the most popular is the wet chemistry techniques based on chemical reactions in solutions yielding AuNPs of varying shapes, sizes and dielectric environments. An impressive procedure for AuNPs synthesis is the two-phase reduction method (Brust et al. 1994) using $NaBH_4$ as the reducing agent. Another simple and widely used method to prepare AuNPs suspension in aqueous medium is the reduction of $HAuCl_4$ (aqueous solution) by tri-sodium citrate solution under boiling condition (Turkevich et al. 1951) (Frens 1973). In this method citrate acts both as a reducing agent and a capping agent for AuNPs and size of the citrate capped AuNPs can be tuned over a wide range by controlling the ratio of $HAuCl_4$ to trisodium citrate. The chemical reaction involved in Turkevich method for AuNPs synthesis is as follows (Balasubramanian et al. 2010):

$$2HAuCl_4 + 3Na_3C_6H_5O_7 + 1.5\,H_2O \longrightarrow 2\,Au^0 + Na_2C_5H_6O_5 + 3CH_3COONa + 4NaCl + 0.5\,C_3H_6O + 5.5\,CO_2 + 4Cl^- + 2H^+$$

However, citrate capped AuNPs are prone to environmentally induced aggregation (Cho et al. 2009). AuNPs are characterized by their typical absorption in the visible range (usually between 510 nm to 550 nm) arising from the characteristic surface plasmon resonance absorption (Ghosh & Pal 2007). The peak maxima and width of the absorption peak of AuNPs provide idea regarding the size and size distribution range of the nanoparticles respectively.

1.4.1 Fabrication of polymer stabilized Gold Nanoparticles

In order to develop AuNPs based DDS, the AuNPs must be suitably functionalized ensuring longevity in the systemic circulation and ability to carry the payload safely to the desired site of action. At present, the design of core-shell nanoparticles is very popular as it not only improves the stability and surface chemistry of the core nanoparticle but also provides materials with unique structures and properties that are not obtainable from the nanomaterial alone. Polymers are excellent candidates for stabilizing AuNPs and polymer stabilized AuNPs are really lucrative vehicles to carry hydrophobic drugs, proteins, DNA, RNA and other biomolecules safely. Polymer capping not only imparts long term stability to AuNPs system but also helps adjusting the solubility and amphiphilicity of AuNPs, modify the properties of AuNPs, promote compatibility and provide scope for further conjugation (with targeting ligands/drug/other biomolecules). Polymers can be used to decorate the surface of a preformed AuNPs (alkane thiol or citrate capped AuNPs) utilizing the 'ligand replacement' approach. In this case polymers comprising of sulfur atom/group are preferred for exploiting the 'Au-S' chemistry. On the other hand, polymers can be physically adsorbed onto the surface of AuNPs (e.g., water soluble/ block polymers, nanoreactors etc.). In order to fabricate polymer stabilized AuNPs *via* covalent bonding, two approaches namely (i) grafting from and (ii) grafting to techniques are mainly used. In 'grafting from' technique polymer chains grow from the small initiators that have been pre-anchored to the particle surface, but in 'grafting to' technique polymer chains are grafted to the nanoparticle surface via chemisorption. In order to obtain well-controlled molecular weights of the polymers and well-defined chain architectures, living/controlled radical polymerization

techniques (Matyjaszewski & Xia 2001) (Boyer et al. 2009) have been extensively employed to graft polymer brushes from AuNPs. Parallel growth of polymer science and nanotechnology has really improved the field of polymer protected AuNPs (Shan & Tenhu 2007). In addition, the method of generation and stabilization of AuNPs using suitable polymers in a single step is also an advantageous approach. Various polysaccharides, natural polymers, peptides etc. (e.g. dextran, chitosan, hyaluronic acid, alginate, glutathione) have recently been used for the fabrication of stable functionalized AuNPs. This synthetic approach has several advantages such as: (i) hazardous chemicals need not be used as the reducing agent (ii) additional stabilizing agent need not be used (iii) easy single step is followed for generation and stabilization of AuNPs (iv) in most of the cases medium of reaction is aqueous and (v) lengthy purification steps need not be followed.

1.4.2 Functionalized Gold Nanoparticles in anticancer drug delivery

AuNPs is widely used as a potential drug delivery vehicle due to its several distinctive attributes such as facile synthetic procedure, convenient surface modification, excellent stability, low cytotoxicity etc. (Giljohann et al. 2010). Moreover, functionalized AuNPs with smaller size are highly desirable for (i) passive tumor targeting *via* EPR effect and (ii) RES clearance (Torchilin & Trubetskoy 1995) (Gref et al. 1994). Suitably functionalized AuNPs has the potential to incorporate multiple therapeutic agents and targeting moieties due to its tunable and multivalent surface construction. Thus AuNPs based DDS can be made highly site specific resulting in augmented therapeutic efficacy and reduced side effects. Polymer stabilized AuNPs ensures unimpeded release of conjugated drugs from the DDS and AuNPs based DDS with stimuli responsive (such as pH, temperature etc.)

release of therapeutic agents can also be engineered simultaneously. In addition to this, AuNPs based DDS have been proved to be useful for photothermal therapy and photodynamic therapy for cancer treatment (Wang et al. 2010) (Cheng et al. 2008).

1.5 Aliphatic photoluminescent polymers as Drug Delivery Systems

To date fluorescent biomaterials are of high demand in the field of cellular fluorescence labeling, biosensing, immunology, drug delivery and tissue engineering etc (Chen et al. 2013) (Wadajkar et al. 2012). At present widely used fluorescent biomaterials include fluorescent organic dyes (such as rhodamines, fluoresceines etc.), fluorescent proteins (green and blue fluorescence protein), quantum dots etc. and all of them are associated with several drawbacks such as poor photostability and severe toxicity etc. The synthetic fluorescent polymers consisting of conjugated phenyl rings are potential source of toxicity and therefore, these are not useful in biomedical field (Huang et al. 2007). However, development of aliphatic, amino acid based, biodegradable polymers (BPLPs) with intrinsic photoluminescence is revolutionary discovery in this regard (Yang & Gautam 2013).

1.5.1 Development of amino acid based aliphatic fluorescent polymers

The family of amino acid based BPLPs was synthesized by Yang et al. *via* melt polycondensation technique (Yang et al. 2009) and the fluorescence of the materials was due to their unique structural feature (Serrano et al. 2011) (Zhang & Yang 2013). The synthetic scheme for BPLPs is shown in Figure 4A. Both water soluble and insoluble BPLPs can be prepared by selecting suitable diols (e.g. PEG can be chosen for water soluble BPLPs). The 6-membered ring structure formed during melt polycondensation, is responsible for the intrinsic fluorescence of BPLPs. The 6-membered rings in BPLPs consist of both amide and ester bonds (as shown in

Figure 4B) which are resonance stabilized and the lone pairs on the N and O atoms occupy p-orbitals in conjugation with the *p*-orbitals on the C=O. Electrons in the C–C bond at the central C (C* in Figure 4A) and the C–H or C–C bond at the α-C in the amino acids in the 6-membered rings can strongly associate with *p*-orbitals in the neighboring C=O, N and O atoms to extend the hyperconjugative effect throughout the ring system. The 6-membered ring is also associated with a pendant group that varies with variation of the amino acid (R in Figure 4A) used and this flanking pendant group can also influence the degree of hyperconjugation present in the ring structure of the polymer. The typical blue fluorescence of BPLP-Cys is shown in Figure 4C.

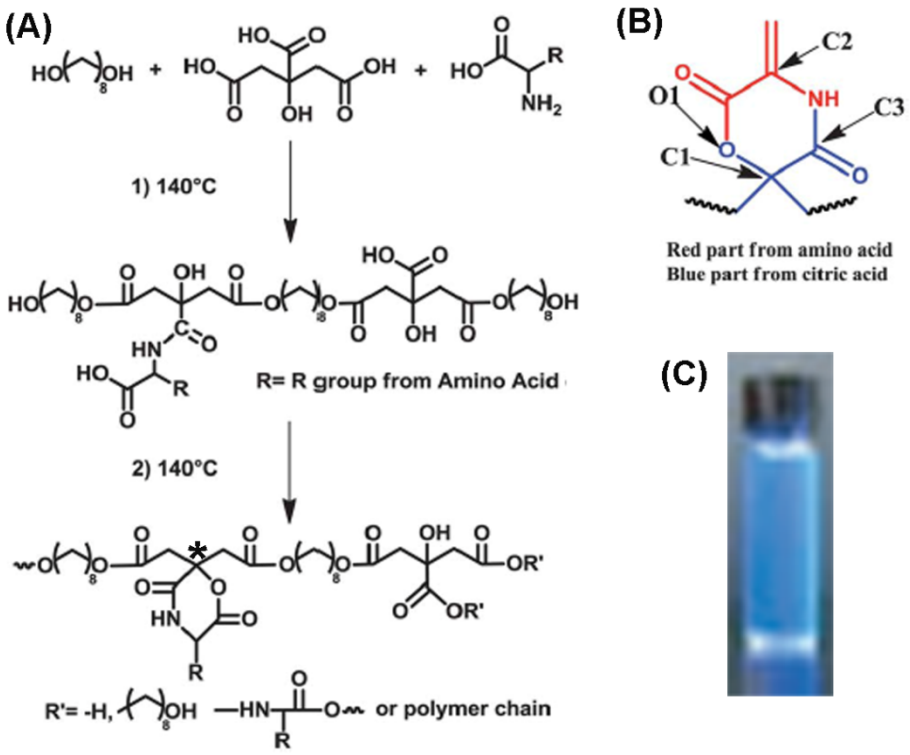

Figure 4: (A) Synthetic routes for the development of BPLPs; (B) six-membered cyclic structural part of the polymer chain containing both amide and ester linkages (Zhang and Yang 2013) and (C) picture of blue fluorescence emission of BPLP-Cys solution under UV light (Yang et al. 2009).

1.5.2 Amino acid based aliphatic fluorescent polymers in drug delivery

The novel family of fluorescent polymers is excellent candidate for the development of new fluorescent DDS. The polymers are based on amino acids which are inevitable part of living organism. Water insoluble BPLPs are biodegradable and biocompatible (Yang et al. 2009) and hence can be used as the hydrophobic building block of DDS for encapsulation of hydrophobic anticancer agents. Water soluble BPLPs can be generated using PEG of different molecular weights and can be used for drug conjugation or for construction of other DDS as well. For the water soluble BPLPs PEG being the polymer backbone, it can be useful in stabilizing metallic nanostructures like AuNPs etc. The synthetic strategy and structure of BPLPs indicate ample scope of structural modification. Thus the system can be useful for making multifunctional DDS too. The prime importance of the polymer lies in the fact that the highly fluorescent materials can be helpful in label-free cellular imaging avoiding the use of hazardous fluorescent probes/ materials as labeling agent in anticancer drug containing DDS. Exploiting the intrinsic fluorescence of this biodegradable, biocompatible polymer system, it is possible to develop highly efficient track-able DDS for cancer therapy.

1.6 Potential anticancer drugs for chemotherapy

1.6.1 Curcumin

Curcumin (diferuloylmethane), a natural polyphenolic compound identified as 1,6–heptadiene–3,5–dione–1,7–bis(4–hydroxyl–3–methoxyphenyl)–(1*E*,6*E*), is extracted from the rhizome of the plant *Curcuma longa* (known as turmeric, the well known spice mostly consumed in south-east Asia). In curcumin (Ccm) two aromatic ring systems are connected by α,β-unsaturated carbonyl groups and the molecule can

exist in both diketonic form and stable enol form (as shown in Figure 5). Ccm is hydrophobic in nature and gets dissolved in organic solvents (like DMSO, ethanol, acetone etc.) giving rise to a bright yellow solution. Practically Ccm has a very poor aqueous solubility and in aqueous medium Ccm degrades very fast.

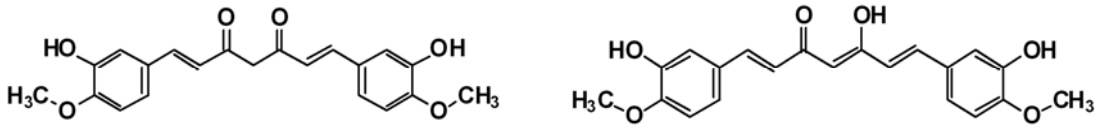

Curcumin (di-Keto form) **Curcumin (Enol form)**

Figure 5: Chemical structure of curcumin (in di-Keto and more stable Enol forms).

Within the last couple of decades, extensive research work has revealed a variety of pharmacological activities of Ccm such as antioxidant, anti-inflammatory, antiproliferative and antiangiogenic activities (Aggarwal et al. 2003) (Shi et al. 2006) (Motterlini et al. 2000) (Lantz et al. 2005) (Aggarwal & Sung 2009). It has Also been proved that -OH groups in Ccm are required for its antioxidant activity, its -OMe groups are essential for its anti-inflammatory and antiproliferative activity (Ravindran et al. 2009). Recent work also established that Ccm holds the potential to prevent protein aggregation in incapacitating diseases such as Alzheimers and Parkinsons (Wang et al. 2013) (Mythri & Bharath 2012). Interestingly, Ccm does not have toxic effect to human body as evident from the long dietary use and it has also been established by several other studies (Lao et al. 2006). On the contrary, Ccm is known to have chemopreventive activity (Duvoix et al. 2005). The medicinal assets of Ccm make it an excellent candidate for prevention and treatment of several health hazards of human being including cancer.

1.6.1.1 Curcumin: anticancer mechanism

Several studies have proved Ccm to be an effective chemotherapeutic and chemopreventive agent. It has been revealed by intense research that Ccm can inhibit cell proliferation, invasion, metastasis and angiogenesis by suppressing multiple cell signaling pathways. The transcription factor NF-κB, constitutively expressed in almost all cancer types suppresses apoptosis in a wide variety of tumors (Aggarwal 2004). NF-κB is the chief controller of inflammation, cell proliferation, apoptosis, and resistance in cells. Ccm has the potential to suppress the activity of NF-κB (Shishodia et al. 2005) resulting in a subsequent down-regulation of many NF-κB regulated genes which are involved in tumorogenesis (e.g. TNF, COX-2, cyclin D1, c-myc and interleukins etc.). Ccm potentially suppresses a variety of growth factors including VEGF, COX-2, MMPs and ICAMs and consequently inhibits tumor angiogenesis and metastasis (Aggarwal et al. 2003) (Aggarwal et al. 2004). Ccm can upregulate p16 and p53 resulting in stimulation of apoptosis (Ravindran et al. 2009). Recent research has unveiled that Ccm can also down-regulate multi drug resistance proteins and P-glycoprotein in cancer cells (Choi et al. 2008) and thus it has the potential to defend the development of multi drug resistance in cancer cells. It is believed that development of resistance to Ccm is very less likely as it induces cellular apoptosis *via* multiple cells signaling pathways. Ccm can show pleiotropic effect due to its ability to inhibit multiple cell signaling pathways. In addition, this polyphenolic drug with its medicinal assets is capable of augmenting antitumor effects of several other antineoplastic agents such as Doxorubicin, Paclitaxel etc. (Chen et al. 2013) (Guo et al. 2014) (Manju et al. 2011). A recent study has shown that Ccm augmented the effect of anticancer drug MTX (Dhanasekaran et al. 2013).

1.6.1.2 Curcumin: drawback and scope for therapeutic application

Although Ccm possesses diverse pharmacological activities including anticancer property, yet the major drawback associated with this natural product is its poor bioavailability. The poor bioavailability originates from extremely low aqueous solubility and instability. Report says that the scanty soluble fraction of Ccm in aqueous medium undergoes rapid hydrolysis at physiological pH (Wang et al. 1997) producing hydrolyzed products with no medicinal values. In spite of the lower bioavailability; the therapeutic efficacy of Ccm against various maladies including cancer, cardiovascular diseases, diabetes etc. has been well documented. Hence, Ccm formulation with enhanced bioavailability can be a potential therapeutic agent.

In order to enhance the aqueous solubility and stability of this hydrophobic drug, several approaches have been proposed. Among them use of liposomes, polymeric micelles or polymer gels, cyclodextrin; formation of Ccm-phospholipid complexes; use of adjuvant like piperine etc. are worthy to be mentioned (Li et al. 2005) (Manju et al. 2011) (Maiti et al. 2007) (Song et al. 2012) (Shoba et al. 1998). The concepts of encapsulation of Ccm inside the hydrophobic core of micelles or inside the hydrophobic cavity of cyclodextrins etc. may seem to be safer carriers for the polyphenolic drug, but such type of DDS are associated with shortcomings like poor loading capacity, batch wise variation in loading amount, impeded drug release etc. However, polymer-Ccm conjugates have been reported to redress these problems to a large extent. In polymer-Ccm conjugates, the covalent conjugation of Ccm to suitable hydrophilic polymers not only augments its aqueous solubility but also provides stability, enhanced time in systemic circulation, improved release kinetics and enhanced therapeutic efficacy of the drug.

1.6.2 Methotrexate

Methotrexate (MTX), an antimetabolite with the IUPAC name (2*S*)-2-[(4-{[(2,4-diaminopteridin-6-yl)methyl](methyl)amino}benzoyl)amino]pentanedioic acid, was first synthesized by the Indian biochemist Yellapragada Subbarow and was clinically developed by American pediatric pathologist Sidney Farber (Mukherjee 2010) . An antimetabolite can be defined as a chemical that can inhibit the use of a metabolite (another chemical that is part of normal metabolism). Antimetabolites generally have structural similarity to the metabolite with which they interfere. Likewise, MTX interferes with Folic acid (FA) and structurally MTX is an analogue of FA (as shown in Figure 6). MTX is used for the treatment of cancer, autoimmune diseases, ectopic pregnancy etc. MTX is a widely used drug for human malignancies such as leukemia, malignant lymphoma, breast cancer and head and neck cancer (Yoon et al. 2010).

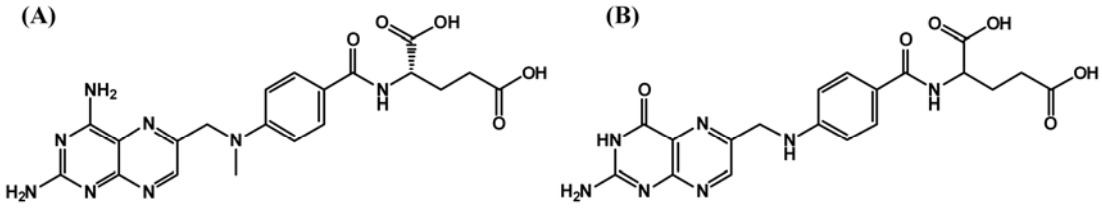

Figure 6: Chemical structure of (A) MTX and (B) FA.

1.6.2.1 Methotrexate: anticancer mechanism

MTX is an antifolate drug that works as an antagonist of FA and consequently can induce cellular apoptosis. FA is an essential component in human body. FA is required for the *de novo* synthesis of nucleoside thymidine which is required for DNA synthesis. Folate is also indispensable for biosynthesis of purine

and pyrimidine bases. But MTX interrupts the FA cycle by tightly binding with the enzyme dihydrofolate reductase (DHFR). DHFR catalyzes the conversion of dihydrofolate to active tetrahydrofolate. MTX contains an amino group at the 4^{th} position of the pteridine ring and this structural change in MTX is critical in its enhanced (almost 1000 fold higher) binding affinity towards DHFR compared to FA. Thus, MTX competitively inhibits DHFR resulting in inhibition of synthesis of DNA, RNA, thymidylates and proteins and subsequent cellular mortality. It is worthy to be mentioned here that MTX being FA analogue, can show targeting effect like FA. Hence, MTX can play the dual role of a targeting agent and a cytotoxic drug to the cancer cells that overexpresses folate receptors (Duthie 2001).

1.6.2.2 Methotrexate: drawback and scope for therapeutic application

Antifolate antimetabolite MTX is undoubtedly a potential anticancer drug and efficient targeting agent. However, the major limitation because of which the clinical efficacy of MTX is often compromised is the development of resistance to the drug in targeted cancer cells. Acquisition of resistance to MTX in cancer cells occurs mainly *via* the drug efflux mechanism (Banerjee et al. 2002). In order to redress this serious problem several approaches have been adopted such as encapsulation of MTX inside polymeric micelles (Nogueira et al. 2013), fabrication of MTX conjugated functionalized nanoparticles (Kohler et al. 2005) etc. Formation of polymer-MTX conjugate is one of the most important approaches in this regard. Upon conjugation to a suitable hydrophilic polymer, the MTX conjugate can be effectively internalized by the targeted cells bypassing the routes for drug efflux and hence the conjugates help in maintaining higher concentration of the drug inside the cell (Riebeseel et al. 2002) (Piper et al. 1983). At the same time, this approach can

improve the release of the drug and redress the problem of MTX associated side-effects.

1.7 Hypothesis

The present study is based on the following hypotheses: (1) Aqueous solubility of hydrophobic anticancer agents can be augmented by appropriate modification to attain improved cytotoxic potential and (2) Suitably engineered nano-structured drug delivery vehicles with potential stability in the systemic circulation can safely carry the anticancer drugs to the desired site and a nano-vector with intrinsic photoluminescence can also facilitate label-free cellular imaging.

1.8 Objectives of the study

The present study deals with the designing of polymer-anticancer drug conjugates and polymer stabilized anticancer drug conjugated AuNPs systems for safer delivery of anticancer drugs (Ccm and MTX) to cancer cells. The main objectives of the study are as follows:

1. To formulate polymer-Ccm conjugate for enhancing the aqueous solubility and stability of the hydrophobic drug. **Biocompatible and non-immunogenic biopolymer Alginate (Alg) was used to design the Alg-Ccm conjugate.**

2. To conjugate Ccm onto the surface of water soluble polymer stabilized AuNPs for augmented aqueous solubility and pH responsive safer delivery of Ccm. **Ccm was conjugated to polymer functionalized AuNPs *via* succinate linker to facilitate pH responsive release of the drug into cancer cells.**

3. To conjugate Ccm and MTX onto the surface of a biopolymer-stabilized AuNPs using minimum reaction steps and through green synthetic route. In order to

fabricate the nano-vector, **AuNPs were generated and stabilized by Alg-Ccm conjugate**. Next, **Alg-Ccm AuNPs were further modified with MTX conjugate of bis(aminopropyl) terminated PEG (MP conjugate).** The hybrid nano-vector **(MP@Alg-Ccm AuNPs) containing two chemotherapeutics was fabricated *via* only two facile steps under green condition (*i.e.*, in aqueous medium and green chemical alginate as the reducing agent).**

4. To fabricate a nano-sized micelle forming fluorescent polymer-Ccm conjugate for safer Ccm delivery and label-free cellular imaging. In order to design the fluorescent nanostructure, a **water soluble, biodegradable, aliphatic, fluorescent polymer with almost no intrinsic toxicity was developed using natural tripeptide Glutathione (GSH) as one of the monomer. This GSH containing fluorescent polymer was therefore used to design the micelle forming fluorescent Ccm conjugate.**

Designing and evaluation of all the four DDS are expected to make a few strides to the cancer research studies and can hopefully provide fundamentals to design a suitable targeted anticancer DDS with improved efficiency, reduced side-effects and better patient compliance. The following chapters are summarized below:

Chapter 2: Literature review; this chapter deals with the relevant published works showing the background and significance of each work done here.

Chapter 3: Materials and methods; this chapter provides with the information of the chemicals used, synthetic routes involved and physicochemical and biological characterizations done for all the four DDS here.

Chapter 4: Results; this chapter delineates the results obtained after synthesis and evaluation of each of the DDS.

Chapter 5: Discussion; the results shown in chapter 4 are critically discussed in this chapter of the thesis

Chapter 6: Summary and conclusion; based on the important results obtained by the study, this chapter summarizes the entire work and also concludes the thesis with the futuristic outlook of further studies that come into view from this research work.

CHAPTER 2

LITERATURE REVIEW

2 Literature Review

2.1 Polymer-Curcumin Conjugates

Within the last couple of decades, extensive research work has unveiled the fact that Ccm, the natural polyphenolic compound has potential medicinal assets (Sharma et al. 2005). In spite of possessing striking chemopreventive and chemotherapeutic effect, extremely low aqueous solubility and instability are the two serious demerits associated with this hydrophobic drug (Duvoix et al. 2005). However, recent studies also suggest that poor absorption and rapid metabolism of Ccm are major factors in the curtailment of its bioavailability (Anand et al. 2007). Ccm has almost no intrinsic toxicity and a dose of 12 g/day is also well tolerated (Lao et al. 2006). Due to poor absorption of Ccm, extremely low level of this drug is often found in serum, even when administered in high doses. It is reported that oral Ccm administration at a dose of 2 g/kg to rats produced a maximum Ccm concentration in serum of 1.35 ± 0.23 μg/mL after 0.83 h, whereas the same dose resulted in almost undetectable low (0.006 ± 0.005 μg/mL at 1 h) Ccm concentration in serum in humans (Shoba et al. 1998). Interestingly, the administration route also plays a significant role in achievable Ccm concentration in serum (Yang et al. 2007). The low absorption of Ccm results in poor biodistribution (Ravindranath & Chandrasekhara 1980). In addition, rapid metabolism and elimination is also a major concern for low bioavailability of this wonderful natural product (Pan et al. 1999). However, co-administration of Ccm with adjuvants which can block the metabolism of the drug is one of the best approaches adopted for reducing its metabolism and systemic

elimination. Piperine is an adjuvant which increases Ccm bioavailability *via* the inhibition of glucuronidation, the major route for Ccm metabolism. In a study by Shoba et al. showed 2000% increment in Ccm bioavailability in humans (receiving 2 g/Kg Ccm) when co-administered with piperine compared to the undetectable Ccm concentration in serum for single administration of the drug (Shoba et al. 1998). However, several other approaches have also been adopted to enhance the bioavailability of Ccm by redressing diverse limitations of the drug such as poor aqueous solubility, instability in aqueous medium etc. Synthesis of polymer-curcumin conjugates is one of the best approaches in this regard, because in one hand the direct covalent conjugation of Ccm to a hydrophilic polymer can enhance the aqueous solubility of the hydrophobic drug. On the other hand the conjugate consisting of both hydrophilic and hydrophobic segments can effectively self-assemble in aqueous medium producing micelle like structure and keeping Ccm safely inside the hydrophobic core of the micelles which in turn resists the hydrolytic degradation of Ccm (c. Manju & Sreenivasan 2011). Several groups have reported polymer-Ccm conjugates using poly(ethylene glycol) (PEG) as the hydrophilic polymer. Safavy et al. have reported that water soluble PEG-Ccm conjugates using urethane linkage exhibited augmented aqueous solubility and improved toxicity of Ccm compared to that of free Ccm (Safavy et al. 2007). Recently, Kim et al. have demonstrated the cellular uptake kinetics of the same PEG-Ccm conjugates (Kim et al. 2011). This study done in 3T3-L1 cell line (an *in vitro* model of adipogenesis) suggested that PEGylation improved water solubility and cellular retention of Ccm resulting in improved delivery of Ccm in preadipocytes and its

antiadipogenic ability. Li et al. reported that PEG-Ccm conjugate has growth inhibitory effects on human pancreatic cancer cell lines (Li et al. 2009). Ccm containing polymers (polycurcumins) were also developed by polycondensation polymerization (b. Tang et al. 2010). In this study Tang et al. included Ccm units in the backbone of polycurcumin as a part of the vehicle. Short PEG chains were also introduced in the backbone as side chains/co-monomers that in turn enhanced the water solubility of polycurcumins. In another interesting study, Tang et al. have reported the development of surfactant like Ccm produrg by conjugation of Ccm with two oligo(ethylene)glycol chains *via* beta-thioester bonds (a. Tang et al. 2010). This Ccm conjugate showed stimuli (redox) responsive release as the beta-thioester bonds are labile in the presence of intracellular glutathione and esterase. Of late, Pandey et al. have projected the use of novel PEGylated Ccm analogues for improvement in solubility of Ccm (Pandey et al. 2011). Manju et al. have conjugated Ccm with hyaluronic acid to enhance the aqueous solubility and stability of the drug and it was shown that the conjugate potentially enhanced the cytotoxic effect of Ccm (a. Manju & Sreenivasan 2011). This Ccm conjugate of hyaluronic acid is interesting with respect to targeted drug delivery as hyaluronic acid has targeting ability. In a recent study Yang et al. have reported the fabrication of biodegradable, amphiphilic polymer-Ccm conjugate micelles (Yang et al. 2012). The polymer segment of the conjugate was composed of hydrophilic PEG and hydrophobic poly(lactic acid) (PLA) and Ccm was conjugated to PLA *via* ester linkage using tris(hydroxymethyl)aminomethane (Tris) linker. Free Ccm was also encapsulated inside the hydrophobic core of mPEG-PLA-Tris-Ccm conjugate micelles. These

polymer-Ccm conjugates can be used as drug delivery vehicles and at the same time they can be used to fabricate other smart DDS (b. Manju & Sreenivasan 2011). In the present study, Ccm was conjugated to two different polymers and these are (i) water soluble biopolymer Alginate and (ii) water soluble, synthetic, fluorescent polymer, *via* ester linkage to enhance the aqueous solubility, stability and improved cytotoxicity of Ccm.

2.2 Gold Nanoparticles Based Drug Delivery Systems

The application of gold nanoparticles (AuNPs) as DDS is a fast expanding field. AuNPs are highly desirous in fabrication of nano-sized drug delivery vehicles due to their small size, facile synthesis and ease of surface modification. The well tunable surface construct is a potential platform for further modification. Exploiting ligand-exchange reactions, multifunctional monolayers can be created onto the surface of AuNPs and this structural diversity enables AuNPs based DDS to carry multiple targeting agents (like anti body, folic acid etc.), chemotherapeutics, labeling agents for imaging (such as fluorescent probes) etc. (Duncan et al. 2010). Suitably functionalized AuNPs, in one hand can carry the drug safely and on the other hand can provide longer time for systemic circulation and improved cytocompatibility. There are many reports on the application of functionalized AuNPs as vehicles for the delivery of diverse drug molecules, proteins, nucleic acids and several other biomolecules. AuNPs based nano vectors are also well reported for anticancer drug delivery. Paciotti et al. used AuNPs functionalized with tumor necrosis factor (TNF), PEG and anticancer drug paclitaxel

(PTX) as a solid tumor targeted, multifunctional drug delivery vehicle (Paciotti et al. 2004) (Paciotti et al. 2006). PEG is the most commonly used non-ionic polymer with stealth potential for the functionalization of AuNPs (Knop et al. 2010). The PEGylated AuNPs not only has reduced tendency towards aggregation but also provides reduced opsonisation resulting in longevity in systemic circulation. In addition PEGylated AuNPs based formulations are found to have increased stability during storage and application. Aryal et al. have reported AuNPs based DDS for pH responsive Doxorubicine (DOX) delivery (Aryal et al. 2009). In order to fabricate the DDS, they first synthesized AuNPs *via* borohydride ($NaBH_4$) reduction and stabilized the AuNPs using thiolated methoxy-PEG. To this thiolated methoxy-PEG capped AuNPs, DOX was conjugated through a hydrazine linker. They demonstrated the enhanced DOX release from the DDS at pH 5.3 compared to that at pH 7.4 due to the presence of acid-labile hydrazine linker. This type of AuNPs based DDS with external/internal stimuli-responsive characteristics are also well studied (Hong et al. 2006). Wang et al. have reported a DDS by tethering DOX onto the surface of PEGylated AuNPs *via* an acid labile linker and have demonstrated the efficiency of the DDS in inhibiting the growth of multidrug resistant MCF-7/ADR cancer cells by enhanced cellular uptake and acid responsive DOX release (Wang et al. 2011). The small sized, duly functionalized AuNPs are excellent candidates for anticancer drug delivery as they can take the advantage of leaky tumor vasculature to facilitate enhanced cellular internalization via EPR effect. However, AuNPs based targeted DDS have also been developed by various research groups to take the advantage of both active and passive targeting for improved

therapeutic effect. In a recent study, Kumar et al. have fabricated neuropilin-1 (Nrp-1) targeted AuNPs based DDS for enhanced therapeutic efficacy of Platinum (IV) drug for prostate cancer therapy (Kumar et al. 2014). For Nrp-1 targeted AuNPs fabrication they utilized AuNPs stabilized by glutathione, a natural tripeptide with antioxidant property leading to cancer regression. Researchers have fabricated anti-epidermal growth factor receptor (EGFR) coated AuNPs to target human oral squamous cell carcinoma (Jain et al. 2007) (Huang et al. 2007). In these works El-Sayed et al. have also exploited the potential of AuNPs to produce local heating effect upon light irradiation to study the photothermal destruction of tumor tissues. Methotrexate (MTX) is another interesting antimetabolite that not only plays the role of an anticancer drug but also has the targeting property like FA. Functionalized AuNPs are proved to be an excellent vector for MTX delivery to various cancer cells (Chen et al. 2007) (Durgadas et al. 2012). In an interesting study, Zhang et al. have reported a DOX delivery vehicle based on tiopronin functionalized ultra small AuNPs for effective killing of apoptosis resistant cancer cells (Zhang et al. 2011). The natural polyphenolic anticancer agent Ccm loaded multifunctional water soluble hybrid nanogel comprising of Au/Ag nanoparticles with a hydrophobic (PS)/hydrophilic(PEG) double layer gel shell has been reported for thermoresponsive release of Ccm (Wu et al. 2011). However, one of the serious drawbacks associated with the development of hydrophobic drug conjugated AuNPs based DDS is that they are fabricated following multistep synthetic steps in most of the cases. In addition, frequently hazardous organic solvents are utilized for the conjugation of anticancer drugs onto the surface of functionalized AuNPs. Multiple synthetic steps

may make the AuNPs prone to aggregation. In this aspect single step generation and stabilization of AuNPs is more interesting and appealing. In some recent reports, Ccm conjugated AuNPs have been developed using Ccm as both the reducing and stabilizing agents (Singh et al. 2013) (Sindhu et al. 2014). Manju et al. have reported the generation of AuNPs in a single step in aqueous medium utilizing hyaluronic acid-Ccm conjugate and evaluated the *in vitro* anticancer potential of the FA targeted, conjugate stabilized AuNPs. In this study the drug conjugate played the dual role of reducing and stabilizing agents for AuNPs (Manju and Sreenivasan 2012). In the present study, two different polymer stabilized AuNPs based DDS were developed. In the first hybrid nano-structured DDS, Ccm was covalently conjugated to a thiol containing low molecular weight polymer stabilized AuNPs through succinate ester linkage to design a pH responsive Ccm delivery vehicle. In the second DDS, AuNPs were generated and stabilized by water soluble Alginate-Ccm conjugate (Alg-Ccm) in a single step followed by conjugation of anti-folate, antineoplastic drug MTX onto the surface of Alg-Ccm stabilized AuNPs. Here the AuNPs based DDS containing dual drug was fabricated following two synthetic steps using water as the green reaction medium.

2.3 Amino Acid Based Aliphatic Fluorescent Polymers in Drug Delivery

Fluorescent materials are of prime importance in the field of biomedical applications. DDS with fluorescent characteristics can fulfill two requirements, (i) they can carry therapeutic agents to the desired site and (ii) they can be used for imaging too. Fluorescent DDS can be used as *in vivo* tracers for the detection and therapy of cancer (Sumer and Gao 2008) and can also be used as probes for scrutinizing cellular

internalization and intra-cellular trafficking of drugs, genes or other biomolecules carried by the respective DDS (Lu et al. 2011). In order to confer photoluminescent property to a nano-vector, usually different types of organic dyes, fluorescent proteins and quantum dots are utilized (Jamieson et al. 2007) (Mauring et al. 2007). But considerable cytotoxic potential of the above mentioned fluorescent materials is one of the major concerns in using these materials for the fabrication of fluorescent DDS (Mancini et al. 2008). Development of fluorescent polymers could not help in this regard as these are composed of conjugated phenyl rings and hence, are highly carcinogenic and toxic in nature. Applications of these fluorescent polymers are thus restricted to non-biological fields only (Huang et al. 2007). Several other photoluminescent polymers such as poly(amidoamines) (PAMAM) and poly(propyleneimine) (PPI) dendrimers, hyperbranched poly(amino esters) etc. are worthy to be mentioned here (Lee at al. 2004) (Wang and Imae 2004) (Wu et al. 2005). However, of late there has been growing interest in developing biodegradable materials with inherent fluorescence and reduced intrinsic toxicity. The development of the novel family of aliphatic, biodegradable, photoluminescent polymers (BPLPs) based on the natural amino acids is really a breakthrough in the field of fluorescent biomaterials (Yang et al. 2009). The BPLPs being devoid of any conjugated phenyl rings do not have carcinogenic potential. The biodegradability and cytocompatible characteristics are excellent qualities for drug delivery applications. Most importantly, the inherent fluorescence originating from their structural feature makes them the potential candidates for drug delivery, imaging and other biomedical applications (Zhang and Yang 2013). The free functional groups

available in BPLPs can be conjugated to other polymeric systems to generate fluorescent polymeric micelles. Drug conjugates can also be developed using the water soluble BPLPs for development of fluorescent DDS. In addition, BPLPs can be used to fabricate fluorescent nanoparticles too (Yang et al. 2009). Recently, Zhang et al. have reported the development of a new class of urethane-doped biodegradable fluorescent polymers (UBPLPs) and their crosslinked variants (CUBPLPs) (Zhang et al. 2013). UBPLPs were also fabricated into stable nanoparticles and showed a high loading efficiency (91.84 %) and sustained release of anti-cancer drug 5-fluorouracil. Both UBPLPs and CUBPLPs showed high quantum yield and excellent cytocompatibility. The fluorescence of the materials was non-invasively detected *in vivo*. Another recent and noteworthy study by Gyawali et al. reports the formation of fluorescent amphiphilic copolymer based on BPLPs by conjugating BPLP-Cysteine (hydrophobic) with methoxy-PEG-COOH (hydrophilic) (Gyawali et al. 2013). The amphiphilic copolymer self-assembled forming fluorescent micelles in which PTX was encapsulated as an anticancer drug. The report shows the biodegradable fluorescent polymeric micelle to be an efficient drug carrier and compatible probe for imaging. Wadajkar et al. have reported an interesting study on dual imaging and cancer cell targeting using water soluble and insoluble BPLPs (Wadajkar et al. 2012). In this work, Wadajkar et al. have modified super paramagnetic iron oxide (Fe_3O_4) nanoparticles (MNPs) by conjugating with both water soluble and insoluble BPLP and this conjugation did not affect the magnetic properties of MNPs. The photoluminescent polymer modified MNPs exhibited magnetic targeting and as well as dual imaging. The MNPs in core helped in magnetic resonance imaging (MRI) and

the fluorescent polymer layer facilitated optical imaging. The nanoparticle system was fully-biodegradable and compatible. Most interestingly, these nanoparticles exhibited cancer cell selectivity for cellular uptake. Conjugation of specific anticancer drug to these nano-vectors may give rise to a multifunctional DDS. Thus the amino acid based fluorescent polymers (both water soluble and insoluble) are very promising candidates for fabrication of fluorescent DDS. Exploiting the functional groups in amino acids it is possible to modify the fluorescent polymers to certain extent keeping the fluorescence property intact. In the present study, a water soluble biodegradable fluorescent polymer was designed utilizing natural tripeptide glutathione. Glutathione (GSH) has antioxidant property and it helps in cancer regression. GSH was incorporated in the polymer backbone formed by PEG and citric acid generating a fluorescent polymer. In addition, nano-sized micelle forming Ccm conjugate was also fabricated using this fluorescent polymer for simultaneous Ccm delivery to cancer cells and label free cellular imaging.

CHAPTER 3

MATERIALS AND METHODS

3 Materials and Methods

3.1 Development of Alginate-Curcumin Conjugate for Enhanced Aqueous Solubility and Stability of Hydrophobic Drug Curcumin

3.1.1 Materials

Curcumin (Ccm; 95% total curcuminoid content) from turmeric rhizome was obtained from Alfa Aesar (Bangalore, India). Sodium alginate (Alg, M_w 4×10^5) was purchased from SD fine chemicals (Mumbai, India). 1,3-dicyclohexylcarbodiimide (DCC), 4-dimethyl aminopyridine (DMAP) and 1-Pyrenecarboxaldehyde (1-PyCHO) were purchased from Sigma-Aldrich (Bangalore, India). Dimethyl sulfoxide (DMSO) and ethanol were obtained from Merck (Mumbai, India). Ultra pure water (18.2 mΩ resistivity) was obtained from a Mili-Q water purification system. Deionized water was used all through the reactions and purification steps in this study.

L-929 cells (mouse fibroblast cells) were obtained from ATCC (Bangalore, India), 3-(4,5-Dimethylthiazol-2-yl)-2,5-diphenyl tetrazolium bromide (MTT reagent), fetal bovine serum (FBS) and minimum essential medium (MEM) were obtained from Sigma-Aldrich (Bangalore, India).

3.1.2 Synthesis of Alginate-Curcumin conjugate (Alg-Ccm)

500 mg Alg was added in portions to water/DMSO mixture (50 mL, 1:1 v/v) and stirred vigorously for 12-16 hrs to obtain finely suspended Alg. DCC (40 mg) and DMAP (15 mg) were added to it and the reaction mixture was stirred for one hour at 25 °C to activate the carboxylate groups. To the activated Alg, Ccm (15 mg dissolved in 10 mL DMSO) was slowly added under N_2 (g) atmosphere. The mixture was stirred well

for about 7 hrs at 60 °C. Resultant solution was then cooled to room temperature and dialyzed for one day against DMSO followed by three days against deionized water using a dialysis membrane of molecular weight cut-off (MWCO) 3500 to remove the unreacted molecules. Finally, Alg-Ccm conjugate was lyophilized and stored in refrigerator for further studies.

3.1.3 Physicochemical Characterizations

3.1.3.1 Fourier Transform Infrared Spectroscopy (FTIR)

FTIR spectra were recorded in the range of 4000 – 500 cm^{-1} using a Nicolet 5700 FTIR Spectrometer (Madison, USA) using KBr pellets.

3.1.3.2 Ultraviolet-Visible (UV-Vis) and Fluorescence Spectroscopy

The absorbance range of Alg-Ccm was monitored using Ultraviolet-Visible (UV-Vis) spectrophotometer (Carry model 100 bio UV-Vis spectrophotometer, Melbourne, Australia). The emission spectrum of Alg-Ccm was recorded using a spectrofluorometer (Carry Eclipse model EL 0507, Melbourne, Australia) after dissolving the conjugate in water/EtOH mixture (1:1 v/v) and exciting it at 427 nm.

3.1.3.3 Nuclear Magnetic Resonance Spectroscopy (^{1}H NMR)

^{1}H NMR spectra were recorded on a NMR Spectrometer (Bruker Avance DPX 300) using D_2O as the solvent.

3.1.3.4 Determination of critical micelle concentration (CMC) of Alg-Ccm

The CMC value of Alg-Ccm was determined to find out the concentration above which Alg-Ccm can form aggregated structure in aqueous solution. The self-aggregation behavior of Alg-Ccm was investigated by both absorption and emission spectroscopy

using 1-PyCHO as the probe molecule. The absorption characteristic of 1-PyCHO was estimated by using UV-Vis spectrophotometer at 25 ºC in the range of 200-700 nm. The emission spectra of 1-PyCHO were recorded in a spectrofluorometer with slit openings (both excitation and emission) of 5 nm at 25 ºC from 400 to 600 nm after exciting the fluorescent probe at 368 nm. A stock solution of Alg-Ccm in water (1 mg/mL) was prepared and the concentration was varied from 10^{-3} mg/mL to 1 mg/mL by diluting the stock solution of Alg-Ccm with distilled water. 8 µL of the stock solution of 1-PyCHO was mixed with 5 mL of each diluted aqueous solution of Alg-Ccm to maintain a final concentration of the probe at 2.4×10^{-6} (M) in each of the solutions. The solutions were incubated for 45 minutes in dark at 25 °C before measuring the absorbance. Similar procedure was followed to determine the CMC of the conjugate by fluorescence measurement.

3.1.3.5 Dynamic Light Scattering (DLS)

The hydrodynamic diameter and zeta potential of Alg-Ccm conjugate micelles in aqueous medium were determined by DLS (Malvern Zetasizer Nano ZS, UK) with a He-Ne laser beam at a wavelength of 633.8 nm. The DLS study was done at 25 °C in aqueous buffer solution (at pH 7.4).

3.1.3.6 Transmission Electron Microscopy (TEM)

The size and morphology of the micelles formed by Alg-Ccm in aqueous solution were visualized by TEM (Hitachi H-7650; Tokyo, Japan). Sample for TEM analysis was prepared by depositing a drop of Alg-Ccm solution (in water, 1 mg/mL) on a 200 mesh copper TEM grid with formver film and air dried at room temperature.

3.1.3.7 Evaluation of curcumin content and aqueous solubility of the conjuagte

The amount of Ccm content in Alg-Ccm conjugate was evaluated using UV-visible absorption spectroscopy. Free Ccm in H_2O/EtOH mixture (1:1 v/v) was used to generate a calibration curve (R^2 = 0.99). Concentration of Ccm in Alg-Ccm was estimated from the absorption intensity of the conjugate solution (in water/EtOH, 1:1 v/v) in the standard calibration curve at 427 nm.

To evaluate the aqueous solubility of Alg-Ccm conjugate, an excess amount of Alg-Ccm was added to an aqueous buffer solution (pH 7.4). The mixture was vortexed for few minutes and then centrifuged at 14,000 rpm for 5 min. Water layer was separated and diluted with EtOH. Thus concentration of Ccm was determined from the optical density calculation as mentioned above.

3.1.3.8 Determination of stability of Alg-Ccm in aqueous medium

The hydrolytic stability of both free Ccm and Alg-Ccm conjugate was determined in phosphate buffered saline (PBS) at physiological pH (pH = 7.4) by determining the change in the absorbance of Ccm. Solutions of free Ccm and Alg-Ccm conjugate in PBS were incubated at 37 °C for 6 h and in 1h interval, portion of the solutions were taken to check the absorbance using UV-Vis spectrophotometer.

3.1.4 Cytotoxicity studies

3.1.4.1 Evaluation of in vitro cytotoxicity by test on extract method

The evaluation of *in vitro* cytotoxicity of Alg-Ccm conjugate was carried out according to the ISO standards (ISO 10993-5, 2009) by using a monolayer of L-929 mouse fibroblast cells. In brief, cells were subcultured from stock culture by

trypsinization and seeded into multi well tissue culture plates. Cells were fed with MEM supplemented with FBS and incubated at 37 ºC in an atmosphere of 5% CO_2. Samples were prepared using Alg-Ccm conjugate maintained in MEM and supplemented with FBS to attain a concentration of 10 mg/mL and then two other samples of the conjugate with concentration of 5 mg/mL and 2.5 mg/mL were obtained by dilution. 100 µL of each of different concentration of conjugate samples, negative control and positive control were placed in triplicate on subconfluent monolayer of L-929 mouse fibroblast cells and the cells were incubated at 37 ± 2 ºC for 24 ± 2 h. Then cell culture was examined microscopically (Leica inverted fluorescence microscope, DMI 6000; Leica Microsystems, Wetzlr, Germany) for testing the cellular response.

3.1.4.2 Evaluation of in vitro cytotoxicity by MTT assay

Quantitative assessment of the cytotoxic potential of Alg-Ccm was carried out by MTT assay which evaluates the metabolic reduction of yellow colored MTT reagent to purple colored formazan crystals in viable cells. Conjugate samples were prepared as mentioned in section 3.1.4.1. Equal volume (100 µL) of various dilutions of test samples (2.5, 5 and 10 mg/mL, *i.e.*; equivalent to 27.25 µg, 54.5 µg and 109 µg/mL Ccm respectively) and free Ccm were placed on subconfluent monolayer of L-929 cells. After incubation of the cells for 24 ± 2 h at 37 ± 2 °C, free Ccm and conjugate sample medium were replaced with 50 µL MTT reagent (1mg/mL in serum free MEM) and cells were again incubated at 37 ± 2 ºC for 2 h. After discarding the MTT medium, 100 µL of isopropanol was added to each well and kept in an orbital shaker (Labline Instruments, Melrose Park, Illinois, USA) at 50 revolution per minute (rpm) for 20 min. Absorbance

of the resulting solutions were read at 570 nm immediately using an automated microplate reader (Bio-Tek Instruments, Winsooski, Vermont, USA). After blank (only medium) subtraction, the results were expressed as optical density. The mean value of three replicates (for each sample) is reported here.

3.2 Conjugating Curcumin to Water Soluble Polymer Stabilized Gold Nanoparticles via pH Responsive Succinate Linker

3.2.1 Materials

Hydrogentetrachloroaurate(III)trihydrate ($HAuCl_4$, $3H_2O$), sodium citrate tribasic dihydrate, citric acid (CA), Polyethylene glycol of average molecular weight 200 (PEG), L-Cysteine (L-Cys), Succinic anhydride (SA), 4-Dimethylaminopyridine (DMAP), 1,3-Dicyclohexylcarbodiimide (DCC) and Triethylamine (TEA) were purchased from Sigma-Aldrich (Bangalore, India). Curcumin (Ccm), from turmeric rhizome and 95% total curcuminoid content, was obtained from Alfa Aesar (Chennai, India). Dimethyl sulfoxide (DMSO) and ethanol (EtOH) were obtained from Merck (Mumbai, India). Hydrochloric acid (HCl) and sodium hydroxide (NaOH) were purchased from Merck (Mumbai, India). In all the experiments ultrapure water (18.2 mΩ resistivity, obtained from Milli-Q water purification system) was used.

Glioma cells (C6 cells, from rat brain tumor) were obtained from the National Centre for Cell Sciences (NCCS), Pune, India. 3-(4,5-Dimethylthiazol-2-yl)-2,5-diphenyl tetrazolium bromide (MTT reagent), fetal bovine serum (FBS), minimum essential medium (MEM), Dulbecco's Modified Eagle's Medium (DMEM)/Nutrient F-

12 Ham and Trypsin/EDTA were purchased from Sigma-Aldrich (Bangalore, India). Fluorescence isothiocyanate (FITC) was purchased from Invitrogen (Bangalore, India).

3.2.2 Synthesis of water soluble low molecular weight polymer P1 and P1 stabilized AuNPs

The water soluble, low molecular weight polymer P1 was synthesized as reported elsewhere with a little modification (Yang et al. 2009). In brief, equimolar amounts of CA and PEG were taken in a three necked round bottom flask fitted with a mechanical stirrer. Reactants were melted at 160 °C temperature with gradual addition of L-Cys (molar ratio of L-Cys: CA 0.2) under inert atmosphere. Reaction mixture was allowed to react at 160 °C for about 15 min and then the temperature was kept at 140 °C for about one hour with constant stirring. The highly viscous polymer P1 was transferred to a separate beaker in hot condition and then cooled to room temperature. P1 was purified by dialysis against water and lyophilized. P1 was stored in refrigerator in an amber colored glass bottle for further studies.

P1-AuNPs were generated from citrate-AuNPs via ligand exchange reaction. Citrate-AuNPs were prepared by Turkevich method (Turkevich et al. 1951). Briefly, to a boiling solution of $HAuCl_4$, $3H_2O$ (20 mL, 1.0 mM), 1% (w/v) aqueous solution of sodium citrate tribasic dehydrate (2 mL) was added under constant stirring. The solution showed a color change from pale yellow through bluish-black to wine red. The wine red solution was cooled and mixed with aqueous solution of P1 (1 mg/mL). The solution mixture was kept under moderate stirring at 25 °C for about 10 hours. Finally the solution was centrifuged for 20 min at 10,000 revolutions per minute (rpm) with an

ultracentrifuge (Sigma 3-30 K, Germany) and washed with water to get the P1- AuNPs. The P1- AuNPs were used for further studies.

3.2.3 Covalent conjugation of curcumin to P1-AuNPs

Ccm was conjugated to P1-AuNPs through a succinate linker following a two step synthetic approach. In the first step, the capping polymer P1 bearing free –OH groups was succinylated using excess SA (Chi et al. 2007). To a dispersion of P1-AuNPs in H_2O/DMSO (3:1 v/v) mixture containing catalytic amount of DMAP, SA was added in small portions. The solution was stirred well and pH was maintained at 9 by drop-wise addition of TEA. The reaction mixture was stirred for 16 hrs at 25 °C. Then it was centrifuged (10000 rpm, 20 min) and thoroughly washed with water to get SA-P1-AuNPs.

In the second step, Ccm was conjugated to the succinate linker available in SA-P1-AuNPs. Aqueous suspension of SA-P1-AuNPs (10 mg in 10 mL) was stirred with 200 µL DCC (4 mM, in DMSO) and 150 µL DMAP (4 mM, in DMSO) for 2 hrs at room temperature to activate the –COOH groups on NPs' surface. Upon activating –COOH groups 150 µL Ccm solution (4 mM, in DMSO) was added to it and the reaction mixture was stirred overnight at 25 ºC. The solution was then centrifuged (10000 rpm, 15 min) and washed properly (with both water/DMSO mixture and water) to remove the vestigial molecules. Finally the Ccm conjugated AuNPs (Ccm-SA-P1-AuNPs) were dispersed in ultrapure water (10 mL) and this solution was used for further studies.

3.2.4 Physicochemical characterization

Hydrodynamic diameter and zeta potential analyses at each stage of modification of AuNPs were done as explained in the physicochemical characterization section 3.1.3.5.

3.2.4.1 Fourier Transform Infrared Spectroscopy (FTIR)

FTIR spectra were recorded in the range of 4000 – 500 cm^{-1} using a Nicolet 5700 FTIR Spectrometer with a horizontal ATR accessory containing diamond Crystal (Madison, USA).

3.2.4.2 UV-Vis and Fluorescence Spectroscopy

Formation of citrate-AuNPs and its surface modifications thereafter were analyzed by recording the surface plasmon resonance (SPR) absorption of the AuNPs by UV-Vis spectroscopy (Varian model Cary Win Bio 100 spectrophotometer, Melbourne, Australia) using quartz cuvettes of 1 cm path length. Fluorescence spectrum of P1 and quenching of fluorescence of P1in P1-AuNPs were recorded using a spectrofluorometer (Carry Eclipse model EL 0507, Melbourne, Australia) in aqueous medium.

3.2.4.3 ^{1}H NMR spectroscopy

^{1}H NMR spectra was analyzed by 500 MHz spectrometer (Brucker Avance DPX 500). NMR spectra of P1 and Ccm-SA-P1-AuNPs were recorded in DMSO-D6 and D_2O with a drop of DMSO-D6 solvents respectively, at room temperature.

3.2.4.4 Gel permeation chromatography (GPC)

GPC analysis (Waters Assoc Inc.; Mailford, USA, model 600 pumps) was performed to determine number and weight average molecular weight of P1. Waters

Styragel column (HR5E/4E/2/0.5 columns in series) and THF at a flow rate of 1 mL/min were used as the stationary phase and mobile phase respectively. Polystyrene molecular weight standards were used for column calibration.

3.2.4.5 Transmission Electron Microscopy (TEM)

The morphology of the developed AuNPs at each step of functionalization was viewed by TEM images (HITACHI, H-7650, Tokyo, Japan). Samples for TEM analysis were prepared by depositing 10 μL of aqueous suspension of AuNPs on a 200 mesh copper grid with formver film and air drying it at room temperature.

3.2.4.6 Powder X-ray diffraction (XRD) analysis

The XRD patterns of pure Ccm and Ccm-SA-P1-AuNPs were recorded with an X-ray diffractometer (Bruker D8 Advance; equipped with Cu Kα radiation source) from 10° to 90° (2θ angle).

3.2.4.7 Determination of stability of Ccm-SA-P1-AuNPs

The stability of Ccm-SA-P1-AuNPs in different concentration of NaCl solutions (0.01 – 1M) and at different pH values (1.5-12) were measured by UV-Vis absorption spectroscopy. The pH of the aqueous dispersion of Ccm-SA-P1-AuNPs was adjusted by addition of 0.1 M HCl or 0.1 M NaOH solution.

3.2.4.8 Determination of Ccm content in Ccm-SA-P1-AuNPs

After synthesis and purification of Ccm-SA-P1-AuNPs by centrifugation, the NPs' pellets were fridge dried. A known amount of the dry sample was then added to a known volume of EtOH and the mixture was kept in an orbital shaker for 24 h (at 37 ºC and at 120 rpm). It was then centrifuged (14,000 rpm, 15 min) and the supernatant was

carefully collected. The collected solution was diluted with distilled water and Ccm present in the solution was quantified from a calibration plot (R^2 = 0.997) using UV-Vis spectrophotometer (at λ_{max} = 427 nm).

3.2.4.9 Study of Ccm release from Ccm-SA-P1-AuNPs

The release of Ccm from Ccm-SA-P1-AuNPs was determined by dialysis bag method in aqueous buffer solutions of two different pH (pH 7.4 and 5.3) at 37 °C. Prior to the study, the dialysis membrane (MWCO 500) was soaked in water for 1h. Then Ccm-SA-P1-AuNPs was placed in the dialysis bag with two end fixed by clamps and the dialysis bag was suspended in 10 mL of release medium (of pH = 5.3). The bag was incubated at 37 °C, 120 rpm in a glass vessel. Release medium was removed periodically and an equal volume of fresh buffer solution (pH = 5.3) was added to the glass vessel. The sample removed was diluted with ethanol and analyzed using UV-Vis absorption spectroscopic technique. Similar experiment was carried out with buffer solution of pH = 7.4 to evaluate the release behavior of the nano-carrier under physiological condition.

3.2.5 Evaluation of cytotoxicity

The cytotoxic potential of Ccm-SA-P1-AuNPs was quantified by MTT assay against C6 Glioma cells. In brief, C6 cells were maintained in 50:50 mixture of DMEM/Nutrient F-12 Ham and MEM supplemented with 10% FBS. Then 80% confluent cells were trypsinized and seeded in 48 well plates (5 x10^4 cells) and incubated for 24 h. Then the cells were exposed to fresh medium containing different concentrations of Ccm-SA-P1-AuNPs and free curcumin in a CO_2 (5%) incubator at 37

°C. After 24 h incubation, the medium containing sample and free drug was removed from respective wells and 200 µL of freshly prepared MTT reagent (0.5 mg/mL) in culture medium was added into each well. After 4 h incubation, MTT reagent was carefully removed. DMSO (200 µL) was then added into each well and the plate was gently shaken for 10 min at room temperature to dissolve all precipitates formed. The absorbance of individual wells at 570 nm was then detected by a microplate reader (Tecan Infinite M200, Switzerland). Cell viability was expressed as the mean percentage of sample absorbance relative to untreated cells (control) as shown in the equation below (where A_s is the absorbance of sample and A_c is the absorbance of control). Here each reported value is the mean of three replicates.

$$\text{Cell Viability (\%)} = \frac{A_s}{A_c} \text{ x } 100$$

3.2.6 Cellular uptake study

Cellular images were acquired with a fluorescence microscope (Leica DM IRB, Germany) using C6 cell line. Cells were seeded on a 4-well plate and incubated at 37 °C for 24 h. Then the cells were exposed to FITC tagged Ccm-SA-P1-AuNPs for 3 h. After that, the medium containing the nanoparticles was removed from each well and the cells were washed with PBS (twice) to remove any non-specific binding. After fixing the cell, uptake was detected in fluorescence microscope exploiting the fluorescence emission of FITC.

3.3 Fabrication of Curcumin and Methotrexate Conjugated Biopolymer Stabilized Gold Nanoparticles Based Drug Delivery Vehicles via Green Synthetic Route: Evaluation of Cytotoxicity and Hemolytic Toxicity

3.3.1 Materials

Hydrogentetrachloroaurate(III)trihydrate ($HAuCl_4.\ 3H_2O$), 1,3-dicyclohexyl carbodiimide (DCC), 4-dimethylaminopyridine (DMAP), N-(3-dimethylaminopropyl)-N-ethylcarbodiimide hydrochloride (EDC), N-hydroxysuccinimide (NHS), Bis (aminopropyl) terminated Polyethyleneglycol (PEG), Methotrexate hydrate (MTX) were purchased from Sigma-Aldrich (Bangalore, India). Curcumin (95% total curcuminoid content) from turmeric rhizome was obtained from Alfa Aesar (Bangalore, India). Sodium alginate was purchased from SD fine chemicals (Mumbai, India). Dimethyl sulfoxide (DMSO) and ethanol (EtOH) were obtained from Merck (Mumbai, India). Ultra pure water (18.2 mΩ resistivity) was obtained from a Mili-Q water purification system. Deionized water was used all through the reaction and purification steps in this study.

C6 Glioma cells and MCF-7 (human breast cancer cells) cell lines were obtained from the National Centre for Cell Sciences (NCCS), Pune, India. 3-(4,5-Dimethyl thiazol-2-yl)-2,5-diphenyl tetrazolium bromide (MTT reagent), fetal bovine serum (FBS), minimum essential medium (MEM), Dulbecco's Modified Eagle's Medium (DMEM)/Nutrient F-12 Ham and Trypsin/EDTA were purchased from Sigma-Aldrich (Bangalore, India). RPMI 1640 medium, Hoechst 33342 and Fluorescence isothiocyanate (FITC) were purchased from Invitrogen (Bangalore, India).

3.3.2 Synthesis of Alg-Ccm Conjugate and generation of Alg-Ccm AuNPs

The Alg-Ccm conjugate was prepared according to our previous report (Dey and Sreenivasan 2014). In brief, hydrophobic drug curcumin was covalently conjugated to the C-6 carboxylate functional group of biopolymer Alg via esterification reaction using DCC/DMAP in H_2O-DMSO medium. The conjugate was purified by dialysis (using a dialysis membrane of MWCO 3500) against DMSO for one day and against H_2O for three days to remove any unreacted molecules. Alg-Ccm conjugate was lyophilized and stored in the refrigerator for further study.

AuNPs were generated and stabilized by the Alg-Ccm conjugate in aqueous medium under thermal activation. An aqueous solution of $HAuCl_4$, $3H_2O$ (1 mM) was slowly added to the aqueous solution of Alg-Ccm conjugate (0.41 mg/mL) to maintain a final concentration of 10^{-2} mM of chloroauric acid in the solution. After proper mixing, the solution was heated gently in a water bath and the generation of AuNPs was indicated by a color change of the solution from yellow to pinkish red. The AuNPs solution was cooled to room temperature and dialyzed against deionized water (using a dialysis membrane of MWCO 3500) for 1 day. Finally the solution was lyophilized and stored in refrigerator.

3.3.3 Synthesis of MTX conjugated Alg-Ccm AuNPs (MP@Alg-Ccm AuNPs)

In order to develop MTX conjugated Alg-Ccm AuNPs, at first MTX was conjugated to Bis (aminopropyl) terminated PEG to generate MTX-bis(aminopropyl) teminated PEG conjugate (MP conjugate). To synthesize MP conjugate, MTX was dissolved in PBS (pH = 7.4) and was activated using EDC and NHS (MTX: EDC: NHS

= 1:1.3:1.1 molar ratio) at room temperature for one hour under N_2 (g) blanket in dark. Then solution of bis (aminopropyl) terminated PEG (MTX: bis (aminopropyl terminated PEG = 1:1 molar ratio) in PBS (pH = 7.4) was gradually added to the activated MTX solution and the mixture was allowed to stir at room temperature for around four hours in dark. MP conjugate was purified by dialysis (using dialysis membrane of MWCO 1000) against PBS (pH = 7.4) for one day and against distilled H_2O for one day. Purified MP conjugate was lyophilized and stored for further study.

In the second step, MP conjugate was conjugated to the Alg-Ccm AuNPs utilizing the EDC chemistry. The free carboxyl functionality on Alg-Ccm AuNPs (15 mg) was activated with EDC/NHS (in aqueous carbonate/bicarbonate buffer medium of pH = 8.2) for one hour at 25 °C followed by the addition of aqueous solution of MP conjugate (25 mg) and the reaction mixture was moderately stirred overnight at 25 °C. The reaction mixture was purified by dialysis (MWCO 3500) and lyophilized to obtain MP@Alg-Ccm AuNPs.

3.3.4 Physicochemical Characterization

Determination of hydrodynamic diameter, zeta potential measurement and TEM analysis were done as depicted in the physicochemical characterization section 3.1.3.5 and 3.1.3.6 respectively. Formation of Alg-Ccm AuNPs, MP conjugate and MP@Alg-Ccm AuNPs was confirmed by FTIR spectroscopic analysis as mentioned in 3.2.4.1. The XRD patterns of Alg-Ccm conjugate and Alg-Ccm AuNPs were determined as depicted in physicochemical characterization section 3.2.4.6.

3.3.4.1 UV-Vis Spectroscopy

The generation and stabilization of AuNPs using Alg-Ccm conjugate and its functionalization with MP conjugate to yield MP@Alg-Ccm AuNPs were characterized by recording SPR absorption spectra of respective AuNPs using UV-Vis spectrophotometer (Carry model 100 bio UV-Vis spectrophotometer, Melbourne, Australia). Formation of MP conjugate was also confirmed by comparing the UV-Vis absorption spectra of bis(aminopropyl) terminated PEG and MP conjugate using the same instrument.

3.3.4.2 ^{1}H NMR Spectroscopy

^{1}H NMR spectra of Alg-Ccm AuNPs and MP@Alg-Ccm AuNPs were analyzed by 500 MHz spectrometer (Brucker Avance DPX 500) using D_2O as the solvent.

3.3.4.3 Determination of drug content in MP@Alg-Ccm AuNPs

Total MTX content in MP@Alg-Ccm AuNPs was determined by UV-Vis spectroscopy (at λ_{max} = 369 nm) in PBS (pH = 7.4). In order to determine the total Ccm content in MP@Alg-Ccm AuNPs, a known amount of fridge-dried sample was dispersed in EtOH and incubated for 24 h (at 37 °C and 120 rpm). After that the dispersion was centrifuged (at 14,000 rpm for 15 min) and the supernatant was collected. Using this supernatant solution, total Ccm content was determined by UV-Vis spectroscopy (at λ_{max} = 428 nm).

3.3.5 Evaluation of Cytotoxicity

The quantitative cytotoxic potential of MP@Alg-Ccm AuNPs was determined using two cancer cell lines: (i) C6 cancer cell and (ii) MCF-7 cancer cells. C6 cells were

maintained in 50:50 mixture of DMEM/Nutrient F-12 Ham and MEM supplemented with 10 % FBS. Then 80 % confluent cells were trypsinized and seeded in 96 well plates ($1x10^3$ cells/well) and incubated for 24 h. Then the cells were exposed to a series of doses of MP@Alg-Ccm AuNPs, free MTX and free Ccm in a CO_2 (5 %) incubator at 37 °C. After 24 h incubation, the medium containing sample and free drug was removed from respective wells and 200 µL of freshly prepared MTT reagent (0.5 mg/mL) in culture medium was added into each well. After 4 h incubation, MTT reagent was carefully removed. DMSO (200 µL) was then added into each well and the plate was gently shaken for 10 min at room temperature to dissolve all precipitates formed. The absorbance of individual wells at 570 nm was recorded by a microplate reader (Tecan Infinite M200, Switzerland). Cell viability was expressed as the mean percentage of sample absorbance relative to untreated cells (control) as shown in the equation below (where A_s is the absorbance of sample and A_c is the absorbance of control). Here each reported value is the mean of three replicates.

$$\text{Cell Viability (\%)} = \frac{A_s}{A_c} \text{ x } 100$$

MCF-7 cells were maintained in RPMI Medium (containing 10 % FBS). Then 80 % confluent cells were trypsinized and seeded in 96 well plates ($1x10^3$ cells/well) and incubated for 24 h. The cells were exposed to a series of doses of MP@Alg-Ccm AuNPs, free MTX and free Ccm to estimate the cell viability by adopting the similar procedure as described for C6 cell lines.

3.3.6 Cellular uptake study

Cellular images were acquired with a fluorescence microscope (Leica DM IRB, Germany) using C6 and MCF-7 cell lines. Cells were seeded and incubated on a 4-well plate at 37 °C for 24 h. Then both C6 and MCF-7 cells were exposed to FITC tagged MP@Alg-Ccm AuNPs. After incubation for two and a half hours, Hoechst 33342 solution (10 μM and 15 μL) was added to each well for staining the nucleus. Then, after 30 min of incubation, the medium containing AuNPs and Hoechst was removed from each well and the cells were washed with PBS (twice) to remove any non-specific binding. After fixing the cells, uptake was detected in fluorescence microscope.

In order to confirm the targeting efficiency of MTX, FITC was tagged at the same density on MP@Alg-Ccm AuNPs and Alg-Ccm AuNPs and MCF-7 cells were treated with same concentration of FITC labeled MP@Alg-Ccm AuNPs and FITC labeled Alg-Ccm AuNPs. The cellular uptake in each case was studied following the same procedure as mentioned above.

3.3.7 Evaluation of hemolysis

The hemolytic potential of MP@Alg-Ccm AuNPs was determined by evaluating the percentage of hemolysis. Blood was drawn from a healthy unmedicated human donor and collected in anticoagulant ACD. MP@Alg-Ccm AuNPs was placed in polystyrene culture plates and agitated with PBS before they are exposed to blood. To each plate 10 mL blood was added (to maintain sample concentration of 0.5 mg/mL). 5 mL blood was immediately taken for initial analysis and remaining 5 mL blood (with sample) was incubated for 30 min under agitation at 70 ± 5 rpm using Environ shaker

thermo stated at 35 ± 2 °C. The total hemoglobin (Hb) in the initial blood sample was measured using automatic hematology analyzer (Sysmex-K4500). The free Hb liberated into the plasma after exposure to the samples was estimated in each sample by measuring absorbance of diluted plasma with diode array spectrophotometer (HP 8453, Hewlett-Packard GmbH/Germany). Percentage of hemolysis was calculated from the following formula and the reported value is the mean of three replicates.

$$\% \text{ Hemolysis} = \frac{\text{Free Hb}}{\text{Total Hb}} \text{ x } 100$$

3.4 Synthesis and Characterization of Glutathione Containing Fluorescent Polymer and Its Curcumin Conjugate for Safer Curcumin Delivery and Label-Free Cellular Imaging

3.4.1 Materials

L-Glutathione (reduced; GSH), poly(ethylene glycol) (PEG; Mw = 1000), anhydrous citric acid (CA), 1,3-dicyclohexyl carbodiimide (DCC), 4-Dimethylaminopyridine (DMAP) and Nile Red (NR) dye were purchased from Sigma-Aldrich, Bangalore, India. Curcumin (Ccm; 95% total curcuminoid content) from rhizome of turmeric was obtained from Alfa Aesar. Dimethyl sulfoxide (DMSO) and Ethanol (EtOH) were obtained from Merck, Mumbai, India. Deionized water was used during all the reaction and purification process and ultra pure water (18.2 mΩ resistivity) was obtained from the Milli-Q water purification system.

Glioma cells were obtained from the National Centre for Cell Sciences (NCCS), Pune, India. 3-(4,5-Dimethylthiazol-2-yl)-2,5-diphenyl tetrazolium bromide (MTT

reagent), fetal bovine serum (FBS), minimum essential medium (MEM), Dulbecco's Modified Eagle's Medium (DMEM)/Nutrient F-12 Ham and Trypsin/EDTA were purchased from Sigma-Aldrich (Bangalore, India).

3.4.2 Synthesis of GSH containing fluorescent biodegradable polymer (GSHBP)

In order to obtain GSHBP, in a three neck round bottom flask PEG and CA (1:1 by no. of mole) were allowed to react under N_2 (g) blanket at 160 °C with gradual addition of GSH (molar ratio GSH: CA = 0.5). The reactants were melted at 160 °C with constant stirring and kept at that temperature for about 20 min. Then the temperature was brought down to 135 °C and the reaction was continued for nearly 2 h. The highly viscous polymer was collected from reaction vessel in hot condition and it was purified after cooling by dialysis against deionized water (using dialysis membrane of molecular weight cut off MWCO 1000). Finally, the product was lyophilized and refrigerated in amber colored glass bottle for future use.

3.4.3 Synthesis of GSHBP-Curucmin conjugate (GSHBP-Ccm)

GSHBP (500 mg) was dissolved in 10 mL DMSO and the free carboxylate groups in GSHBP were activated using DCC in presence of catalytic amount of DMAP by stirring the mixture at room temperature for 1h. Then Ccm (4.07 mM in DMSO) was added to it and the reaction mixture was stirred at 65 ºC temperature under N_2 for 8 hours. The reaction mixture was cooled to room temperature and purified by dialysis against DMSO for 1 day followed by distilled H_2O for 2 days using a dialysis membrane of MWCO 1000. Finally the dialyzed intense yellow colored product was lyophilized and stored in refrigerator in an amber colored glass bottle for further use.

3.4.4 Physicochemical Characterizations

FTIR, UV-Vis absorption and fluorescence emission spectra of GSHBP and GSHBP-Ccm conjugate were obtained as depicted in physicochemical characterization sections 3.2.4.1 and 3.1.3.2 respectively. Determination of hydrodynamic diameter and zeta potential of GSHBP-Ccm conjugate micelles was done as explained in physicochemical characterization section 3.1.3.5.

3.4.4.1 Nuclear Magnetic Resonance Spectroscopy (^{1}H and $^{13}CNMR$)

Both ^{1}H and ^{13}C NMR spectra were analyzed by 500 MHz spectrometer (Brucker Avance DPX 500) in DMSO-D6 solvent at room temperature.

3.4.4.2 Gel permeation chromatography (GPC) and Liquid chromatography (LC)

Molecular weight of the polymer and its degradation behavior was determined using GPC and LC (Waters Assoc Inc.; Mailford, USA, model 600 pumps). For GPC analysis, Styragel column and THF were used as stationary phase and mobile phase respectively. Refractive index (RI) detector was used to generate the GPC traces. Whereas, in LC analysis C18 Reprobond column was used as the stationary phase and 0.1 % H_3PO_4 aqueous solution was employed as the mobile phase. UV detector was used in LC analysis (using $\lambda = 214$ nm for citric acid).

3.4.4.3 Estimation of fluorescence quantum yield of GSHBP

Fluorescence quantum yield (Q.Y.) of GSHBP was determined by William's method (Williams and Winfield 1983) using anthracene as the reference compound. An aqueous solution of GSHBP polymer was prepared to determine the excitation

wavelength at which the polymer gives highest intensity of fluorescence emission and then the absorbance of the solution at that optimal excitation wavelength was measured. From this solution, six solutions were prepared (by dilution with gradient concentration) such that the absorbance of each of the six solutions lies in the range of 0.01 – 0.1. Fluorescence emission spectra for the set of solutions were recorded (keeping both the emission and excitation slit width as 5 nm) and the integrated fluorescence intensity (area under the curve) for each solution was calculated. Finally, the integrated fluorescence intensity against absorbance was plotted for all the six solutions with different concentrations. Similar plot was also done for the reference compound and the fluorescence Q.Y. was calculated based on the following equation.

$$\phi_s = \phi_r . \frac{Slpoe_s}{Slope_r} . (n_s/n_r)^2$$

Where, Φ = Q.Y., Slope = slope of integrated fluorescence intensity Vs absorbance plot, n = refractive index of the solvent used, s = sample r = reference. Here we used ethanolic solution of anthracene as the reference (Φ_r = 0.27) (Yang et al. 2009).

3.4.4.4 Determination of critical micelle concentration for GSHBP-Ccm conjugate

The CMC value of GSHBP-Ccm conjugate micelles was determined using NR dye as the fluorescence probe (Chen et al. 2011). A stock solution of NR dye (2.5 x 10^{-6} M) was prepared in acetone. Aqueous solutions of GSHBP-Ccm conjugate (with concentration ranging from 3 μg/mL to 1000 μg/mL) were prepared. To each of the 5 mL solution of GSHBP-Ccm of different concentrations, 25 μL of NR solution was added and kept in dark under constant shaking for 1h at room temperature. Each solution

was excited at 540 nm (excitation and emission slit widths as 5 nm) and fluorescence emission spectrum was recorded at room temperature from 580 nm to 750 nm.

3.4.4.5 Transmission Electron Microscopy (TEM)

Morphology of the nano-sized micelles in aqueous dispersion was visualized by recording the TEM images (TEM; JEM-2100, JEOL, Japan) under cryogenic condition.

3.4.4.6 Determination of Ccm content and release of Ccm under physiological condition

In order to determine the total Ccm content in GSHBP-Ccm conjugate, a known amount of GSHBP-Ccm was dissolved in water/ethanol mixture and the amount of Ccm was obtained from the calibration plot (λ_{max} = 428 nm; R^2 = 0.995).

Release of Ccm from GSHBP-Ccm conjugate was determined by dialysis bag method in phosphate buffer solution (PBS of pH 7.4) at 37 °C. Prior to the study, the dialysis membrane (MWCO 1000) was soaked in water for 2h. GSHBP-Ccm conjugate (10 mg) was placed in the dialysis bag with two end fixed by clamps and the dialysis bag was suspended in 10 mL of release medium (PBS of pH = 7.4). The bag was incubated at 37 °C, 120 rpm in a glass vessel. Release medium was removed periodically and an equal volume of fresh PBS (pH = 7.4) was added to the glass vessel. Amount of released Ccm in the medium was then analyzed by UV-Vis spectroscopy.

3.4.5 Cytotoxicity evaluation for GSHBP and GSHBP-Ccm conjugate

The cytotoxic potential of GSHBP and GSHBP-Ccm conjugate was assessed by MTT assay against C6 cells. In brief, C6 cells were maintained in 50:50 mixture of DMEM/Nutrient F-12 Ham and MEM supplemented with 10% FBS. Then 80% confluent cells were trypsinized and seeded in 48 well plates (5 x10^4 cells/well) and

incubated for 24 h. Then the cells were exposed to a series of doses of GSHBP, GSHBP-Ccm conjugate and free Ccm in a CO_2 (5%) incubator at 37 °C. After 24 h incubation, the medium containing sample and free drug was removed from respective wells and 200 μL of freshly prepared MTT solution (0.5 mg/mL) in culture medium was added into each well. After 4 h incubation, MTT solution was carefully removed. DMSO (200 μL) was then added into each well and the plate was gently shaken for 10 min at room temperature to dissolve all precipitates formed. The absorbance of individual wells at 570 nm was then detected by a microplate reader (Tecan Infinite M200, Switzerland). Cell viability was expressed as the mean percentage of sample absorbance relative to untreated cells. Here each reported value is the mean of three replicates.

3.4.6 Cellular imaging using fluorescent GSHBP-Ccm conjugate micelles

Cellular images were acquired with a fluorescence microscope (Leica DM IRB, Germany) using C6 cell line. Cells were seeded on a 4-well plate and incubated at 37 °C for 24 h. Then the cells were exposed to GSHBP-Ccm micelles for 4 h, the medium containing GSHBP-Ccm was removed from each well and the cells were washed with PBS (twice) to remove any non-specific binding. After fixing the cell, uptake was detected in fluorescence microscope exploiting the self-fluorescence of polymer as well as the fluorescence emission of Ccm.

3.4.7 Evaluation of percentage of hemolysis

In order to know whether the polymer or its Ccm conjugate can exhibit hemolytic toxicity, % hemolysis study of GSHBP and GSHBP-Ccm conjugate was evaluated. Blood was drawn from a healthy unmedicated human donor and collected in

anticoagulant ACD. GSHBP was placed in polystyrene culture plates and agitated with PBS before they are exposed to blood. To each plate, 10 mL blood was added (to maintain a concentration of 6.4 mg/mL of the polymeric sample). From this 5 mL blood sample was collected immediately for analysis. Rest 5 mL of the blood (with sample) was incubated for 30 min under agitation at 70 ± 5 rpm using environ shaker thermostated at 35 ± 2 °C. The total hemoglobin (Hb) in the initial blood sample was measured using automatic hematology analyzer (Sysmex-K4500). The free Hb liberated into the plasma after exposure to the samples was estimated in each sample by measuring absorbance of diluted plasma with diode array spectrophotometer (HP 8453, Hewlett-Packard GmbH/Germany). Percentage of hemolysis was calculated from the following formula and the reported value is the mean of three replicates.

$$\% \text{ Hemolysis} = \frac{\text{Free Hb}}{\text{Total Hb}} \text{ x } 100$$

Similar procedure was followed for the percent hemolysis study of GSHBP-Ccm (for the final concentration of 6.4 mg/mL for the sample).

CHAPTER 4

RESULTS

4 Results

4.1 Development of Alginate-Curcumin Conjugate for Enhanced Aqueous Solubility and Stability of Hydrophobic Drug Curcumin

4.1.1 Synthesis and physicochemical characterization of Alg-Ccm conjugate

In order to obtain a potential Ccm conjugate for therapeutic applications with improved aqueous solubility and stability of the drug, Alg-Ccm conjugate was synthesized. To synthesize Alg-Ccm, extremely hydrophilic polymer alginate was first finely dispersed in water/DMSO (1:1 v/v) mixture and then phenolic –OH group of Ccm was conjugated to the activated C-6 carboxylate functionality of alginate via esterification using DCC/DMAP as shown in Scheme 1. Dialysis and lyophilization resulted in solid, yellow colored Alg-Ccm conjugate.

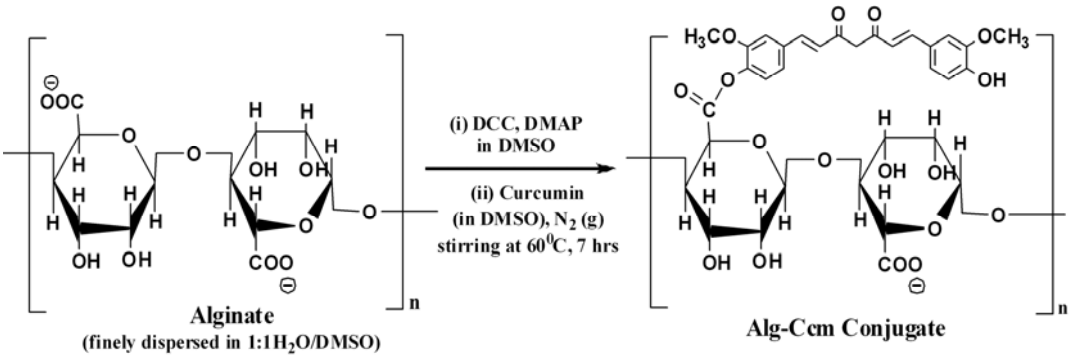

Scheme 1: Schematic view of the synthetic strategy of Alg-Ccm conjugate.

The formation of Alg-Ccm conjugate was verified by FTIR spectra shown in Figure 7. Figure 7A shows the FTIR spectrum of sodium alginate in which a broad band around 3421 cm^{-1} was assigned to the O-H stretching, peak around 2925 cm^{-1} was due to aliphatic C-H stretching and the sharp peak at 1608 cm^{-1} was assigned to the carboxylate

C-O stretching. Figure 7B depicts the FTIR spectrum of the conjugate in which the O-H stretching appears at 3441 cm^{-1} and the peak is relatively sharper as the conjugate contains phenolic O-H moieties from Ccm. The peak at 1617 cm^{-1} was assigned to the stretching vibration of C=O (enol) functionality of Ccm in Alg-Ccm. The peaks seen around 1658 cm^{-1} and 1217 cm^{-1} were attributed to the C=O and C-O stretching frequencies of ester linkage respectively. The aliphatic C-H stretches in Alg-Ccm were also nicely manifested through the peaks at 2928 cm^{-1} and 2847 cm^{-1}.

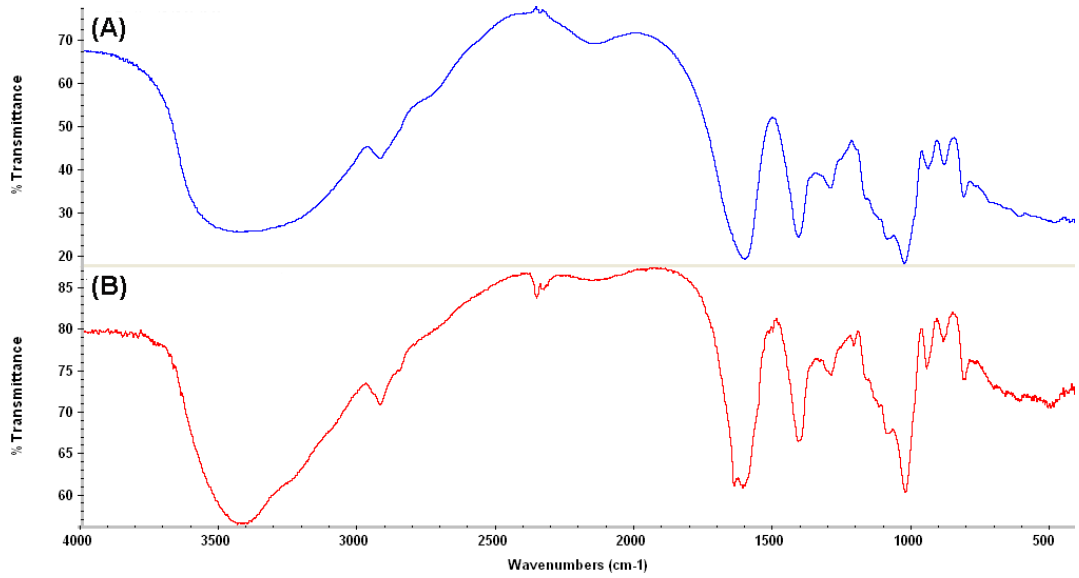

Figure 7: FTIR spectra of (A) Sodium alginate and (B) Alg-Ccm conjugate.

In order to further confirm the formation of Alg-Ccm, ^{1}H NMR spectra of the conjugate was recorded. The ^{1}H NMR spectrum of alginate is illustrated as the *inset* picture in Figure 8 in which the signals between 3.5 to 5 ppm are due to the methine protons of hexuronic acid residues of alginate (Yang et al. 2007) (Li et al. 2011). Figure 8 depicts the ^{1}H NMR spectrum of the conjugate in which the additional peaks from 6.7

to 7.9 ppm (due to aromatic protons in Ccm) clearly indicated the conjugation of curcumin to alginate backbone. However, the characteristic signal at 3.81 ppm assigned for methoxy proton of curcumin might have merged with the peak of C-5 methine proton of mannuronic acid (M) unit of alginate in the conjugate.

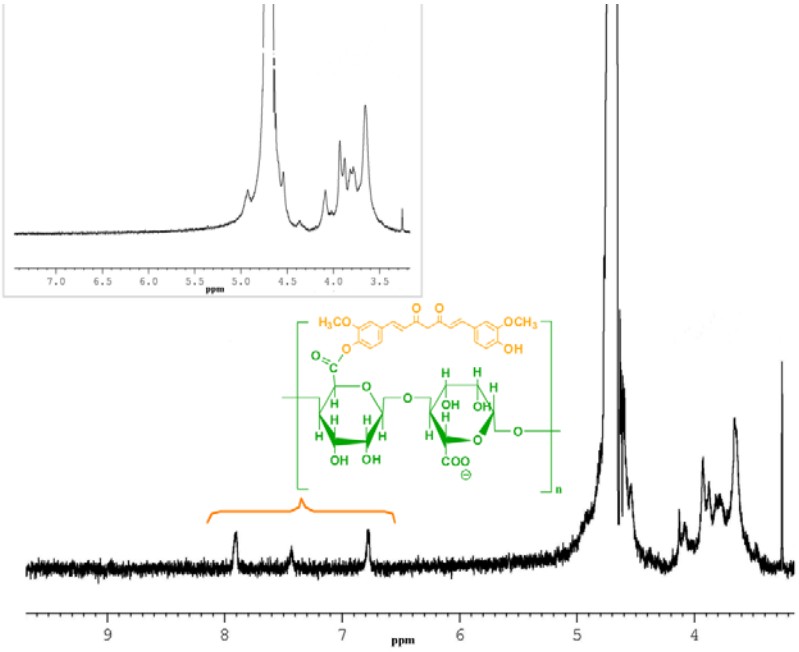

Figure 8: ^{1}H NMR spectrum of Alg-Ccm conjugate (*inset:* ^{1}H NMR spectrum of Alg).

The characteristic UV-Vis absorption spectrum of Alg-Ccm conjugate is shown in Figure 9A. The absorption maximum of Ccm was red-shifted to 427 nm in the conjugate. Figure 9B shows the fluorescence emission spectra of Alg-Ccm in water/EtOH medium in comparison with that of pure curcumin. A hypsochromic shift by ~11 nm in the emission spectrum of Alg-Ccm compared to pure Ccm was observed.

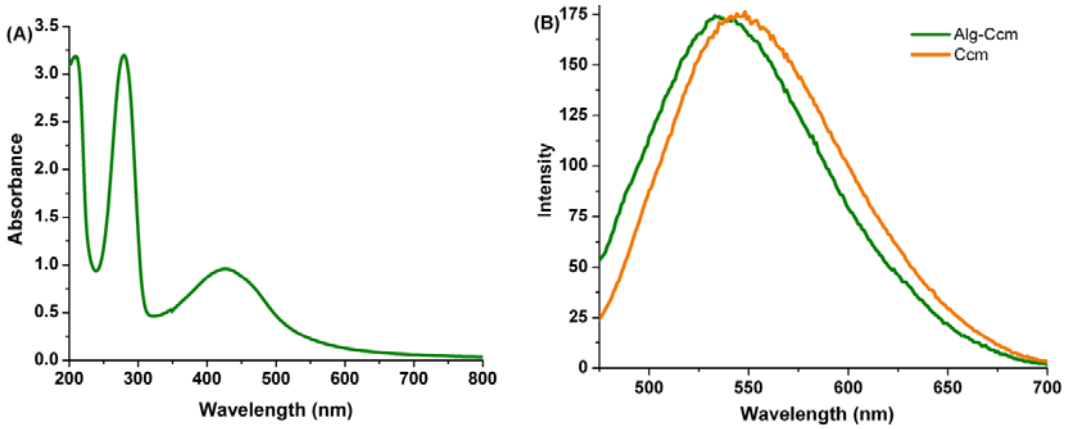

Figure 9: (A) UV-Vis absorption spectrum of Alg-Ccm conjugate and (B) fluorescence emission spectra of Alg-Ccm conjugate compared to free Ccm (λ_{ex} = 427 nm).

To scrutinize the possibility of self-assembly of Alg-Ccm conjugate, the aqueous solution of the conjugate was analyzed by DLS which indicated the formation of nano-sized micelle like structures with an average hydrodynamic diameter of 459 ± 0.32 nm as shown in Figure 10A. It was further confirmed by the TEM images of the conjugate shown in Figure 10B and 10C. The TEM images depicted spherical particles with an average diameter of 62.5 ± 11 nm. The zeta potential of Alg-Ccm micelles was found to be – 45.43 ± 0.2 mV (at 25 °C and pH 7.4).

The self-assembly behavior of Alg-Ccm conjugate in aqueous medium was characterized by determining the CMC of the conjugate using 1-PyCHO as the probe molecule. Figure 11A shows the absorption spectra of 1-PyCHO in water with increasing concentration of Alg-Ccm conjugate. CMC value of Alg-Ccm was determined by plotting the absorbance ratio (A/A_0) (at 368 nm) against – log [conjugate] as shown in Figure 11B. A and A_0 represent the absorbances of 1-PyCHO in presence and absence of Alg-Ccm. The break point in the curve indicated the

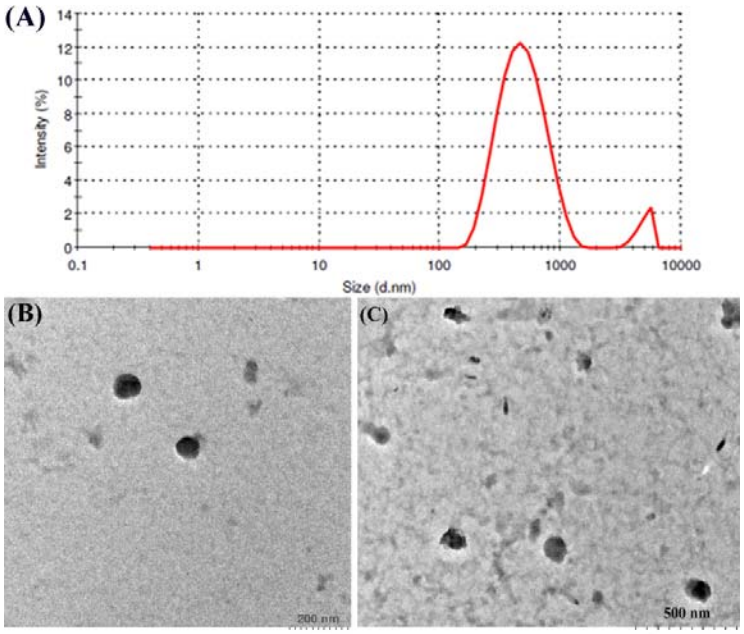

Figure 10: (A) Particle size distribution plot of Alg-Ccm in aqueous solution and (B) and (C) TEM images of Alg-Ccm conjugate micelles at two different magnifications.

CMC value of Alg-Ccm (Figure 11B) and the CMC values are tabulated in Table 1. In order to confirm the CMC value obtained by the UV-Vis spectroscopic method, CMC of Alg-Ccm conjugate was also determined by fluorescence spectroscopic technique using 1-PyCHO as the fluorescent probe. On exciting the probe at 368 nm, it showed an emission spectrum with λ_{max} at 474 nm and Figure 11C illustrates the relative lowering of fluorescence intensity of 1-PyCHO at 474 nm with increasing concentration of Alg-Ccm conjugate. Fluorescence intensities in presence of conjugate (F) at 474 nm relative to the intensities in absence of conjugate (F_0) were plotted against – log [conjugate] as depicted in Figure 11D and the break point indicated the CMC value of Alg-Ccm (see Table 1). The CMCs obtained by absorption and emission studies (Table 1) were in good agreement with each other.

Table 1: CMC values of Alg-Ccm determined by different methods

Sample Name	CMC (mg/mL) by absorption spectroscopy	CMC (mg/mL) by emission spectroscopy
Alg-Ccm	**0.21**	**0.25**

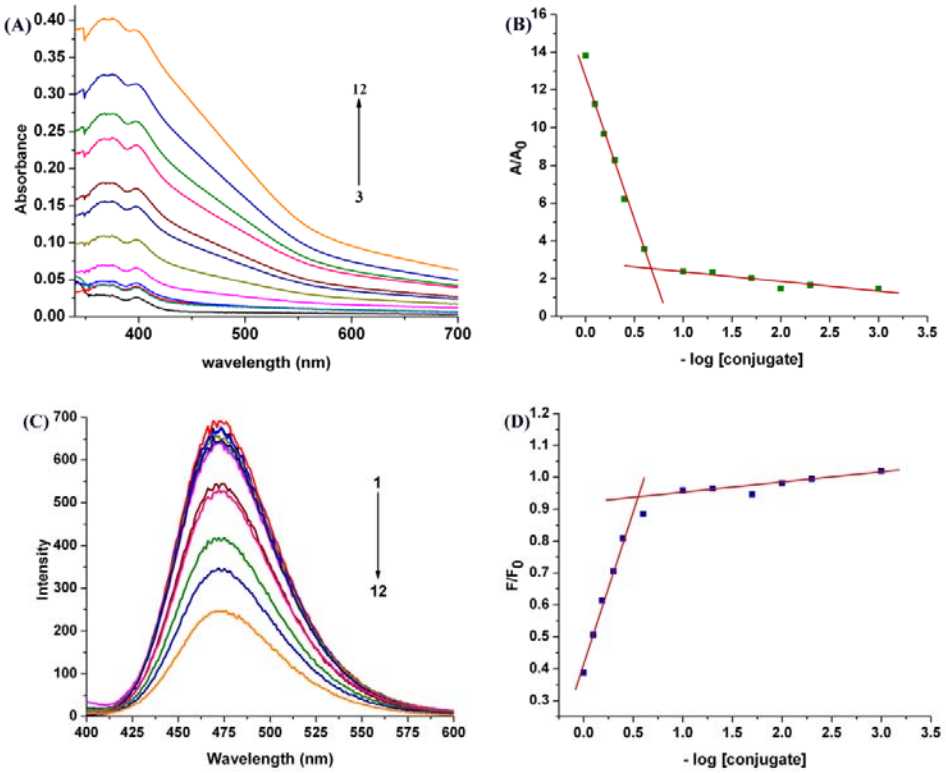

Figure 11: Spectral data for the CMC determination of Alg-Ccm conjugate: (A) absorbance spectra of 1-PyCHO in water with increasing concentration of Alg-Ccm conjugate (B) plot of A/A_0 Vs – log [conjugate]; (C) emission spectra of 1-PyCHO in water with increasing concentration of Alg-Ccm conjugate (D) plot of F/F_0 Vs – log [conjugate].

The Alg-Ccm conjugate exhibited an intense yellow color with an average Ccm content of 1.09 ± 0.053 mg in 100 mg of the conjugate. Alg-Ccm conjugate dissolved readily in water and aqueous buffer solution (pH = 7.4). The aqueous solubility of Alg-

Ccm conjugate was found to be more than 10 mg/mL, which corresponds to 109 µg/mL of Ccm. Free Ccm in fact, exhibits an extremely low aqueous solubility but its aqueous solubility was improved after conjugation with highly hydrophilic polymer alginate and the images shown in Figure 12A support this fact. Ccm undergoes rapid hydrolysis into smaller fragments that contribute negligibly towards the absorption of light (Agarwal, & Shishodia, 2006). Hence a decrease in the absorbance intensity can indicate the proportional decrease in concentration of Ccm in solution. Here to study the stability of Ccm in conjugated state, solutions of free Ccm and Alg-Ccm in PBS (pH 7.4) was incubated for 6 hrs at 37° C and estimated absorbances of each solution at 1 h intervals. It was observed that free Ccm degraded rapidly where as Ccm in Alg-Ccm conjugate was highly stable (as shown in Figure 12B).

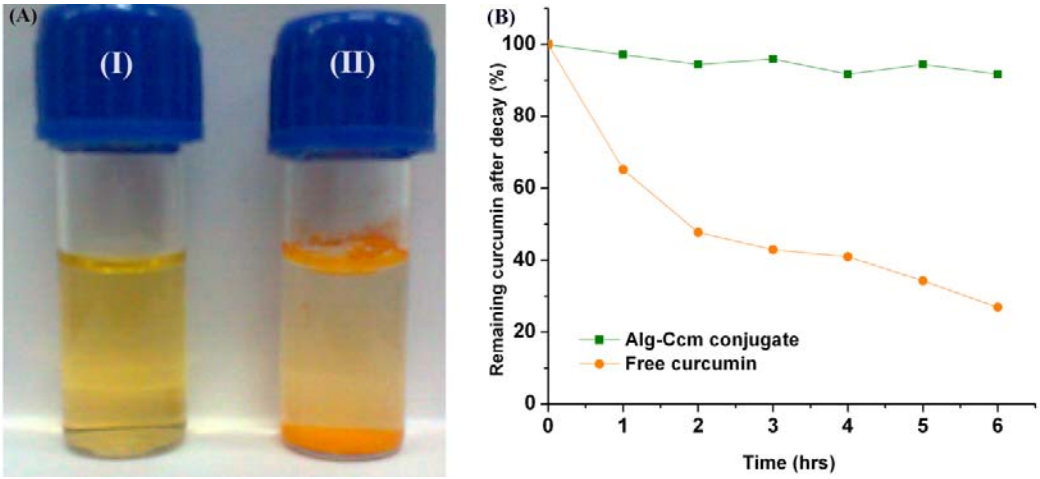

Figure 12: (A) Images of solutions of (I) Alg-Ccm conjugate and (II) free curcumin in PBS at pH 7.4, the conjugate gives a clear yellow solution but free curcumin forms flakes indicating poor solubility; and (B) Plot showing degradation of free curcumin and Alg-Ccm conjugate in PBS at pH 7.4.

4.1.2 Evaluation of cytotoxic potential of Alg-Ccm conjugate

In order to confirm whether conjugation of curcumin to a hydrophilic polymer can exert any effect on the intrinsic potential of curcumin to kill cells, the cytototoxicity of Alg-Ccm was qualitatively evaluated with L-929 mouse fibroblast cells. Figure 13 shows the morphological changes in L-929 cells after exposing the cells with different concentrations of Alg-Ccm. Figure 13A and 13B showed almost complete destruction of the original spindle shape morphology of the cell layers indicating toxicity of the conjugate towards L-929 cells. Figure 13C indicated moderate cytotoxic reactivity (due to lower concentration of Ccm) towards the cells.

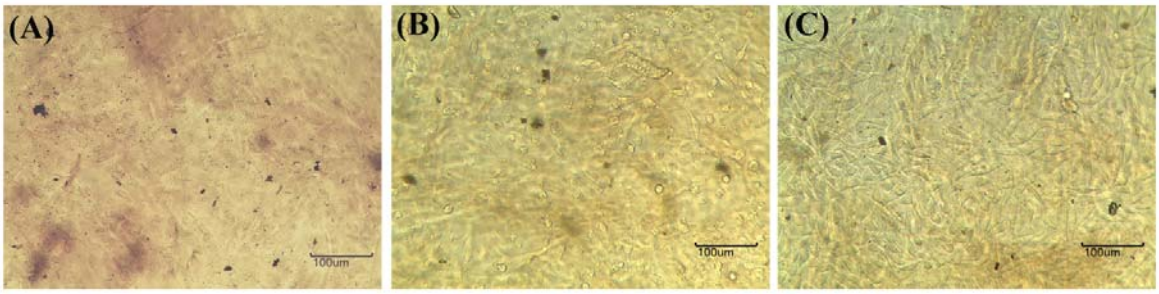

Figure 13: Microscopic images showing the morphology of L-929 cells after contact with different concentrations of Alg-Ccm conjugate solution corresponding to curcumin equivalent of (A) 10.9 µg, (B) 5.4 µg and (C) 2.7 µg.

Besides, the cytotoxicity of the conjugate was quantitatively assessed using MTT assay against L-929 cells. The percentage of cell viability quantified from MTT assay is shown in Figure 14. The MTT assay revealed that the different dilution of Alg-Ccm solutions corresponding to Ccm equivalent of 10.9 µg, 5.4 µg and 2.7 µg killed nearly 85%, 62% and 44% of the cells respectively. The result represented (Figure 14A) a

concentration dependent decrease in cell viability. The percentage of viable cells increased as there was a decrease in the concentration of equivalent Ccm. The comparison of cytotoxic effect of conjugated Ccm with free Ccm (maximum amount of free Ccm *i.e.*10.9 µg is shown here) also reflected the improvement in cytotoxic potential of the conjugate (Figure 14B).

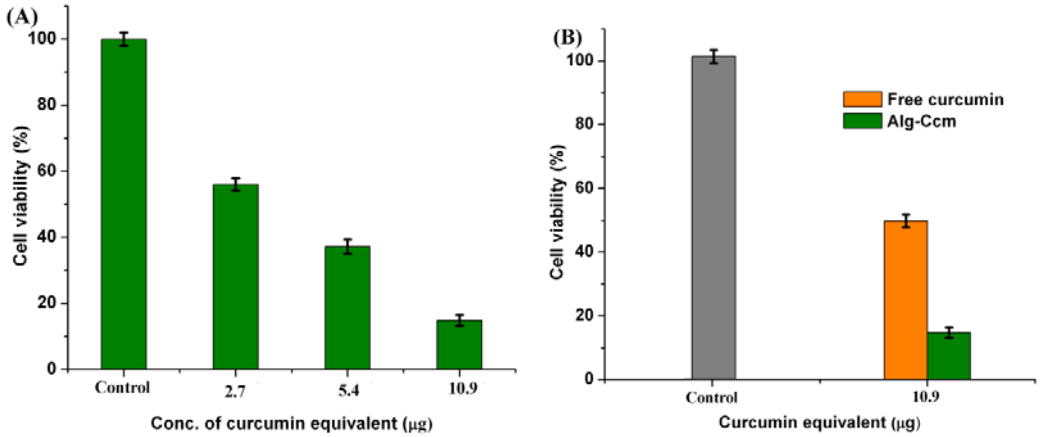

Figure 14: (A) Cytotoxic activity of Alg-Ccm conjugate against L-929 cells, and (B) comparison of cytotoxic activity of Alg-Ccm conjugate and free Ccm against L-929 cells. Cell viability (%) of the extract prepared using the negative control (ultrahigh density polyethylene) is taken as 100%. The error bars indicate mean value ± standard deviation (n = 3).

4.2 Conjugating Curcumin to Water Soluble Polymer Stabilized Gold Nanoparticles via pH Responsive Succinate Linker

4.2.1 Synthesis and characterization of water soluble polymer (P1)

In this study Ccm was conjugated to water soluble polymer stabilized AuNPs. The hydrophilic, low molecular weight, natural amino acid L-Cys containing polymer

(P1) was synthesized by solvent free melt polycondensation reaction of PEG, CA and L-Cys as depicted in Scheme 2. P1 was characterized using a variety of techniques. The

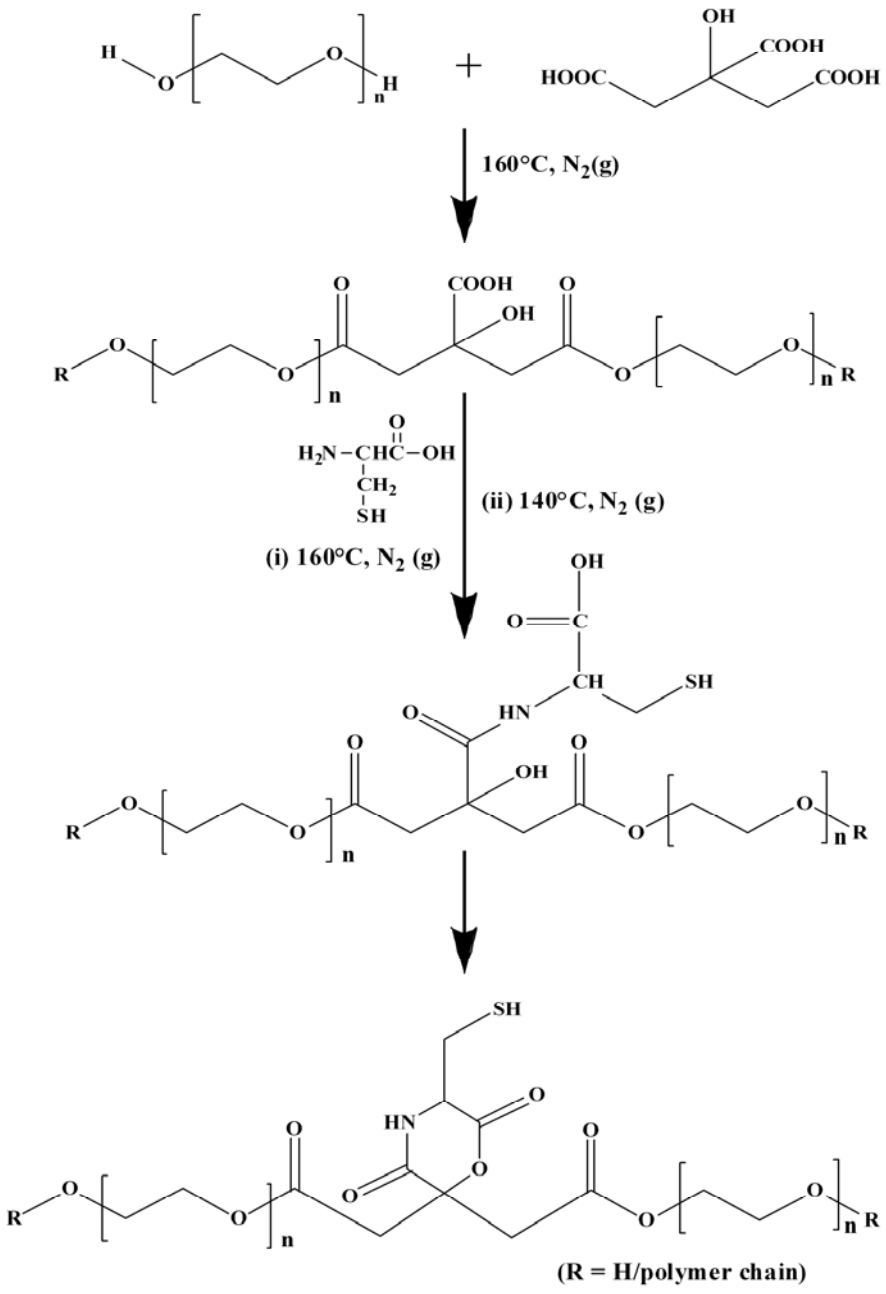

P1

Scheme 2: Schematic presentation for the synthesis of P1.

number and weight average molecular weights and the polydispersity index (PDI) of P1 were determined by GPC. Data obtained from GPC are tabulated in Table 2. Aliphatic polymer P1 devoid of conjugated phenyl chromophores was found to be photoluminescent in nature. The characteristic UV-VIS absorption spectra and fluorescence spectra of P1 (aqueous solution, 0.5 % w/v) are shown in Figure 15A and 15B respectively.

Table 2: GPC analysis data of polymer P1

M_n	M_w	MP	PDI
1533	**2174**	**1932**	**1.418**

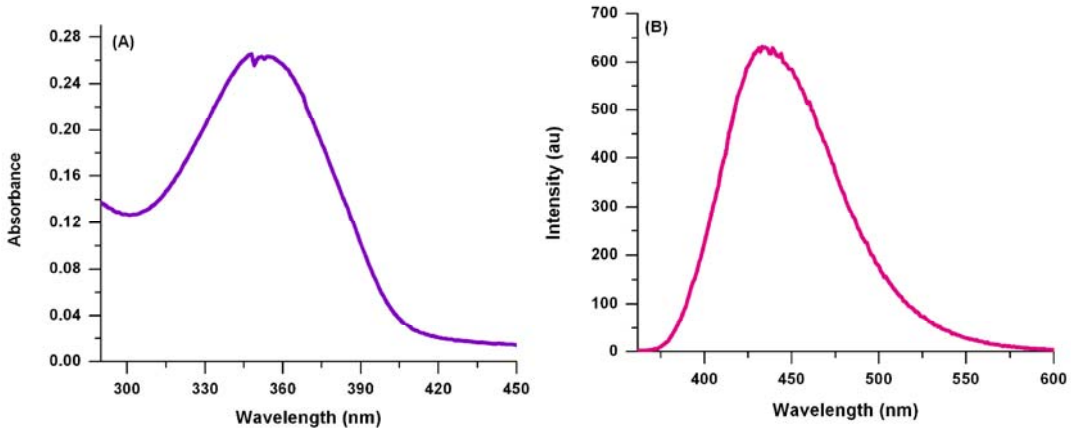

Figure 15: (A) UV-Vis absorption spectrum of P1; (B) fluorescence emission spectrum of P1 (λ_{ex} = 347 nm).

FTIR spectrum (shown in Figure 16A) of P1 confirmed the presence of characteristic functionality like –C=O (1727 cm^{-1}), -C(=O)NH- (1520 cm^{-1}) and -S-H (2515 cm^{-1}) in the polymer chain.

4.2.2 Fabrication of Ccm conjuagted P1 stabilized AuNPs

The AuNPs based curcumin delivery system (Ccm-SA-P1-AuNPs) was synthesized following a stepwise synthetic route as shown in Scheme 3. In the first step, citrate-AuNPs were prepared by Turkevich method (Turkevich et al. 1951) and the citrate-AuNPs were modified with P1 following ligand exchange route. P1 bearing free thiol linkage could bind strongly to the surface of AuNPs via Au-S bond and hence imparted excellent stability to the AuNPs. In the second stage of synthesis, P1-AuNPs was succinylated in aqueous alkaline medium (pH = 9) using excess amount of succinic anhydride. The succinylated product (SA-P1-AuNPs) contained free carboxyl groups which were then activated using DCC. The activated –COOH groups in the succinate linker reacted with phenolic –OH group of Ccm in presence of catalytic amount of DMAP in H_2O/DMSO mixture resulting in Ccm-SA-P1-AuNPs.

4.2.3 Physicochemical characterization

Surface modification of AuNPs at each step of synthesis was confirmed by FTIR analysis as shown in Figure 16. Figure 16A and 16B show the FTIR spectrum of pure P1and P1-AuNPs respectively. The low intensity sharp peak of –SH functionality (at around 2515 cm^{-1}) seen in Figure 16A was found to be missing in Figure 16B indicating chemical adsorption of P1 onto the surface of AuNPs via Au-S covalent bond. Besides, Figure 16B displays peaks attributed to –C=O stretching frequency at 1711 cm^{-1}, -C-H stretching frequency at 2924 cm^{-1} and 2854 cm^{-1}, free –O-H stretching frequency at 3647 cm^{-1} and –N-H bending vibration at 1462 cm^{-1}. In Figure 16C a broad band near

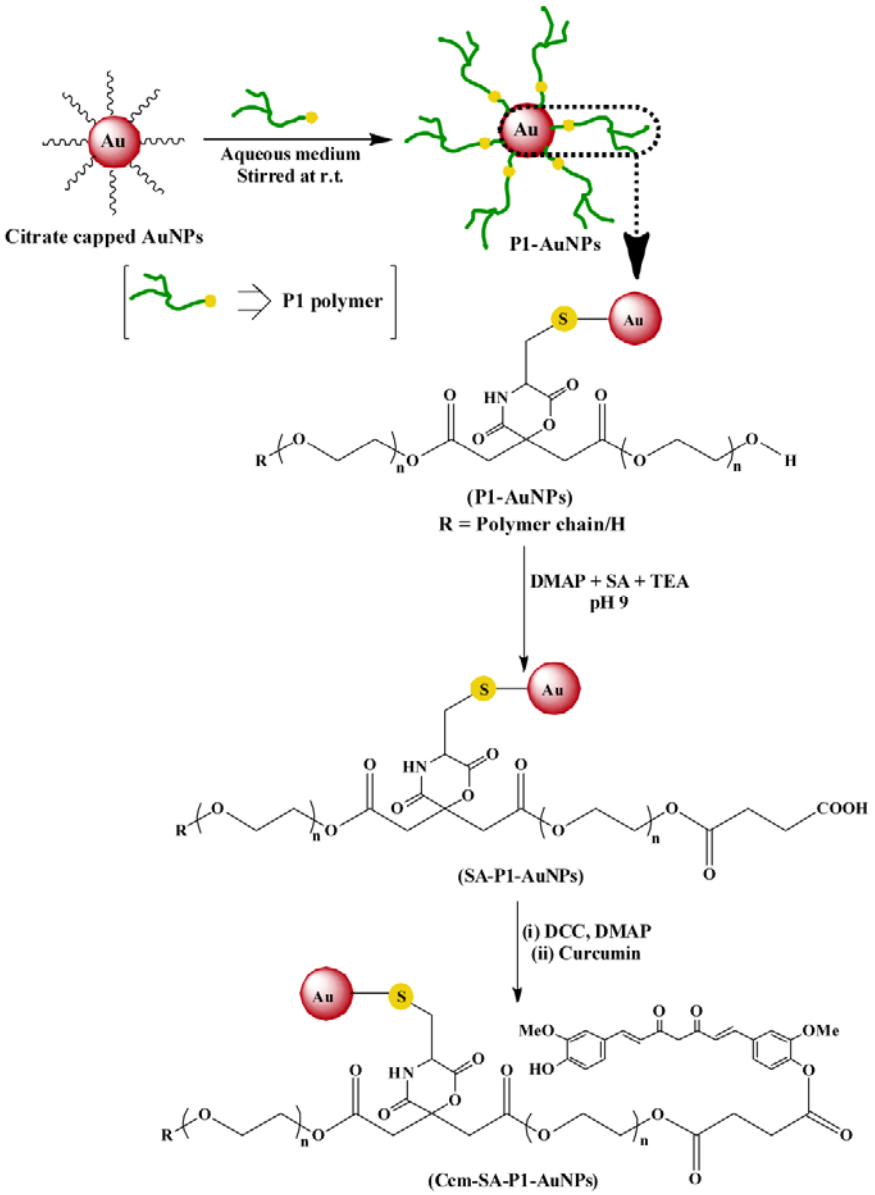

Scheme 3: Schematic presentation for the synthesis of Ccm-SA-P1-AuNPs.

3411 cm^{-1} assigned to the –O-H stretching frequency and the peak at around 1603 cm^{-1} attributed to the -C-O stretching of carboxylate anion confirms the succinylation reaction. The peak around 1603 cm^{-1} vanished as shown in Figure 16D after Ccm conjugation pointing out $–COO^-$ as the reaction site. In addition to this, in Figure 16D a

relatively sharp peak at 3420 cm^{-1} is associated with the phenolic –OH in Ccm and the peaks at around 1703 cm^{-1} and 1670 cm^{-1} are assigned to the ester C=O stretching frequency and ketonic functionality in Ccm respectively. A peak at 1290 cm^{-1} attributed to the –C-O stretching frequency of ester reflects conjugation of Ccm onto AuNPs via esterification reaction.

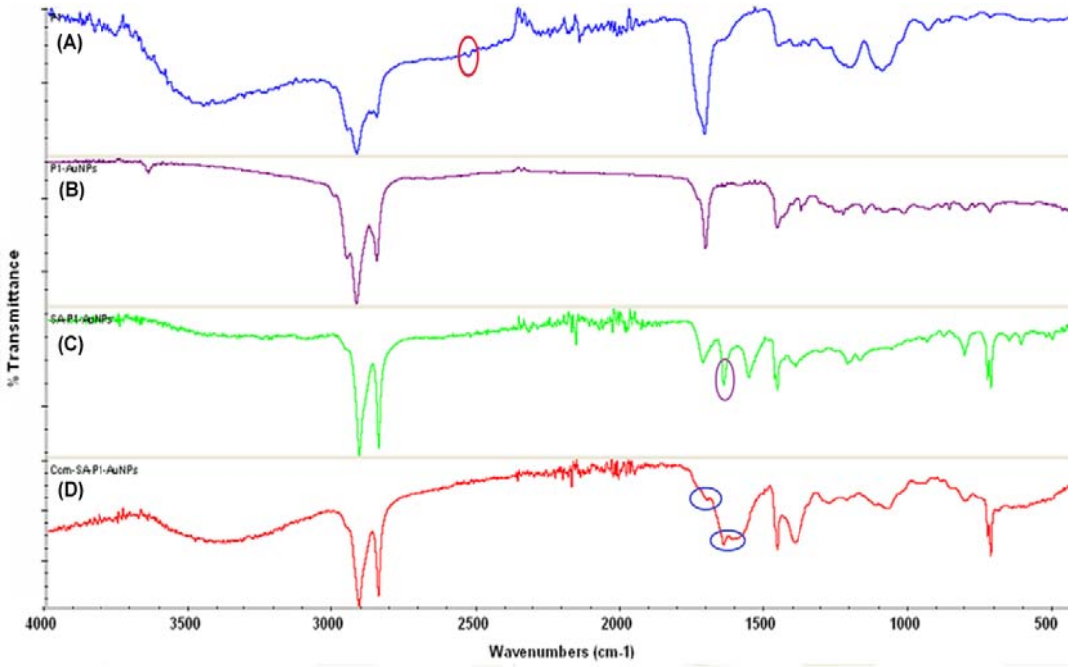

Figure 16: FTIR spectra of (A) P1; (B) P1-AuNPs; (C) SA-P1-AuNPs and (D) Ccm-SA-P1-AuNPs.

Formation of Ccm-SA-P1-AuNPs was further confirmed by ^{1}H NMR spectra as shown in Figure 17. In ^{1}H NMR spectra of pure P1 (Figure 17A), the peaks at $\delta \approx 2.7$ ppm can be assigned to the $-C\underline{H}_2$ protons of citric acid. Peaks at $\delta \approx 4.3$ ppm are due to the $-CH_2-C\underline{H}_2-O$ protons from PEG. The characteristic peak at $\delta = 1.3$ ppm (triplet as

shown, on expansion, in the inset of Figure 17A, due to –S<u>H</u> proton) confirms the presence of thiol functionality in P1. Presence of multiple peaks at around 3 ppm can be attributed to the –C<u>H</u>$_2$-SH protons in P1. In the ^{1}H NMR spectra of Ccm-SA-P1-AuNPs (in Figure 17B), the appearance of new peaks between δ = 6.5 to 7.9 ppm (due to the aromatic protons of Ccm) and at δ = 3.8 ppm (due to the characteristic –OC<u>H</u>$_3$ protons of Ccm) confirmed Ccm conjugation to polymer stabilized AuNPs.

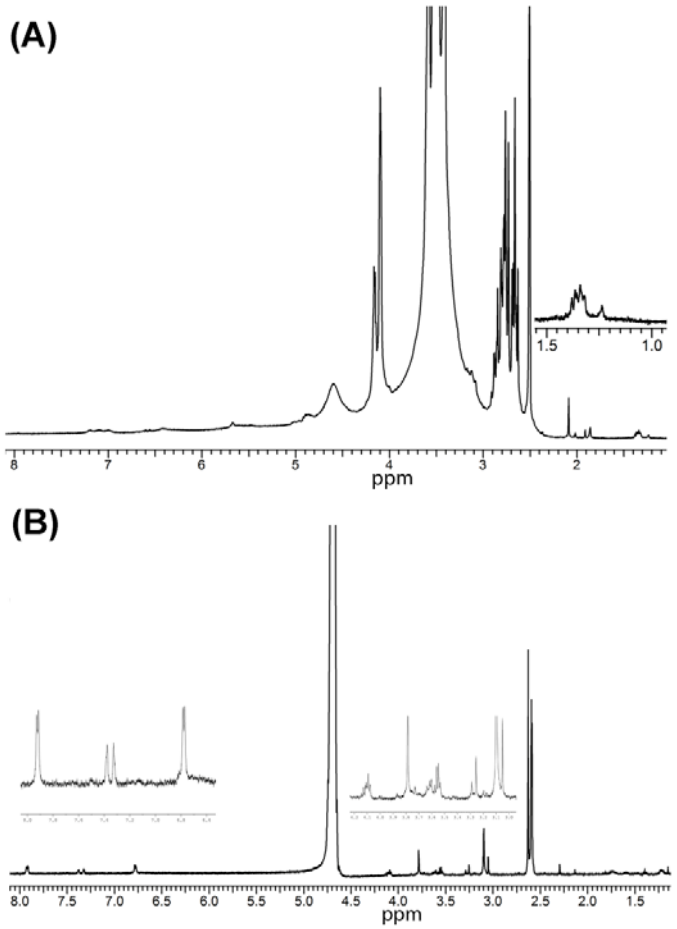

Figure 17: ^{1}H NMR spectra of (A) P1 polymer and (B) Ccm-SA-P1-AuNPs.

Changes in the SPR absorption were monitored during each step of synthesis of Ccm-SA-P1-AuNPs. Citrate-AuNPs showed a characteristic SPR at ~ 521 nm which was red shifted to ~ 524 nm in P1-AuNPs indicating chemisorption of P1 onto the surface of AuNPs (Figure 18A). Figure 18B showed further red shift of SPR absorption of P1-AuNPs upon succinylation and Ccm conjugation to ~ 527 nm and ~ 531 nm respectively. It is to be noted that the distinct and characteristic absorption peak of Ccm at ~ 420 nm was not seen in the spectrum as it merged with the intense SPR absorption of AuNPs but another absorption peak of Ccm at ~ 280 nm was clearly noted (Figure 18B).

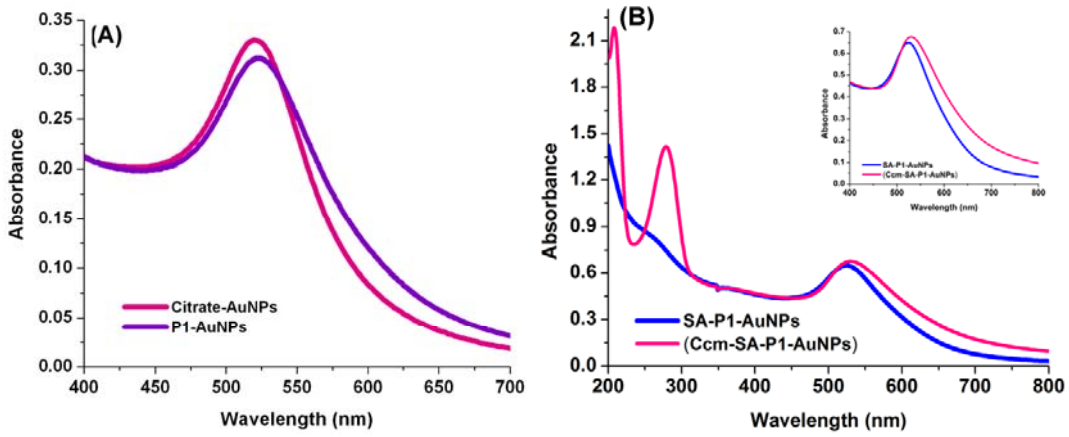

Figure 18: SPR absorption of AuNPs at various stages of modifications (A) red shift in absorbance for P1-AuNPs synthesis from citrate-AuNPs and (B) further red shift in absorbance in formation of SA-P1-AuNPs and Ccm-SA-P1-AuNPs (*inset* absorption spectra of SA-P1-AuNPs and Ccm-SA-P1-AuNPs in the visible range).

The characteristic strong fluorescence emission of P1 was quenched as the AuNPs were functionalized with P1 (Figure 19A).

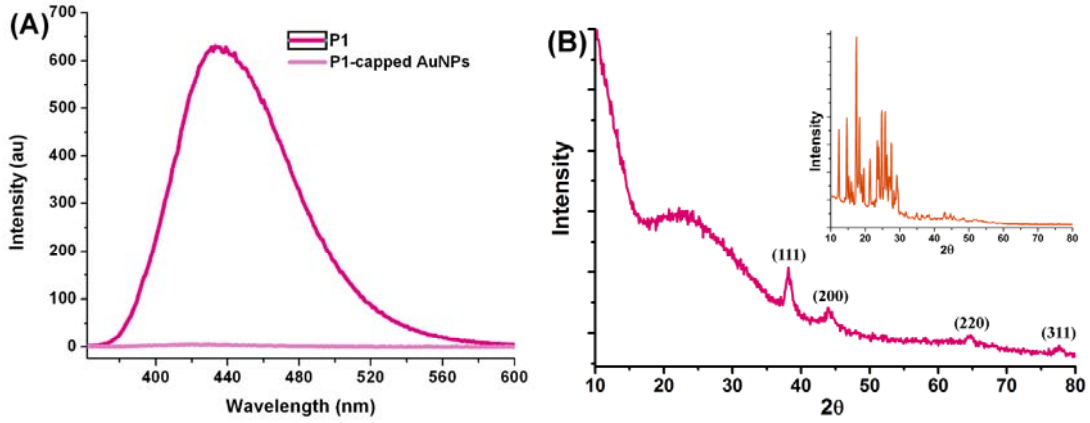

Figure 19: (A) Fluorescence spectra of P1 and P1-capped AuNPs showing fluorescence quenching of P1 after conjugation onto the surface of AuNPs (λ_{ex} = 347 nm) and (B) XRD pattern of Ccm-SA-P1-AuNPs (*inset*: XRD pattern of pure Ccm)

Figure 19B compares the XRD patterns of pure Ccm and Ccm-SA-P1-AuNPs. The X-ray diffractogram of Ccm-SA-P1-AuNPs clearly depicted the characteristic peaks of face centred cubic (FCC) crystal lattice of drug conjugtaed polymer stabilized AuNPs. In the XRD pattern of Ccm (shown as the *inset* in Figure 19B) a number of sharp peaks (in the 2θ range of 10° to 30°) indicated the crystalline nature of the hydrophobic drug. However, in Ccm-SA-P1-AuNPs no such crystalline peak of curcumin was observed.

The hydrodynamic diameter and zeta potential (ζ) of the AuNPs measured by DLS at pH 7.4 (in aqueous buffer at 25 ºC) at various steps of modification are tabulated in Table 3. TEM images of AuNPs at each stage of modification are also shown in Figure 20 (A to D). Though the surface charge was reduced to certain extent after Ccm conjugation, yet there was sufficient repulsive force present in the system to prevent it from aggregation and the TEM image shown in Figure 20D supported this fact.

Table 3: Sizes and zeta potential values of AuNPs solution (25 °C, pH = 7.4) after each step of surface modification.

Systems	Hydrodynamic diameter (nm)	Zeta potential (mV)
Citrate-AuNPs	15.6 ± 0.11	- 40.2 ± 0.3
P1-AuNPs	19.7 ± 0.06	- 23.1 ± 0.2
SA-P1-AuNPs	25.8 ± 2.3	- 40.9 ± 2.74
Ccm-P1-AuNPs	43.1 ± 1.8	- 32 ± 0.65

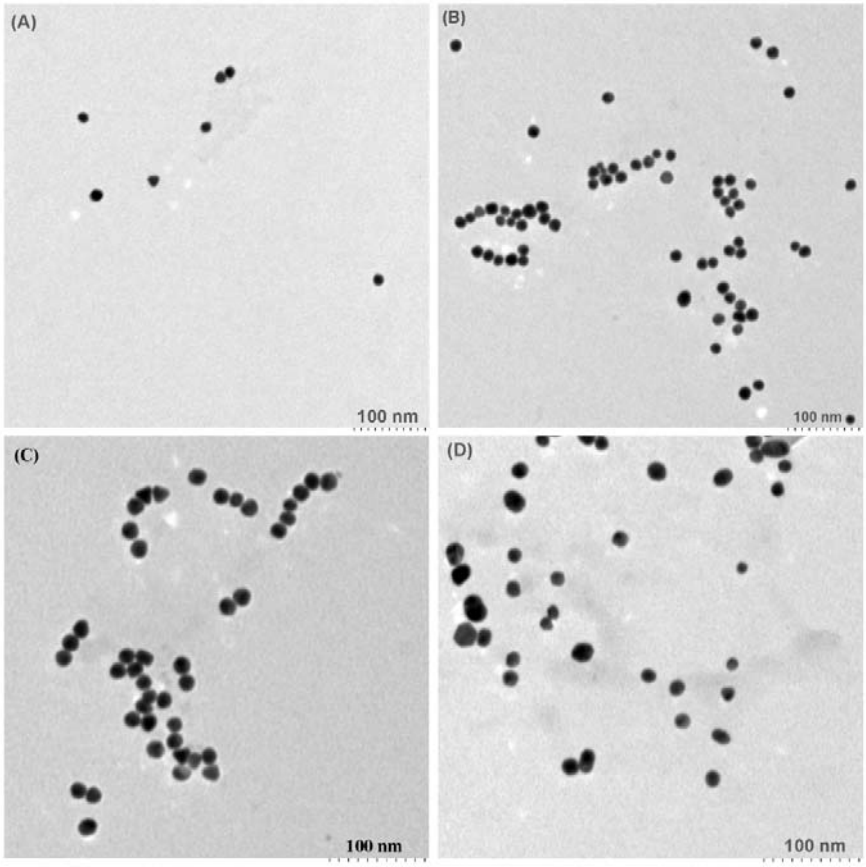

Figure 20: TEM images of AuNPs at different stages of modification: (A) Citrate AuNPs (B) P1-AuNPs (C) SA-P1-AuNPs and (D) Ccm-SA-P1-AuNPs

In order to check the stability of Ccm conjugated P1-AuNPs, the NPs were treated with varying concentrations of NaCl. Ccm-SA-P1-AuNPs were found to withstand high salt concentration (highly stable in 0.1 M NaCl environment; Figure 21A). In addition to this, Ccm-SA-P1-AuNPs also showed good stability in the physiological pH (pH = 7.4; Figure 21B).

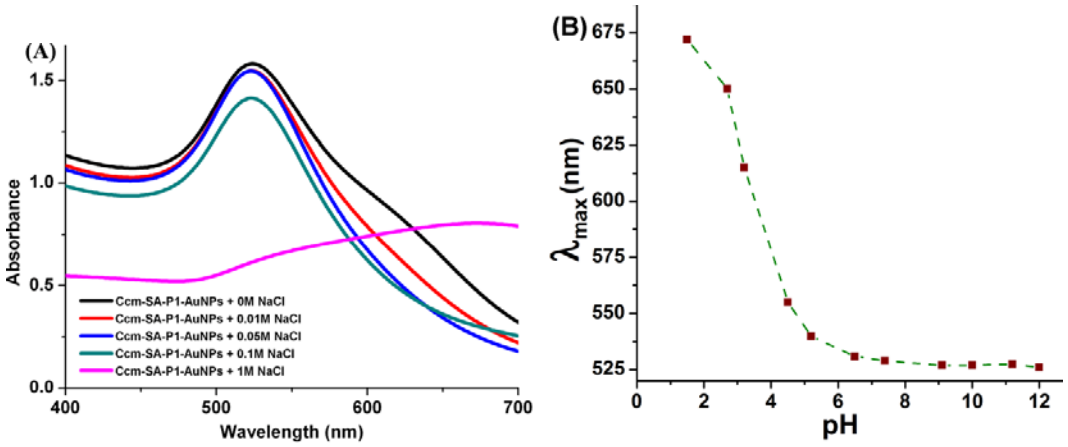

Figure 21: (A) UV-Vis absorption spectra in different concentrations of NaCl and (B) Change in SPR absorption maxima against pH (1.5 to 12) to determine the stability of Ccm-SA-P1-AuNPs.

4.2.4 Drug release (*in vitro*) from Ccm-SA-P1-AuNPs

The amount of Ccm present in Ccm-SA-P1-AuNPs was 67.5 ± 0.08 µg per 10 mg of the sample. In this study Ccm was conjugated to the polymer stabilized AuNPs *via* succinate ester linker. The drug release profile from Ccm-SA-P1-AuNPs shown in Figure 22 indicated that very low amount of Ccm was released from the nano-carrier at physiological pH over a period of 6 h. Whereas, within the same time span ~ 90 % drug was released at pH 5.3.

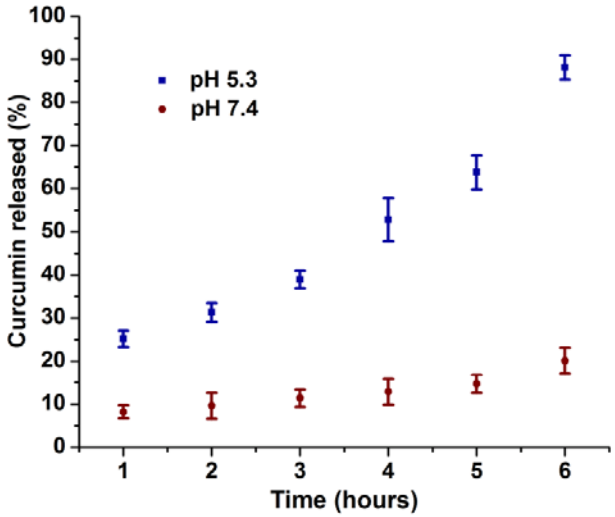

Figure 22: Ccm release profile from Ccm-SA-P1-AuNPs in buffer solution of different pH.

4.2.5 Evaluation of Cytotoxic activity

The cytotoxic potential of Ccm-SA-P1-AuNPs was determined by MTT assay against C6 cancer cell line. Figure 23A shows the cytotoxic response of Ccm-SA-P1-AuNPs towards the cancer cells in comparison with free Ccm. Figure 23B demonstrated that P1-AuNPs were compatible to the cells (cell viability for maximum tested concentration is shown here). Figure 23A clearly depicted a concentration dependent decrease in cell viability (*i.e.*, with increase in equivalent Ccm concentration in Ccm-SA-P1-AuNPs, there was more % of cell death). However, for each concentration toxicity of Ccm-SA-P1-AuNPs was higher than that of free drug.

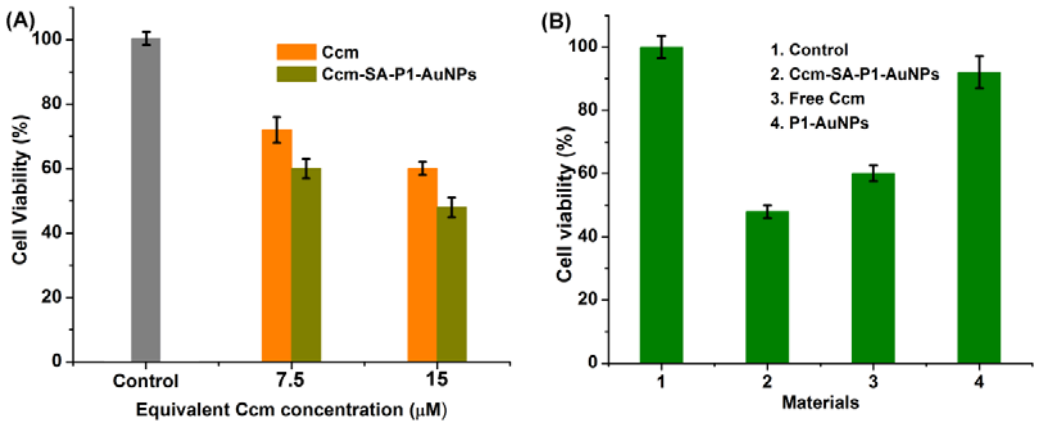

Figure 23: Cell viability (%) of C6 cancer cells as determined by MTT assay (A) showing the cytotoxicity of Ccm-SA-P1-AuNPs in comparison with free Ccm and (B) after interaction with (1) control (medium without any AuNPs) (2) Ccm-SA-P1-AuNPs (with equivalent Ccm concentration of 15 μM) (3) Free Ccm (15 μM) and (4) P1-AuNPs (concentration equivalent to the concentration of Ccm-SA-P1-AuNPs containing 15 μM drug); Control = cells treated with medium only. The error bars indicate mean ± standard deviation (n = 3).

4.2.6 Evaluation of cellular uptake of Ccm-SA-P1-AuNPs

In order to confirm the internalization of Ccm-SA-P1-AuNPs, C6 glioma cells were incubated with FITC tagged Ccm-SA-P1-AuNPs.

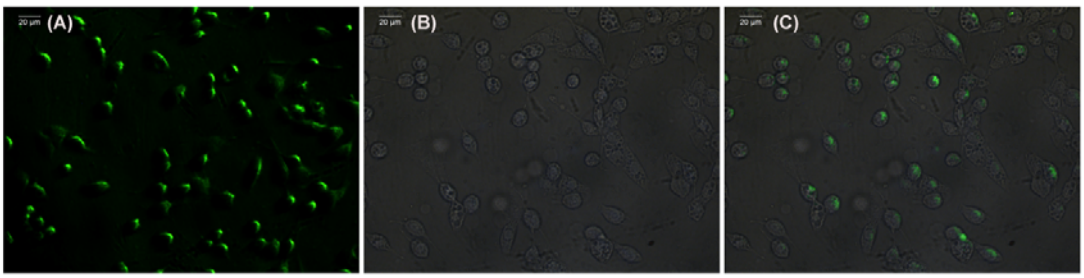

Figure 24: Fluooreescence microscopic images of C6 glioma cells after 3h incubation with FITC tagged Ccm-SA-P1-AuNPs; green fluorescence from FITC (A) fluorescence image (B) bright field image and (C) merged image of green fluorescnec in bright field.

The intracellular fluorescence intensity observed in glioma cells by fluorescence microscopic image (as shown in Figure 24) confirmed the facile uptake of the nanoparticles by cancer cells.

4.3 Fabrication of Curcumin and Methotrexate Conjugated Biopolymer Stabilized Gold Nanoparticles Based Drug Delivery Vehicles via Green Synthetic Route: Evaluation of Cytotoxicity and Hemolytic Toxicity

4.3.1 Synthesis and physicochemical characterizations

In this study AuNPs based dual drug delivery vehicle was fabricated following two simple synthetic steps in aqueous medium. In the first step, biopolymer stabilized Ccm conjugated AuNPs were synthesized by reduction of chloroauric acid with Alg-Ccm conjugate. In the second step, MTX conjugate of bis(aminopropyl) terminated PEG (MP conjugate) was covalently conjugated onto the surface of Alg-Ccm AuNPs in aqueous medium to generate MP@Alg-Ccm AuNPs. The green synthetic route is depicted in scheme 4. In order to develop MP conjugate, MTX was conjugated to bis(aminopropyl) terminated PEG *via* EDC chemistry in aqueous buffer solution (as shown as *inset* in scheme 4). Generation and stabilization of AuNPs by Alg-Ccm conjugate was confirmed by the distinctive SPR absorption of Alg-Ccm AuNPs at 525 nm (Figure 25A). Figure 25B compares the XRD patterns of Alg-Ccm conjugate and Alg-Ccm AuNPs and the diffractogram confirmed face centered cubic (FCC) crystalline geometry of the AuNPs formed through this route.

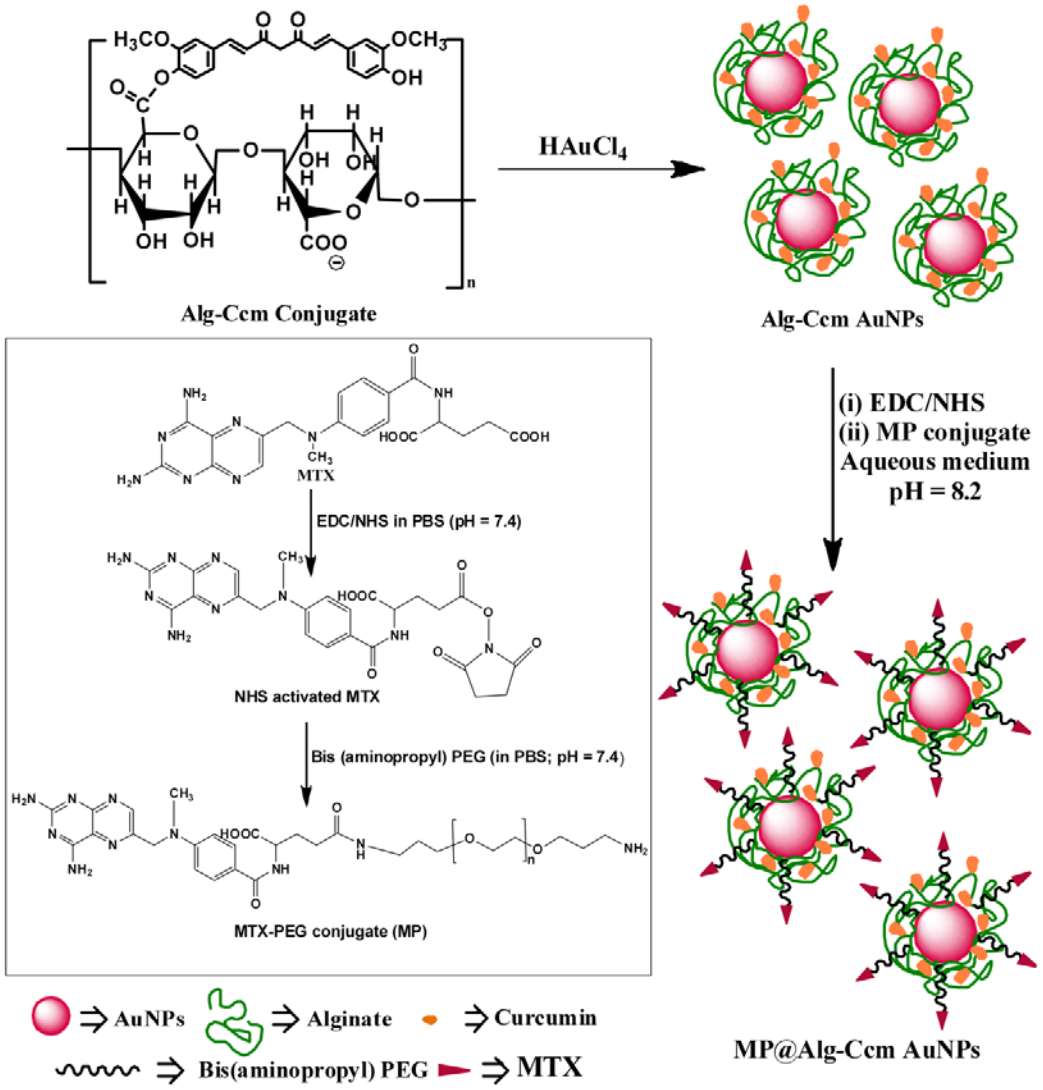

Scheme 4: Pictorial presentation of the synthetic scheme for fabrication of MP@Alg-Ccm AuNPs (*inset:* synthetic scheme for the generation of MP conjugate)

Formation of MP conjugate was assessed by FTIR spectroscopic analysis (Figure 26A). In Figure 26A, two distinct peaks at 3174 cm^{-1}, 3362 cm^{-1} can be attributed to the stretching vibration of primary $–NH_2$ group in MP conjugate and the peak ~ 3500 cm^{-1} can be due to the –NH stretching vibration of secondary amide. The peak at 1641 cm^{-1} is

due to amide –C=O stretching whereas the peaks ~ 1596 cm^{-1} and 1550 cm^{-1} can be attributed to –NH bending vibrations of the secondary amide group present in MP conjugate. Figure 26B compares the UV-Vis absorption spectra of bis(aminopropyl) terminated PEG with that of the MP conjugate. Bis(aminopropyl)terminated PEG does not exhibit any absorption band, where MP conjugate clearly indicated the absorption bands for MTX.

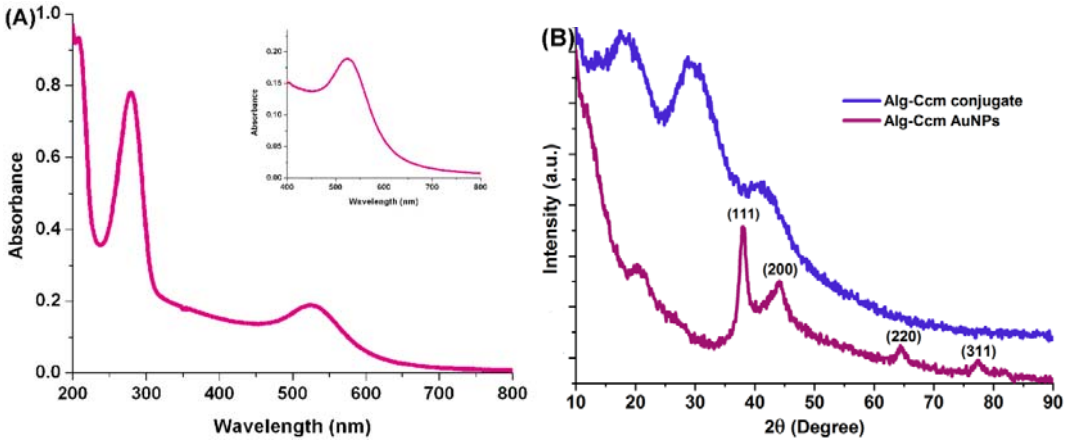

Figure 25: (A) SPR absorption of Alg-Ccm AuNPs (*inset:* picture of the same in the visible range) and (B) XRD patterns of Alg-Ccm conjugate and Alg-Ccm AuNPs

Upon conjugation with MP conjugate, the SPR absorption of MP@Alg-Ccm AuNPs was shifted to 539 nm. The red shift in the SPR band as shown in Figure 27 and appearance of a new absorption peak in MP@Alg-Ccm AuNPs at around 369 nm (see the *inset* in Figure 27) confirmed the successful conjugation of MTX onto the surface Alg-Ccm AuNPs. Fabrication of MP@Alg-Ccm AuNPs was further confirmed by FTIR analysis shown in Figure 28.

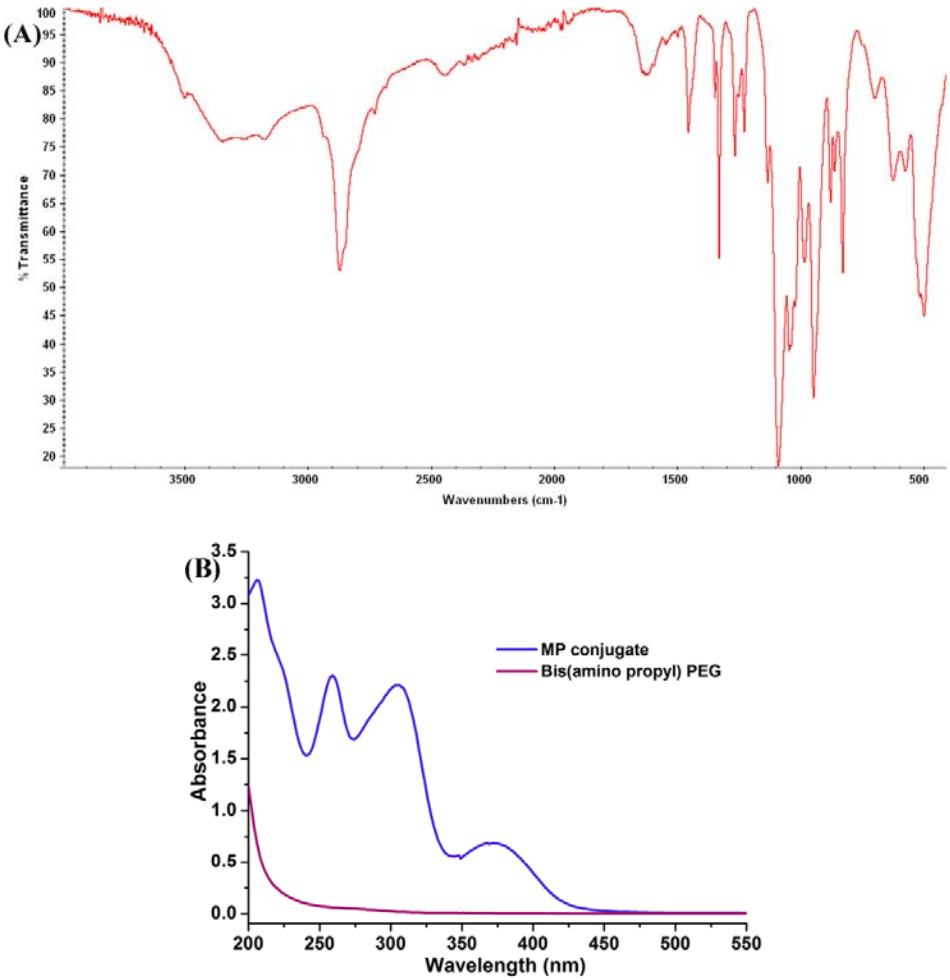

Figure 26: (A) FTIR spectrum of MP conjugate and (B) UV-Vis absorption spectra of bis(aminopropyl)PEG and MP conjugate

In Figure 28A, the peak at 3437 cm^{-1} is assigned to the –OH stretching vibration and peaks at around 1650 cm^{-1} and 1647 cm^{-1} are attributed to the stretching vibration of –C=O functionality in Alg-Ccm AuNPs. The small peak at 1211 cm^{-1} is due to the ester -C-O vibration in the conjugate. In the FTIR spectrum of MP@Alg-Ccm AuNPs (in Figure 28B), the appearance of new peak at around 1409 cm^{-1} clearly indicated the

presence of MTX and the new peak at 1550 cm^{-1} supported the formation of amide linkage.

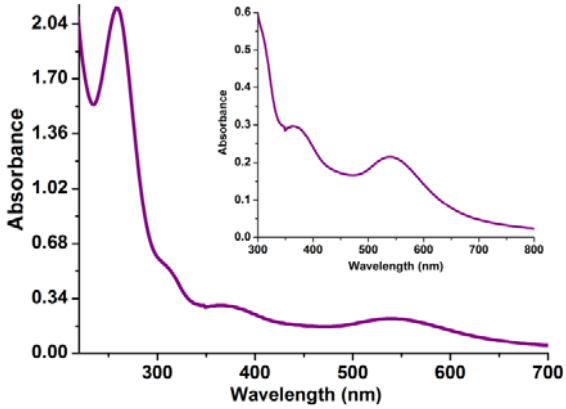

Figure 27: SPR absorption of MP@Alg-Ccm AuNPs (*inset:* picture of the same in the range of 300 to 800 nm)

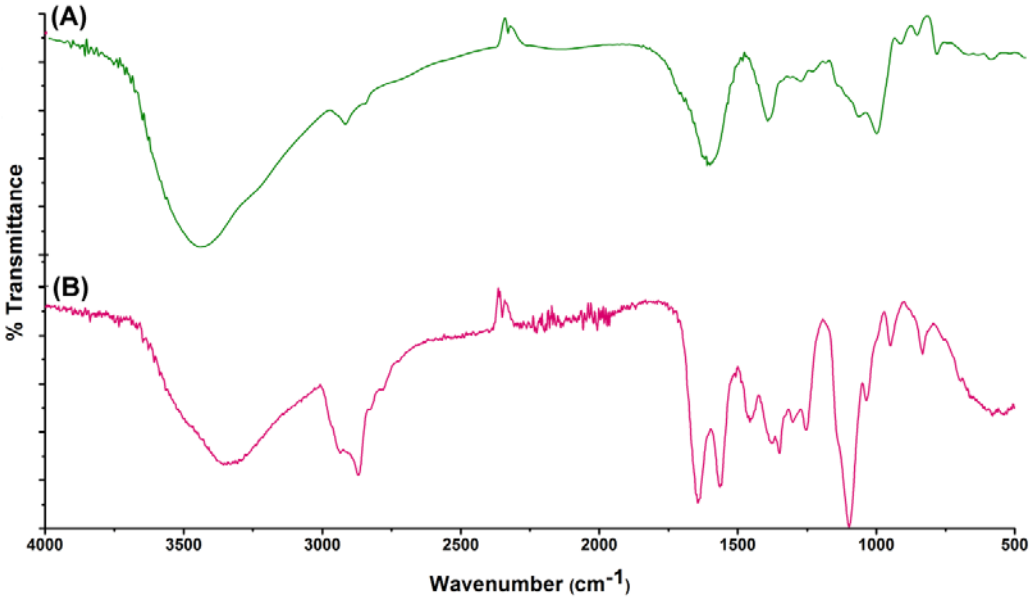

Figure 28: FTIR spectra of (A) Alg-Ccm AuNPs and (B) MP@Alg-Ccm AuNPs

Figure 29 shows the ^{1}H NMR spectra of the DDS at each of the two different stages of modifications. Figure 29A shows the ^{1}H NMR spectrum of Alg-Ccm AuNPs in which the methine protons of hexuronic acid residues of Alg appeared at δ ≈ 3.5 to 5 ppm and the peaks at δ 6.9 and 7.9 are due to the aromatic protons of Ccm. However, the chemical shift due to the characteristic –OC<u>H</u>$_3$ protons of Ccm probably merged with the chemical shift of C-5 methine proton of mannuronic acid (M) unit of alginate (δ ≈ 3.81 ppm).

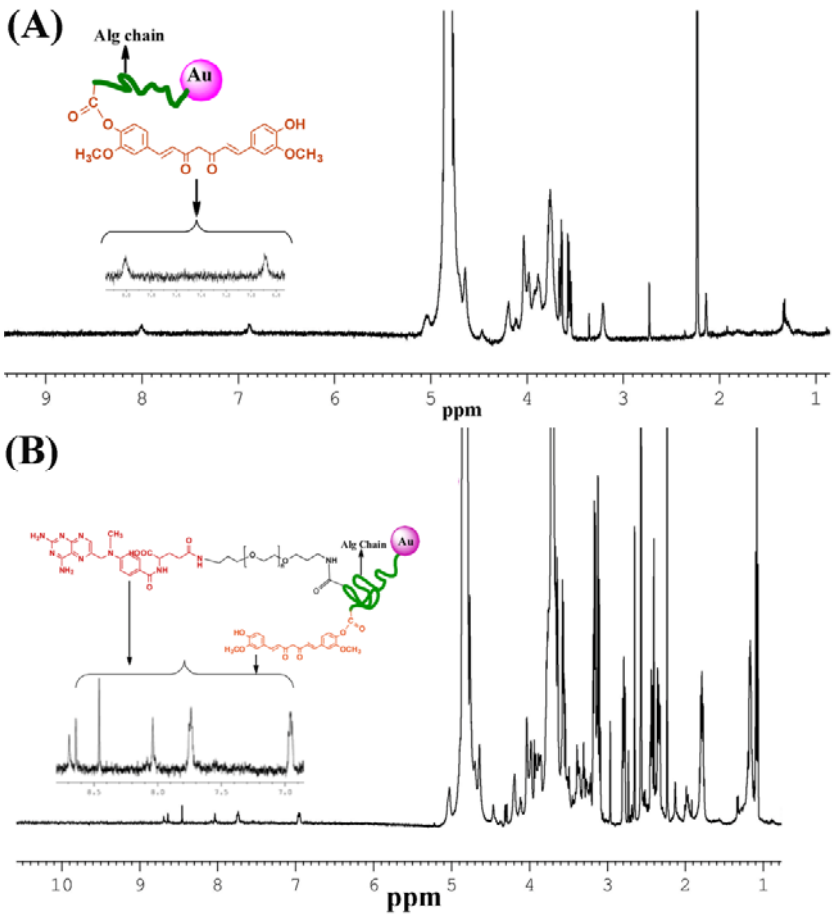

Figure 29: ^{1}H NMR spectra of (A) Alg-Ccm AuNPs and (B) MP@Alg-Ccm AuNPs.

In Figure 29B, the multiple peaks at δ ≈ 1.7 to 3.8 ppm were observed due to the protons from bis (aminopropyl) terminated PEG unit. Some of the peaks merged with that of alginate protons. However, the peaks that appeared in the range of δ ≈ 6.9 to 8.7 ppm can be attributed to the aromatic protons of both Ccm and MTX.

The hydrodynamic diameter and zeta potential of Alg-Ccm AuNPs and MP@Alg-Ccm AuNPs as determined by DLS are summarized in Table 4. In MP@Alg-Ccm AuNPs, the surface charge was lowered compared to that in Alg-Ccm AuNPs. However, the zeta potential was sufficient enough to stabilize the double drug conjugated AuNPs which was further supported by the well-dispersed TEM images of the AuNPs in Figure 30.

Table 4: Sizes and zeta potential values of Alg-Ccm AuNPs (25 °C, pH = 7.4) after each step of surface modification.

Systems	Hydrodynamic diameter (nm)	Zeta potential (ζ, mV)
Alg-Ccm AuNPs	132 ± 2	- 39.5 ± 0.02
MP@Alg-Ccm AuNPs	187 ± 4	-25.8 ± 0.05

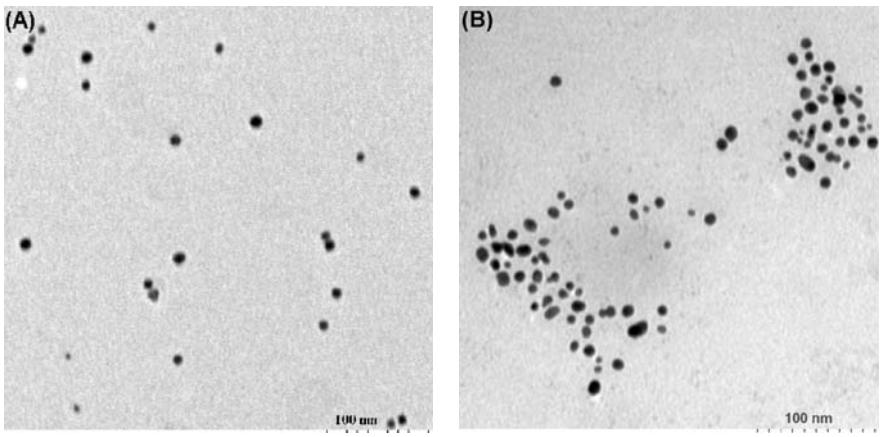

Figure 30: TEM images of (A) Alg-Ccm AuNPs and (B) MP@Alg-Ccm AuNPs

4.3.2 Evaluation of cytotoxicity

From UV-Vis spectroscopic study it was revealed that 100 mg of MP@Alg-Ccm AuNPs contained 1.05 ± 0.01 mg of Ccm and 1.26 ± 0.05 mg of MTX. The cytotoxic activity of MP@Alg-Ccm AuNPs was quantitatively evaluated by MTT assay against C6 glioma cell and MCF-7 cells. Figure 31 shows the cytotoxic activity of MP@Alg-Ccm AuNPs after interaction with the cancer cells in comparison with each of the free drugs of equivalent concentrations. With increase in concentration of the sample, cell viability was decreasing in both the cell lines. For each concentration MP@Alg-Ccm AuNPs exhibited improved toxic response compared to individual administration of MTX/Ccm for both the cell lines.

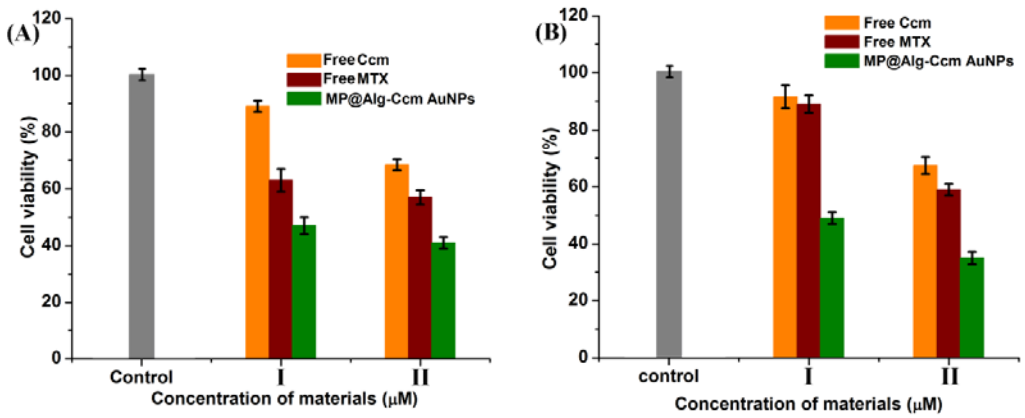

Figure 31: Cell viability of (A) glioma cells and (B) MCF-7 cells after being exposed to different concentrations of MP@Alg-Ccm AuNPs in comparison with equivalent amount of free drugs, where I: 20.5 μM MTX + 21 μM Ccm in DDS & equivalent free drugs and II: 41 μM MTX + 42 μM Ccm in DDS & equivalent free drugs. Control = cells treated with medium only. The error bars indicate mean ± standard deviations and here n = 3.

4.3.3 Cellular uptake studies

Figure 32 (A to F) shows the cellular uptake images of glioma and MCF-7 cells after incubation with FITC labeled MP@Alg-Ccm AuNPs. The green intracellular fluorescence was observed for each cell line. As evident from Figure 32 (A to F), significant amount of FITC labeled MP@Alg-Ccm AuNPs was visible in the cytoplasm and nuclear regions of both the cells.

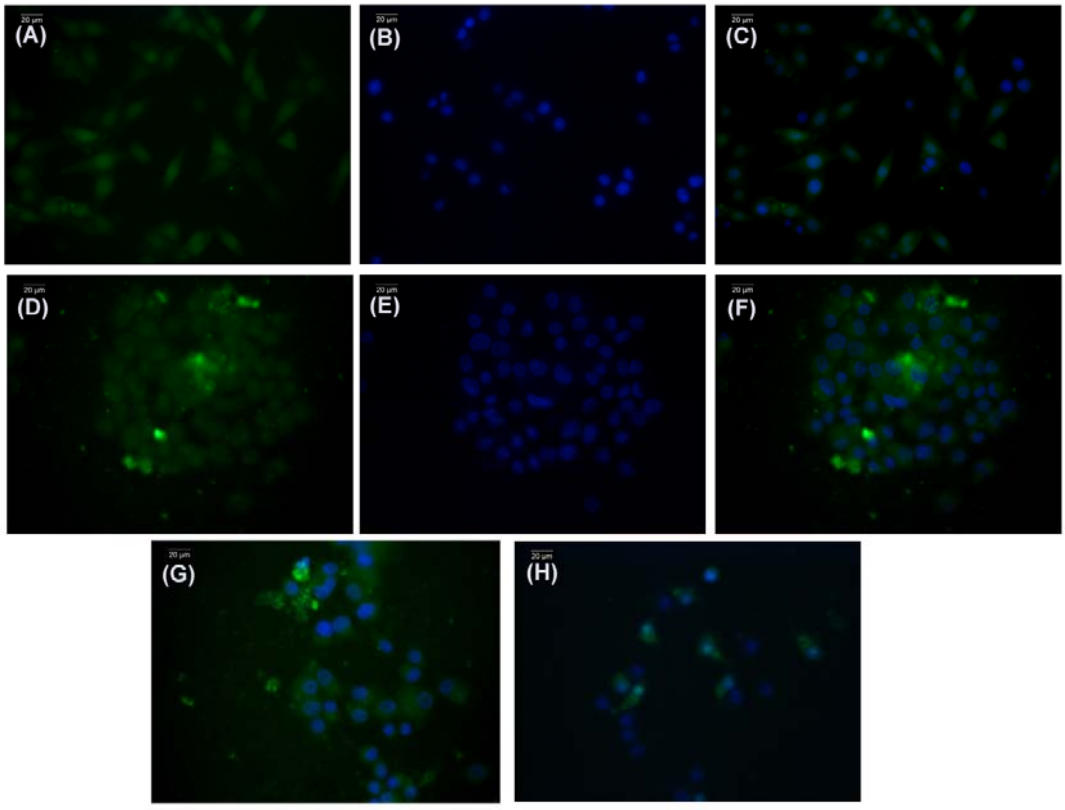

Figure 32: Fluorescence microscopic images after incubation with FITC labeled MP@Alg-Ccm AuNPs for 3 h; glioma cells: (A) fluorescent image (B) Hoechst 33342 stained nucleus and (C) merged fluorescent image; MCF-7 cells: (D) fluorescent image (E) Hoechst 33342 stained nucleus and (F) merged fluorescent image; (G) and (H): merged fluorescent images of MCF-7 cells after being exposed to FITC labeled MP@Alg-Ccm AuNPs and FITC labeled Alg-Ccm AuNPs respectively.

Figure 32G and Figure 32H show the internalization of FITC labeled MP@Alg-Ccm AuNPs and FITC labeled Alg-Ccm AuNPs respectively by MCF-7 cells. It was observed that in case of MCF-7 cells exposed to FITC tagged MP@Alg-Ccm AuNPs, significantly higher number of cells exhibited intracellular fluorescence (merged image in Figure 32G). Whereas, in case of FITC tagged Alg-Ccm AuNPs, very few cells exhibited green intracellular fluorescence (merged image in Figure 32H).

4.3.4 Evaluation of hemolytic toxicity

The hemolytic toxicity of MP@Alg-Ccm AuNPs was evaluated by determination of % hemolysis. For MP@Alg-Ccm AuNPs (0.5 mg/mL concentration) the hemolysis was found to be 0.11 ± 0.001 % and the result was much lower than the acceptable limit of 5 %.

4.4 Synthesis and Characterization of Glutathione Containing Fluorescent Polymer and Its Curcumin Conjugate for Safer Curcumin Delivery and Label-Free Cellular Imaging

4.4.1 Synthesis of GSHBP and GSHBP-Ccm conjugate

The GSH containing polymer GSHBP was synthesized *via* solvent free melt polycondensation reaction of PEG, CA and GSH as shown in Scheme 5A. In order to develop GSHBP-Ccm conjugate, hydrophobic drug Ccm was conjugated to GSHBP *via*

esterification reaction using DCC as the coupling agent in presence of catalytic amount of DMAP (as shown in Scheme 5B).

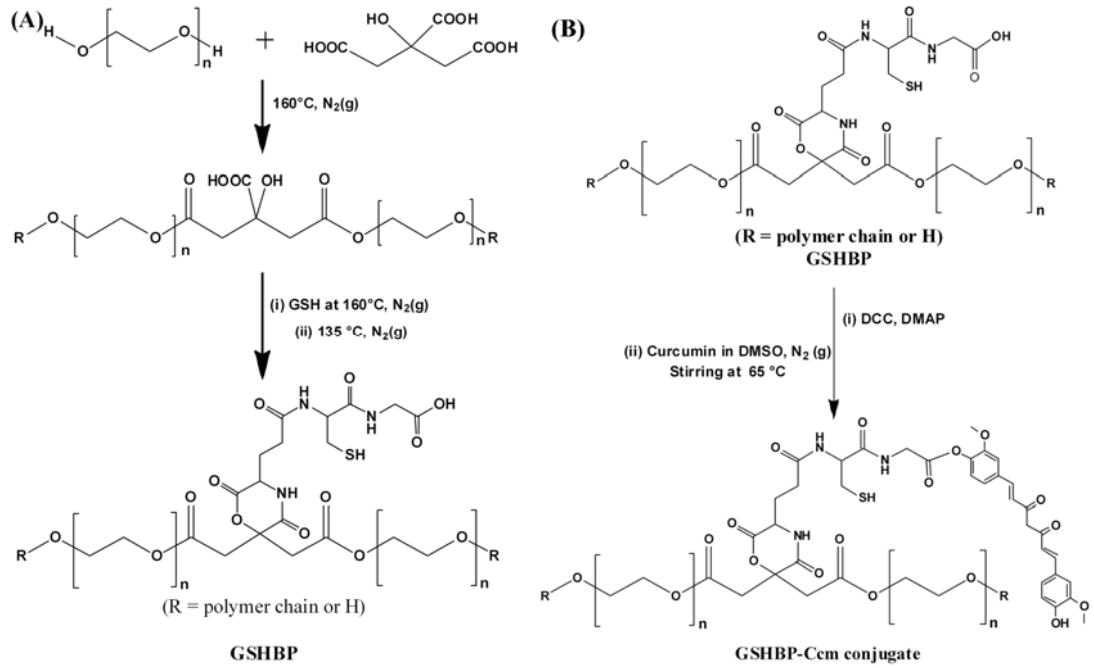

Scheme 5: Schematic presentation of the synthetic route of (A) GSHBP polymer and (B) GSHBP-Ccm conjugate

4.4.2 Physicochemical characterization of GSHBP and GSHBP-Ccm conjugate

A new absorption peak was found at 347 nm for the water soluble polymer GSHBP when compared to the UV-Vis absorption spectra of GSH and pre-GSHBP (i.e. melt polycondensation product of PEG and CA only) as shown in Figure 33A. The UV-Vis absorption spectrum of GSHBP alone is shown in Figure 33B with *inset* showing the absorption band in the visible range. GSHBP exhibited strong fluorescence emission around 431 nm (λ_{ex} = 347 nm, Figure 34A). The spectroscopic data indicated that a

stable six-membered cyclic structure possessing both amide and ester linkage with extensive hyperconjugation was possibly formed (as shown in scheme 5A) (Yang et al. 2009). The fluorescence quantum yield of GSHBP, as determined by William's method with reference to anthracene, was found to be 36 % (Figure 34B).

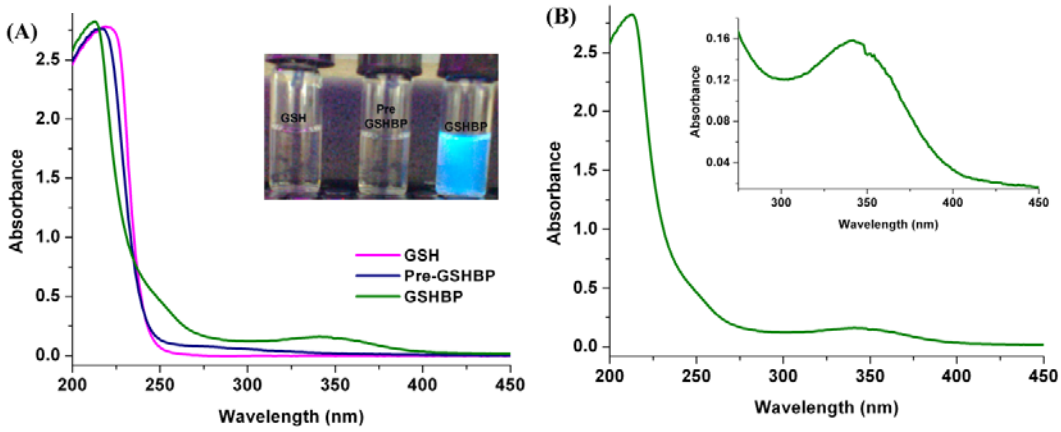

Figure 33: UV-Vis absorption spectra of (A) GSHBP in comparison with GSH and pre-polymer (*inset*: images of corresponding solutions under UV lamp) and (B) GSHBP alone with *inset* picture of the same from 275 nm to 450 nm range.

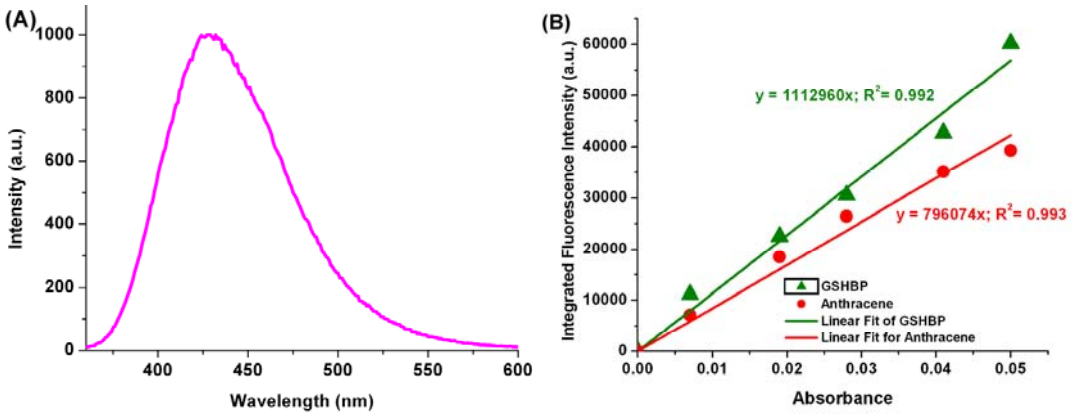

Figure 34: (A) Fluorescence emission spectrum of GSHBP (λ_{ex} = 347 nm) and (B) Plot of integrated fluorescence intensity Vs Absorbance of GSHBP for Q.Y estimation by William's method using anthracene as the standard.

The number average molecular weight of GSHBP obtained from GPC analysis was 4700 Da. Hydrolytic degradation of GSHBP was studied in PBS (pH 7.4) at 37 °C and the extent of degradation was monitored using GPC and LC techniques. CA was found as the major degradation product. The amount of CA in degradation media at different interval was quantified using LC and the time bound variation of CA is shown in Figure 35A. Reduction in molecular weight of GSHBP due to hydrolytic degradation was reflected in the GPC chromatograms (as shown in Fig 35B).

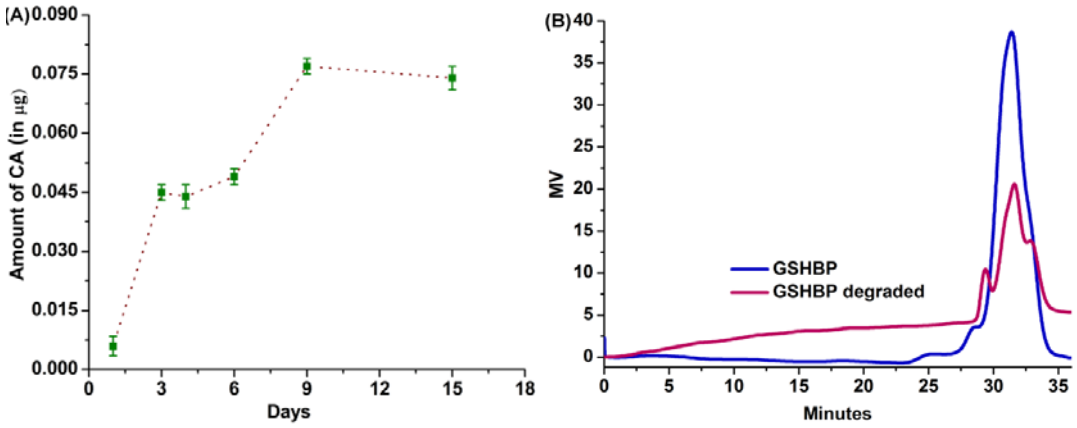

Figure 35: Plots showing the degradation of GSHBP under physiological condition (A) plot of increasing amount of major degradation product CA with time during degradation and (B) comparison of GPC traces of GSHBP before and after degradation (for 15 days).

^{13}C NMR (Figure 36, δ = 28.5 ppm, –CH_2-SH; δ = 60.9 ppm , –(C=O)-CH_2 and δ = 72.2 ppm, carbon forming 6-membered ring from citric acid; δ = 63.9 and 63.2 ppm, –CH_2 carbon from PEG; the peaks near 160 ppm to 187 ppm range can be attributed to the carbonyl carbons (-C=O) in GSHBP) and ^{1}H NMR (Figure 37A; δ = 1.5 ppm , –CH_2-SH; δ ≈ 2.7 ppm, –CH_2 from citric acid; δ = 2.9 ppm, –CH_2-SH) spectra confirmed

the formation of GSHBP. In addition, FTIR spectrum (Figure 38A; 1730 cm^{-1}, -C=O stretch; 1536 cm^{-1}, amide –N-H bending; 2520 cm^{-1}, -S-H stretch) further supported GSHBP formation.

The formation of GSHBP-Ccm was clearly reflected in the ^{1}H NMR of GSHBP-Ccm (Figure 37B) which showed new peaks in the aromatic region (aromatic H of Ccm) and a sharp peak at 3.84 ppm (assigned to –O$C\underline{H}_3$ protons of Ccm).

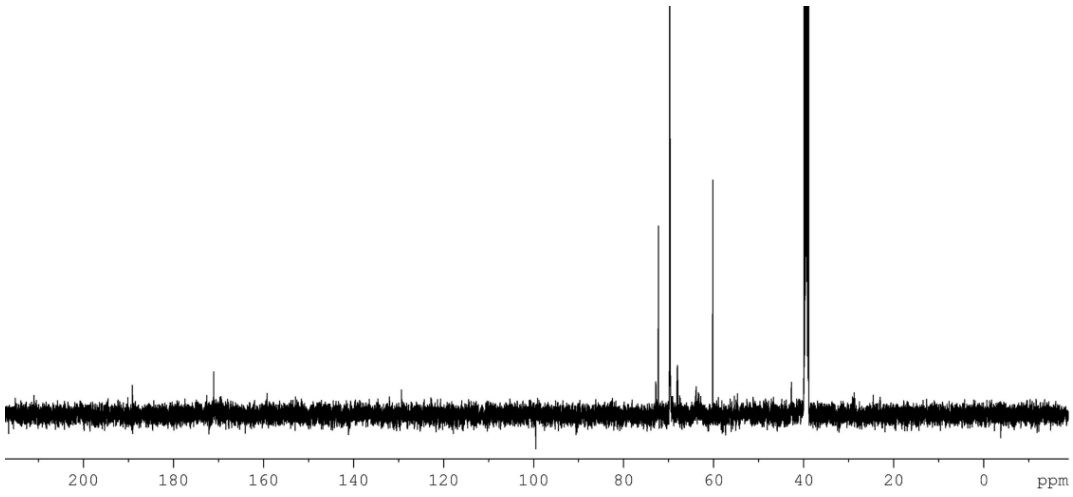

Figure 36: ^{13}C NMR spectrum of GSHBP

FTIR spectrum of the conjugate (Figure 38B) showed new peaks at 1690 cm^{-1} and 1647 cm^{-1} associated with -C=O stretching of Ccm along with other characteristic peaks of GSHBP further confirming the reaction between GSHBP and Ccm.

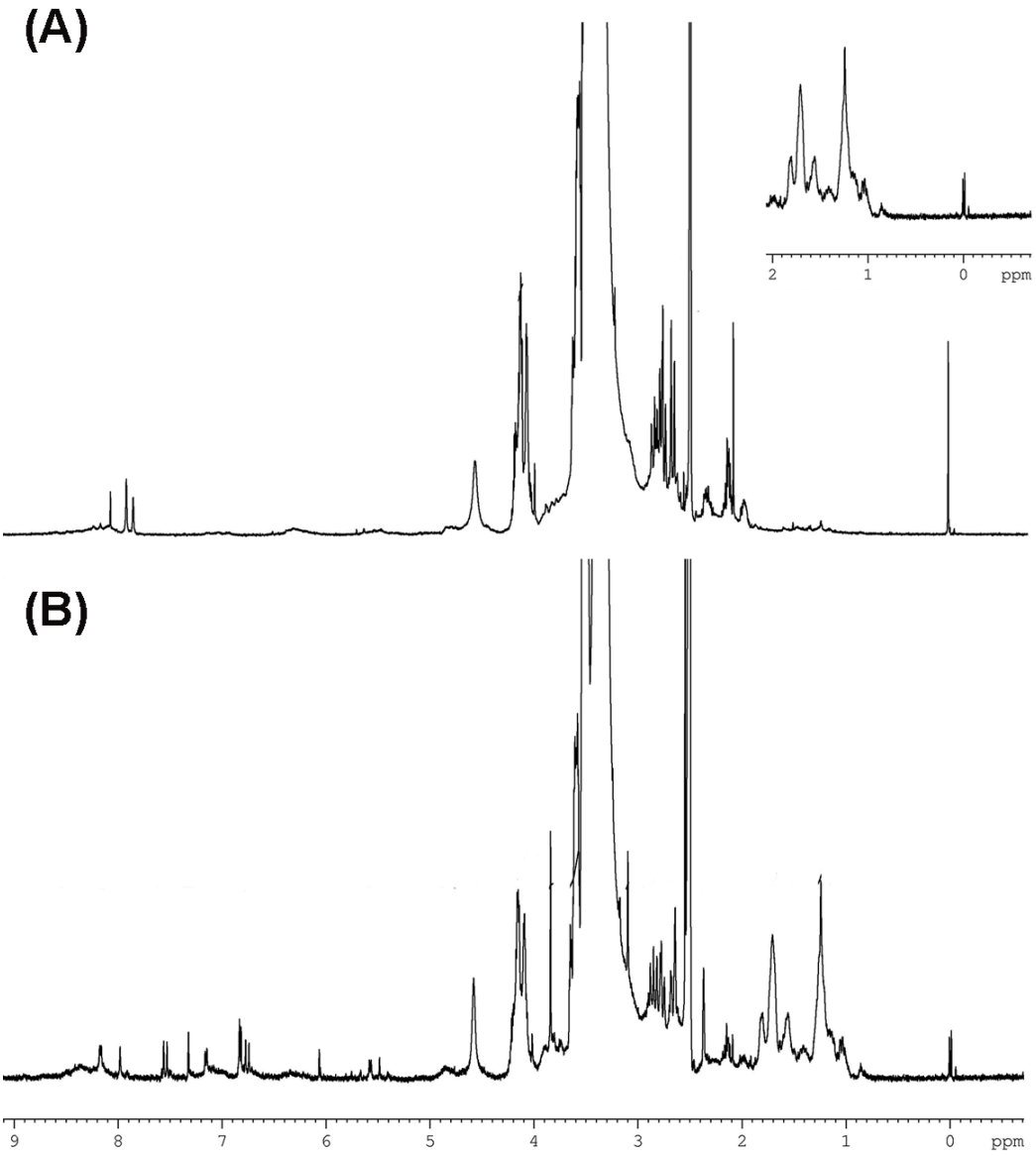

Figure 37: ^{1}H NMR spectra of (A) GSHBP and (B) GSHBP-Ccm conjugate.

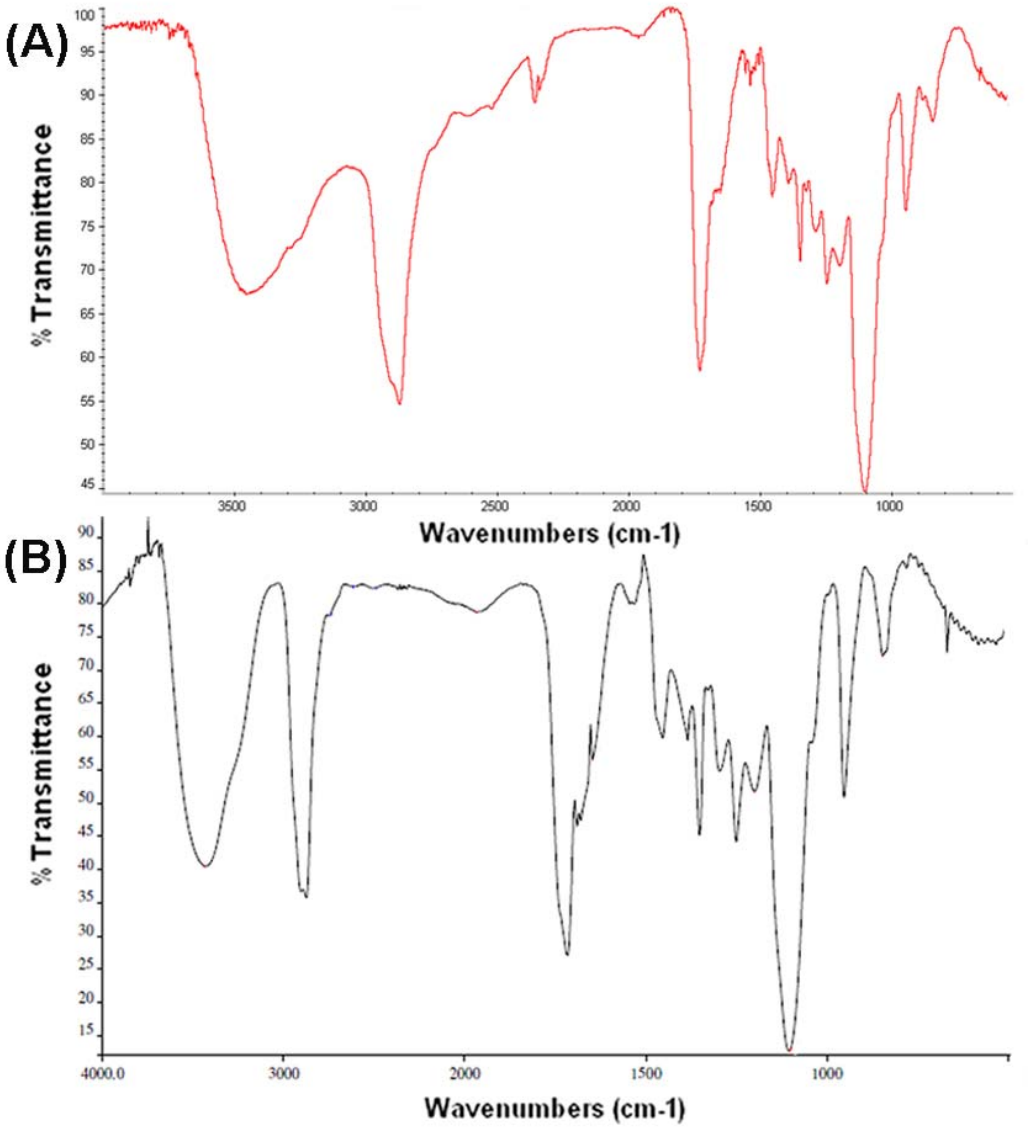

Figure 38: FTIR spectra of (A) GSHBP and (B) GSHBP-Ccm conjugate.

UV-Vis spectra of GSHBP-Ccm exhibited the characteristic absorption band of GSHBP along with the red shifted absorption of Ccm at 428 nm (Figure 39A). GSHBP-Ccm retained the characteristic blue emission of the polymer and at the same time, on

exciting the conjugate at 427 nm, characteristic emission of Ccm was observed (shown as the *inset* in Figure 39B).

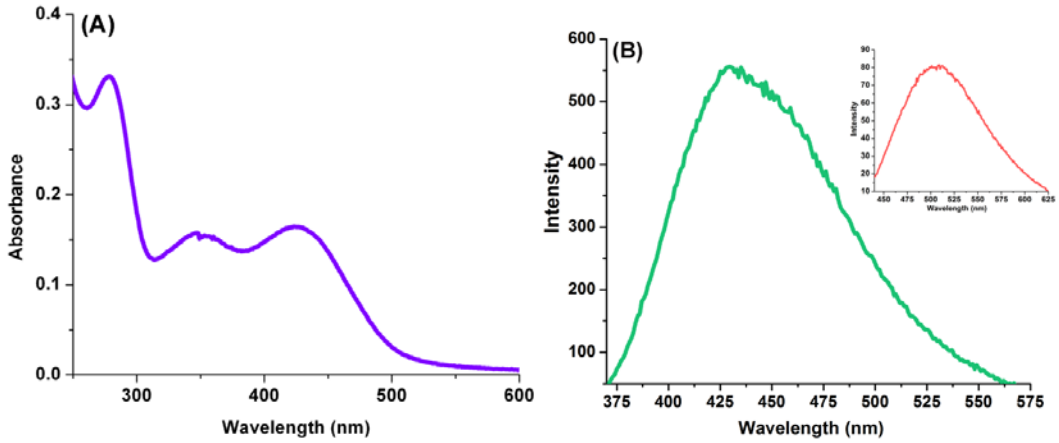

Figure 39: (A) UV-Vis absorption spectra of GSHBP-Ccm and (B) fluorescence emission spectra of GSHBP-Ccm (*inset*: fluorescence emission spectrum of Ccm in GSHBP-Ccm conjugate at λ_{ex} = 427 nm).

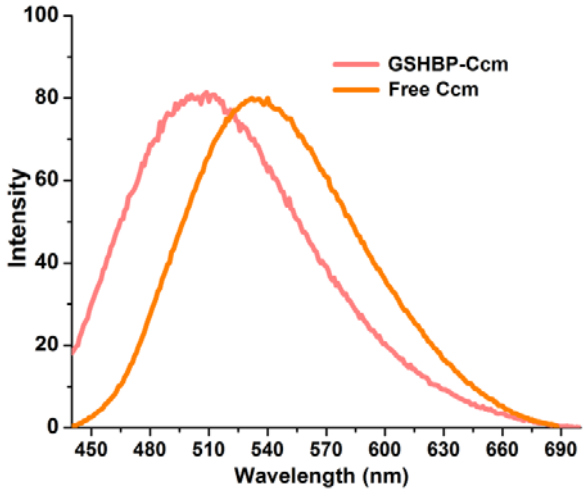

Figure 40: Fluorescence emission spectra of Ccm in pure state and in GSHBP-Ccm conjugate (λ_{ex} = 427 nm).

However, the fluorescence emission of Ccm was blue shifted in the conjugate compared to the emission of free drug (Figure 40). Figure 41A shows the fluorescence emission

spectra of GSHBP and GSHBP-Ccm along with the coloured picture of fluorescence emission (as *inset*, Figure 41A). In addition, the conjugate self assembled in aqueous medium forming micelles which were visualized by TEM images captured under cryogenic condition as shown in Figure 41B. The spherical conjugate micelles with average hydrodynamic diameter of 140.8 ± 0.77 nm (as shown in the size distribution plot in Figure 42A) exhibited low negative zeta potential in the range of – 23.7 mV to – 25.5 mV (at 25 °C in aqueous buffer solution of pH 7.4).

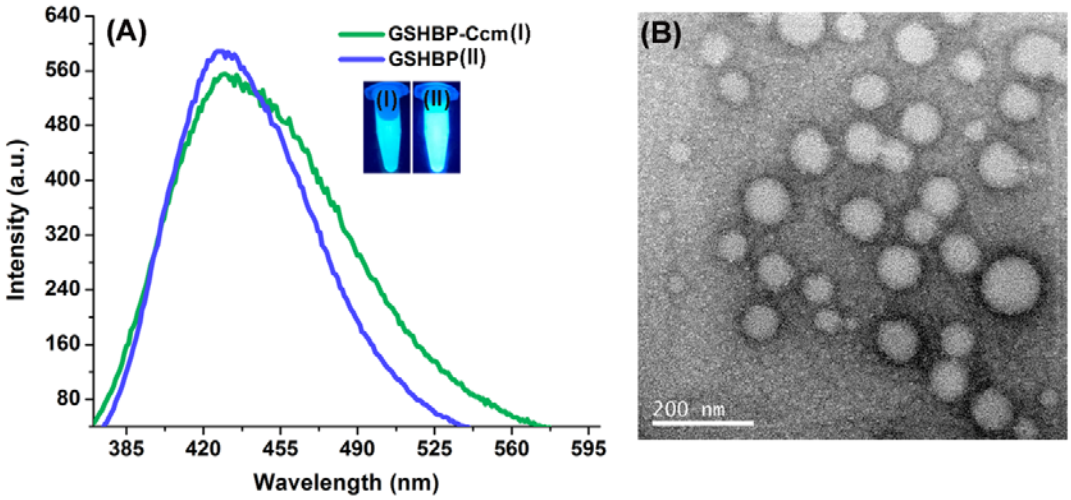

Figure 41: (A) Fluorescence emission of GSHBP and GSHBP-Ccm (λ_{ex} = 347 nm) (*inset:* fluorescent images of the same under UV lamp) and (B) cryo-TEM image of GSHBP-Ccm micelles in aqueous dispersion.

The CMC for the conjugate micelles was determined using NR dye as the hydrophobic fluorescent probe. In order to determine the CMC of GSHBP-Ccm conjugate, the respective fluorescence intensities of the probe molecule were plotted against log [concentration of GSHBP-Ccm]. The plot is shown in Figure 42B and the

inset picture in Figure 42B shows the change in the characteristic fluorescence of the dye with varied concentration of GSHBP-Ccm conjugate in aqueous medium. The break point of the curve indicated the CMC value of GSHBP-Ccm conjugate and it was found to be 0.17 mg/mL.

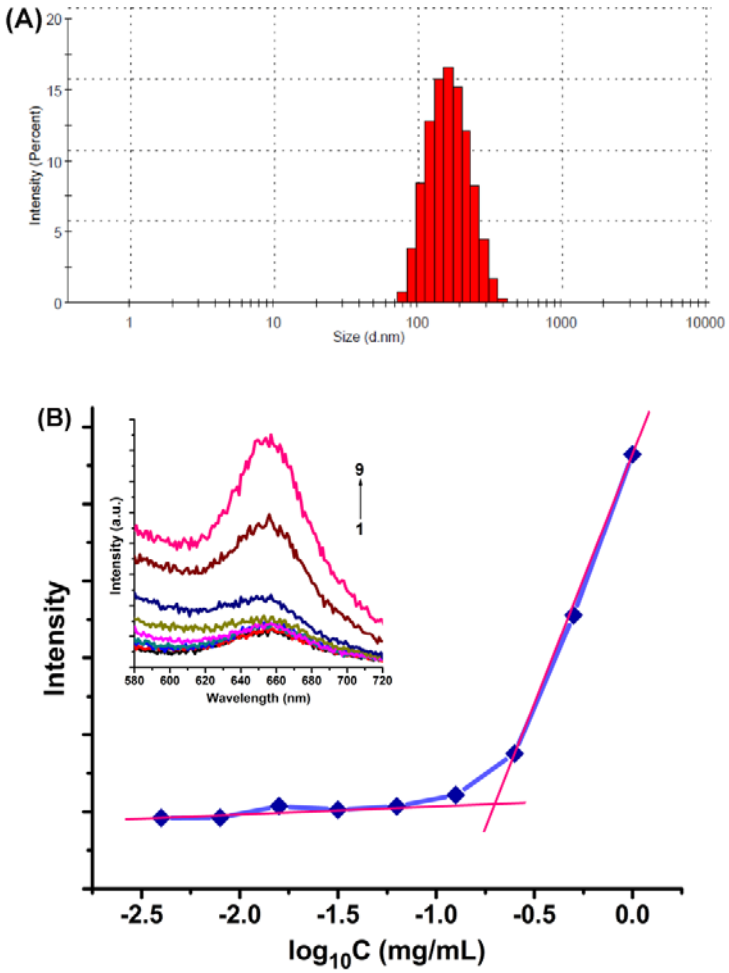

Figure 42: (A) Size distribution plot for GSHBP-Ccm in aqueous buffer solution (of pH = 7.4 at 25 °C) and (B) plot of intensity (a.u.) Vs log [concentration of conjugate] for CMC determination of GSHBP-Ccm conjugate micelles (*inset:* increment in fluorescence intensity of the probe (NR dye; λ_{ex} = 540 nm) with enhanced concentration of the conjugate)

4.4.3 Release of Ccm (*in vitro*) under physiological condition

GSHBP-Ccm showed a high aqueous solubility (more than 30 mg/mL) and 100 mg of the conjugate contained 178 ± 0.01 µg of Ccm. Thus aqueous solubility of Ccm was remarkably increased after its conjugation to the hydrophilic polymer. Here, the drug release from GSHBP-Ccm conjugate micelles was studied under physiological condition (in PBS of pH 7.4 at 37 °C) as shown in Figure 43.

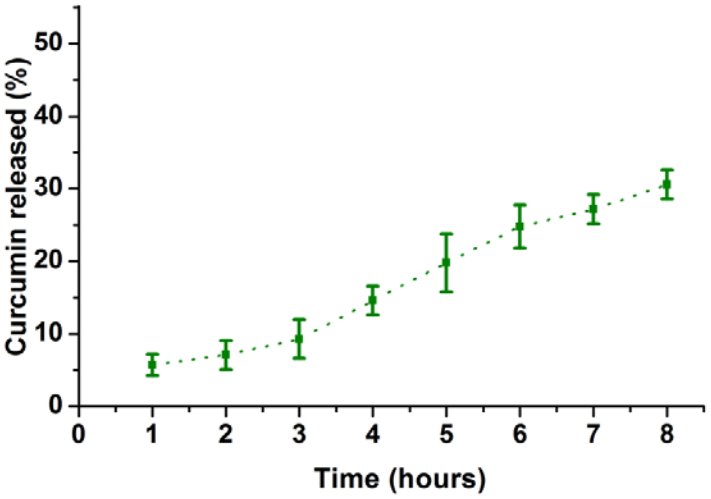

Figure 43: Release profile of Ccm from GSHBP-Ccm conjugates under physiological condition

The Ccm release was found to be slow at the physiological pH and within a period of 8 h ~ 27 % Ccm was released from the core of GSHBP-Ccm conjugate micelles.

4.4.4 Cytotoxicity Evaluation

In this study, the cytotoxic potential of GSHBP polymer was determined by MTT assay analysis against C6 glioma cells.

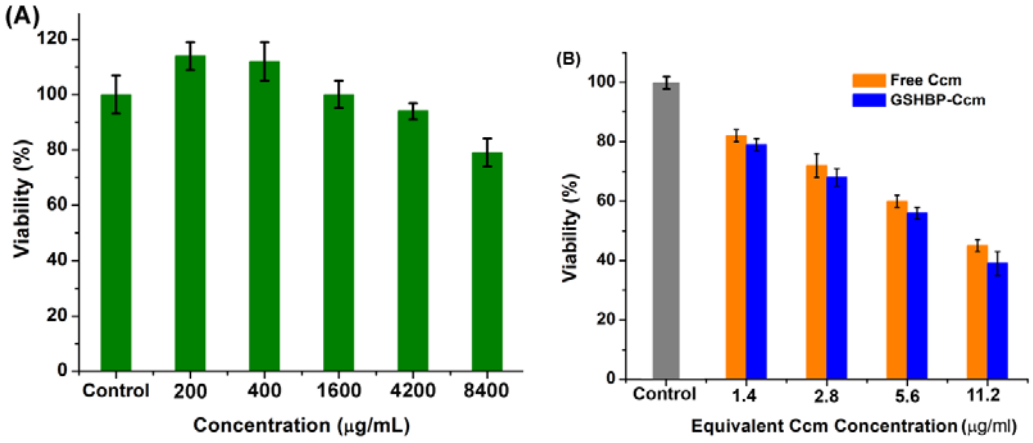

Figure 44: Cell viability (%) of C6 cells as a function of various concentrations (A) GSHBP and (B) GSHBP-Ccm. Control = cells treated with medium only. (Error bar represents average ± standard deviation, n=3).

The cell viability (%) as a function of concentration of GSHBP shown in Figure 44A revealed that GSHBP exhibited no toxicity upto a concentration of 1600 µg/mL. The cytotoxic response of GSHBP-Ccm was also determined in comparison with free Ccm against C6 cancer cells. The conjugate, as shown in Figure 44B, exhibited a concentration dependant toxic response. Ccm in the conjugate also showed better toxic response than that in the bare form.

4.4.5 Evaluation of cellular uptake of GSHBP-Ccm micelles *via* label-free cellular imaging

In order to study the internalization of the nano-sized fluorescent conjugate micelles, C6 cancer cells were incubated with medium containing GSHBP-Ccm conjugate micelles for 3 h at 37 °C and the uptake of nano-sized micelles was visualized using fluorescence microscope exploiting the intrinsic fluorescence of GSHBP. The self-fluorescence (blue) arising from GSHBP as shown in Figure 45A and Figure 45B ascertained that the biocompatible fluorescent polymer can be utilized for label-free

cellular imaging. Fortunately, Ccm also possesses intrinsic fluorescence that was utilized in the present study for cellular imaging application. The green fluorescence associated with Ccm in the conjugate was also readily seen under fluorescence microscope (Figure 45C and 45D). The merged fluorescent image (in bright field) is shown in Figure 45F.

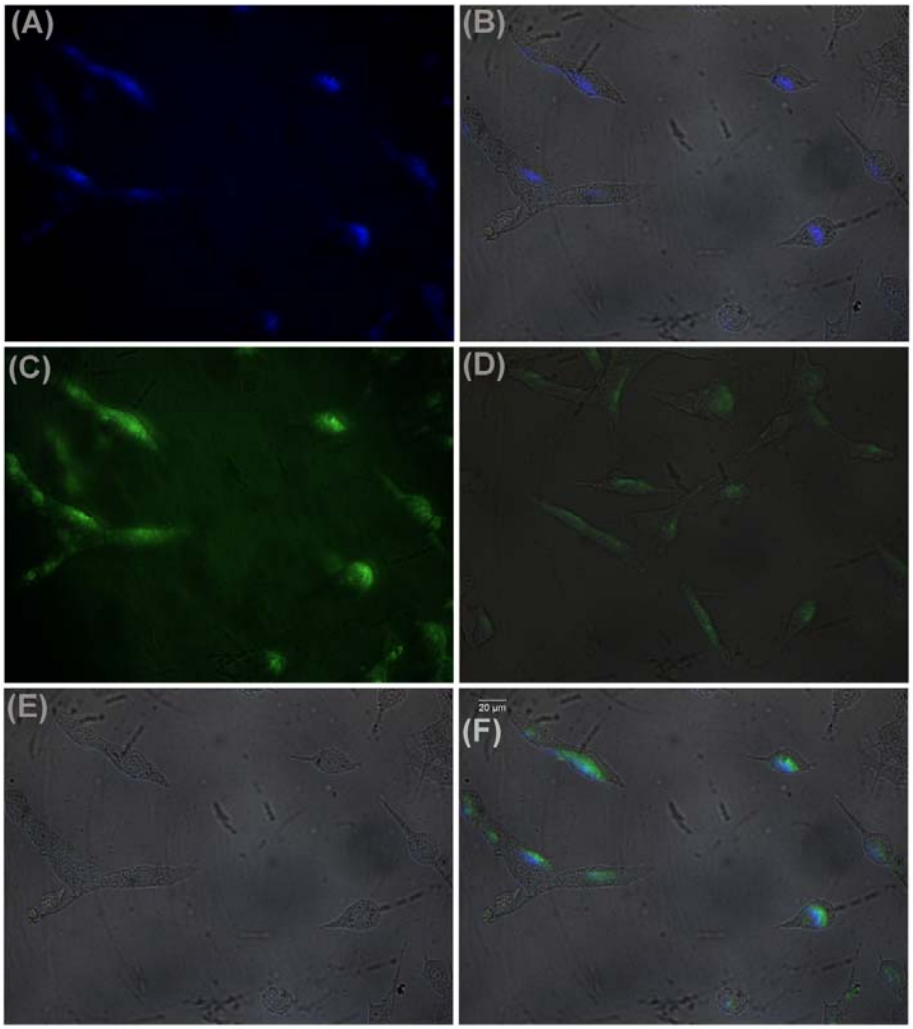

Figure 45: Fluorescence microscopic images of C6 glioma cells incubated with fluorescent GSHBP-Ccm micelles for 3h: blue fluorescence from self-fluorescent GSHBP (A) fluorescence image (B) overlaid image in bright field; green fluorescence of Ccm (C) fluorescence image (D) overlaid image in bright field; (E) bright field image (F) merged image of both blue and green fluorescence in bright field.

4.4.6 Evaluation of percentage hemolysis of GSHBP and GSHBP-Ccm

The hemolytic potential of GSHBP and its Ccm conjugate was determined by *in vitro* hemolysis study. The percentage (%) of hemolysis for GSHBP was 0.05 ± 0.002 and for the GSHBP-Ccm conjugate the value was found to be 0.09 ± 0.005. For both polymer and drug conjugate, the % hemolysis (for a concentration of 6.4 mg/mL) was not only much lower than the acceptable limit (5 %) but also was less than 0.1 % (% hemolysis < 0.1 indicates non-hemolytic nature of a material).

CHAPTER 5

DISCUSSION

5 Discussion

Chemotherapy is undoubtedly an important treatment strategy for cancer. However, the chemotherapeutic agents are incapable to discriminate normal and cancer cells. Hence chemotherapeutics, even under optimal conditions, often causes toxicity to normal cells leading to side effects and unwanted troubles to the patients. In order to redress the problems associated with the non-specific action of chemotherapeutic agents, suitably engineered drug delivery vehicles are of paramount importance to carry the cytotoxic drugs specifically to the site of action. Nano-structured drug delivery vehicles are interesting in this context as they can take the advantage of the leaky tumor vasculature to ensure better cellular internalization exploiting the EPR effect (*i.e.* passive targeting). In this study, different nano-sized delivery vehicles were designed based on polymer-drug conjugates and polymer stabilized AuNPs to carry anticancer drugs (such as Ccm and MTX) to the targeted site with the objective to augment aqueous solubility and stability of the drug, improve cytotoxicity, safer delivery through systemic circulation, better cellular uptake (*via* passive and active targeting) and label-free cellular imaging. The results emerged from the study are critically discussed in this section of the thesis.

5.1 Development of Alginate-Curcumin Conjugate for Enhanced Aqueous Solubility and Stability of Hydrophobic Drug Curcumin

The natural polyphenol Ccm possess tremendous medicinal assets including chemopreventive and chemotherapeutic potential. However, extremely low aqueous

solubility, lack of stability and consequent poor bioavailability are the serious limitations associated with this natural drug. It is well documented that conjugation of hydrophobic drug to hydrophilic polymer can augment the water solubility of the drug and at the same time, polymer-drug conjugates may alter drug pharmacokinetics and biodistribution which are basically useful for those drugs that exhibit rapid metabolism (e.g. Ccm), faster clearance and/or off target toxicities (anticancer drugs) (Larson and Ghandehari 2012). Various water soluble synthetic and natural polymers have been utilized for conjugation of diverse hydrophobic drugs. In this study, biopolymer Alg was chosen for the development of Alg-Ccm conjugate considering its non-immunogenic nature. Alg is an anionic, polysaccharide copolymer consisting of (1 → 4) linked β-D-mannuronic acid (M) and its C-5 epimer α-L-guluronic acid (G) residues. The natural block copolymer contains domains of sequential M-units (M blocks), G-units (G blocks) and atactically organized M and G units. Alg is widely used in biomedical applications owing to its several advantages such as biodegradability, high biocompatibility, non-toxicity, non-immunogenicity and the scope of chemical modification (Li et al. 2011) (Yang et al. 2007). The two secondary C-2 and C-3 hydroxyl groups and the C-6 carboxylate group are the accessible sites in Alg for the desired chemical modifications to develop derivatives with unique characteristics (Pawar and Edgar 2011). In this study, Ccm was directly conjugated to the reactive C-6 carboxylate functional group of Alg through ester linkage in water/DMSO mixture (Scheme 1). Formation of Alg-Ccm conjugate was confirmed by FTIR and ^{1}H NMR spectroscopic analyses as depicted in Figure 7 and Figure 8 respectively. The red shift in UV-Vis absorption spectrum of Ccm

(Figure 9A) and blue shift in the emission maxima of Ccm (Figure 9B) in the conjugate strongly indicated the successful conjugation of Ccm to Alg. A considerable increase in the aqueous solubility of Ccm was observed upon conjugation with highly hydrophilic polymer Alg. As the conjugate contains both hydrophobic (Ccm) and hydrophilic (Alg) segments, hence Alg-Ccm self-assembled in aqueous medium forming micelle like nano-structures. The self-assembly behavior of Alg-Ccm was confirmed by DLS and TEM analyses and CMC was determined as shown in Figure 10 and Figure 11 respectively. The CMC values obtained by UV-Vis absorption and fluorescence emission techniques (as tabulated in Table 1) were very much comparable. Formation of Alg-Ccm conjugate micelles in aqueous medium is schematically represented in Scheme 6.

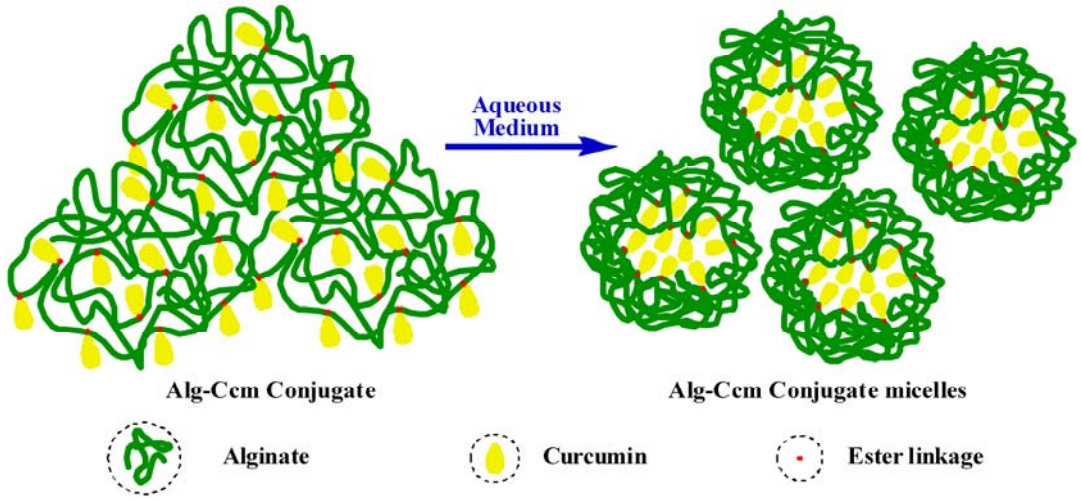

Scheme 6: Schematic presentation of self-assembly of Alg-Ccm conjugates in aqueous medium forming micelle like nano-structures.

Here it is presumed that Ccm being hydrophobic in nature will occupy the inner core of the conjugate micelles and will be safely surrounded by a hydrophilic layer of

Alg. A large discrepancy was found in the size of Alg-Ccm conjugate micelle determined by DLS and TEM analyses. This observation can be attributed to the fact that DLS determines the hydrodynamic diameter, whereas TEM determines the size in dry condition. In this case, highly hydrophilic polymer Alg was probably in swelled condition in aqueous dispersion giving rise to a large hydrodynamic diameter for Alg-Ccm micelles. The high negative surface charge of Alg-Ccm conjugate micelles ensured its potential stability in aqueous medium (Hans, & Lowman, 2002). The rapid hydrolytic degradation of Ccm is one of the major reasons behind its poor bioavailability. Several studies proved that the hydrolytic degradation occurs much faster above the neutral pH (Wang et al., 1997) and these studies also revealed that partially deprotonated Ccm is first fragmented into *trans*-6-(40-hydroxy-30-methoxyphenyl)-2,4-dioxo-5-hexenal which further degrades into smaller fragments like feruloyl methane, vanillin and ferulic acid. As these smaller fragments contribute negligibly towards light absorption, hence decrease in absorbance indicates a proportional decrease in concentration of Ccm in solution. In this study, the same principle was followed to analyze the effect of covalent conjugation towards the stability of Ccm in aqueous medium. Figure 12B shows that formation of Alg-Ccm conjugate protected Ccm from hydrolytic degradation and enhanced the stability of Ccm in water. In aqueous solution, the conjugate remained in self-assembled condition in which hydrophobic Ccm was inside the core of conjugate micelle protected by the hydrophilic Alg shell (as shown in Scheme 6). Thus micelle structure shielded Ccm from hydrolytic degradation to a large extent and made Alg-Ccm highly stable in aqueous medium.

Ccm has the ability to kill cells and it has also been reported that the –OH and –OMe groups in Ccm are responsible for its antioxidant and antiproliferative properties respectively (Ravindran et al. 2009). To get an insight whether conjugation of Ccm to a hydrophilic polymer can exert any effect on the intrinsic potential of Ccm to kill cells, the cytototoxicity of Alg-Ccm was evaluated with L-929 mouse fibroblast cells. Figure 13 qualitatively indicated that the cytotoxic potential of Ccm was retained in the conjugate. Quantitative assessment of cytotoxicity was also done by MTT assay which indicated a concentration dependent decrease in cell viability as shown in Figure 14A. Figure 14B depicts the improved cytotoxic potential of Ccm in conjugated state compared to that of free drug. This observation can be attributed to the enhanced aqueous solubility and stability of Ccm in Alg-Ccm conjugate. Alg-Ccm could get more exposure time and better interaction with the cells due to the enhanced aqueous solubility, better cellular internalization of conjugate micelles and improved stability at physiological condition giving rise to an improved cytotoxic activity.

5.2 Conjugating Curcumin to Water Soluble Polymer Stabilized Gold Nanoparticles via pH Responsive Succinate Linker

AuNPs have emerged as the potential drug delivery vehicle because of its striking features (Giljohann et al. 2010) (Lee et al. 2010) like low cytotoxicity, non-immunogenicity, excellent stability in the nanoscale, easy synthesis and functionalization, tunable surface properties *etc*. Polymers are excellent stabilizing agents for AuNPs. For the surface modification and stabilization of AuNPs, often

ligands or polymers with sulfur atom or groups are chemically adsorbed onto the surface of AuNPs exploiting the superior affinity of Au towards S. In this study AuNPs was stabilized by a water soluble, low molecular weight polymer with free thiol group. The polymer (P1) was synthesized *via* melt polycondensation reaction as shown in Scheme 2. Interestingly, P1 exhibited intense blue fluorescence. Unlike fluorescent polymers, P1 was devoid of any conjugated phenyl chromophores. P1 contained a ring structure resembling *morpholine-2,5-dione* in its polymer chain (Scheme 2). An extensive hyperconjugation present in the heterocyclic ring containing both amide and ester linkages and a pendant $–CH_2SH$ group in close vicinity made P1 fluorescent (Yang et al. 2009). The formation of P1 was confirmed by UV-Vis absorption, fluorescence emission, FTIR and ^1H NMR spectroscopic analyses as shown in Figure 15A, Figure 15B, Figure 16A and Figure 17A respectively. GPC data shown in Table 2 indicated that P1 was basically an oligomer. Then the citrate-reduced AuNPs was modified with P1using the free –SH functionality in it *via* ligand replacement reaction. P1-AuNPs was further modified by succinylation and Ccm conjugation to fabricate the Ccm conjugated P1 stabilized AuNPs (Ccm-SA-P1-AuNPs). The step-wise synthetic route is depicted in Scheme 3. Surface modification of AuNPs at each step of synthesis was confirmed by FTIR analysis as shown in Figure 16. Fabrication of Ccm-SA-P1-AuNPs was further confirmed by ^1H NMR spectrum as shown in Figure 17B. As SPR absorption is highly sensitive to the surface environment of NPs (Liang et al. 2010), hence the red shifts in SPR band of functionalized AuNPs shown in Figure 18 further confirmed each stage of surface modification of AuNPs. Figure 19A shows that the characteristic strong

fluorescence emission of P1 was quenched as the AuNPs was functionalized with P1. Quenching of fluorescence of P1 strongly indicated the chemisorption of P1 on the surface of AuNPs. This type of quenching effect is often observed when a fluorescent species is in close contact with AuNPs (Schneider et al. 2006). XRD pattern (Figure 19B) indicated FCC crystal lattice of Ccm-SA-P1-AuNPs. The XRD data further confirmed that the drug was in amorphous or disordered crystalline phase after its covalent conjugation onto the surface of AuNPs *via* the water soluble capping polymer. The amorphous or disordered crystalline phase of the drug in conjugated state is highly required for unimpeded drug release. The DLS data for the functionalized AuNPs (Table 3) indicated that small sized Ccm conjugated AuNPs might be advantageous to exhibit better EPR effect. The magnitude of ζ-potential of Citrate-AuNPs dropped from -40.2 ± 0.3 mV to -23.1 ± 0.2 mV in P1-AuNPs. This decrease of ζ-potential value may be attributed to PEG (possessing stealth property) which is the backbone for P1 (Manson et al. 2011). SA-P1-AuNPs contained free carboxylate groups on its surface and those carboxylates were in deprotonated state (as $pK_a = 4.2$) at pH = 7.4 (Baek et al. 2009), hence the AuNPs were found to possess surface charge of -40.9 ± 2.74 mV. After Ccm conjugation, the ζ-potential again dropped to -32 ± 0.65 mV in Ccm-SA-P1-AuNPs. Though the surface charge was reduced to certain extent after Ccm conjugation, yet there was sufficient repulsive force in the system to prevent it from aggregation and this was established by the TEM image shown in Figure 20D. As the small sized AuNPs was functionalized with a polymer containing PEG as the backbone and they possess negative surface charge, hence the nano drug delivery vehicle might be able to escape

protein adsorption to a large extent resulting in longer systemic circulation and enhanced EPR effect (Anitha et al. 2011) (Aryal et al. 2009). Results shown in Figure 21 signify Ccm-SA-P1-AuNPs to be pretty stable at physiological condition and the nano system may find potential application as a drug delivery vehicle (Zhang et al.2010). The Ccm conjuagted hydrophilic polymer stabilized AuNPs were found to be readily dispersible in water. Thus conjugation of Ccm to P1 stabilized AuNPs helped in enhancing the aqueous solubility of the hydrophobic drug. In addition, due to the presence of acid cleavable succinate ester linkage (which is fairly stable under physiological condition), Ccm-SA-P1-AuNPs showed slow Ccm release under physiological condition and released the drug efficiently in acidic condition (Figure 22) (Clawson et al. 2011). Thus the release study revealed that Ccm-SA-P1-AuNPs can exhibit pH responsive Ccm release behaviour.

Figure 23A depicts that the intrinsic cytotoxic potential of Ccm was not adversely affected by conjuagtion. In fact, Ccm-SA-P1-AuNPs exhibited superior cytotoxicity to free Ccm towards C6 cancer cells. This observation can be attributed to the augmented solubility of Ccm upon conjuagtion through hydrophilic P1, improved internalization of the small-sized Ccm-SA-P1-AuNPs and facile release of Ccm inside the acidic environment of cancer cells. Fluorescence microscopic images in Figure 24 clearly depicted the facile cellular uptake of the nano-vector by C6 cancer cells.

5.3 Fabrication of Curcumin and Methotrexate Conjugated Biopolymer Stabilized Gold Nanoparticles Based Drug Delivery Vehicles via Green Synthetic Route: Evaluation of Cytotoxicity and Hemolytic Toxicity

It is well established that therapeutic approach of combining two or more anticancer drugs can promote synergism among the different drugs against cancer cells and combination therapy is highly promising in taming MDR in cancer (Hu et al. 2010). At the same time, nano-vectors are capable of enhancing therapeutic efficacy of diverse chemotherapeutics along with improved intracellular uptake and reduction in side-effects. AuNPs based DDS are lucrative from the point of view that they are synthesized in a facile manner, small sized, cytocompatible, suitable for attaching multiple functionality etc. Appropriately functionalized AuNPs as a carrier for drug and other biomolecules are well studied. However, in almost all studies multiple reaction steps are adopted to attach various functionalities onto the surface of AuNPs. Also, many of the reactions are carried out under harsh conditions such as using strong reducing agents, hazardous organic solvents etc. As a result, the modified AuNPs need to go through rigorous purification steps and all these above mentioned factors may have some adverse effect on the stability of engineered DDS. Keeping all these facts in mind, it is reasoned that simultaneous generation and stabilization of AuNPs by mild reducing agent that can work in aqueous medium may be a wise option. Polymers play a significant role in stabilizing AuNPs and provide them with a longer life in systemic circulation. Hence, non-immunogenic biopolymer “alginate” was opted for simultaneous generation and stabilization of AuNPs in “green solvent” water. Biopolymer alginate, existing in brown algae and some bacteria is also considered as a “green chemical” (Yang et al. 2011).

Here it is reasoned that, if we can use the Alg-Ccm conjugate directly for AuNPs synthesis under thermal activation, it may generate Ccm conjugated biopolymer stabilized AuNPs in a single step. Hence, the same route was adopted to get Alg-Ccm AuNPs (as shown in Scheme 4) which was purified in a facile manner by dialysis against water. It has been demonstrated that conjugation of Ccm onto Alginate enhances the aqueous solubility and stability of the hydrophobic drug (Dey and Sreenivasan 2014). Here it was hypothesized that alginate possessing secondary hydroxyl groups can effectively reduce Au(III) to Au(0) and the structure of alginate being oxygen rich, it can effectively stabilize the new born AuNPs and protect them from aggregation. In the present study the main intention was to design a targeted DDS containing two different anticancer drugs to get an idea about the synergistic effect of the two drugs against cancer cells. Here MTX was chosen as the second drug to conjugate onto the surface of Alg-Ccm AuNPs. Because, antifolate drug MTX is structurally analogous to FA and shows targeting effect like FA. Thus MTX can serve both the purpose of active targeting and anticancer drug. However, the main drawback associated with MTX is its cellular efflux and consequent resistance to the drug developed in the targeted cancer cells. In order to offset this fact, MTX conjugates with suitable polymers such as poly (ethyleneglycol), hyaluronic acid, poly (glutamic acid) *etc.* are usually developed for MTX delivery (Riebeseel et al. 2002) (Piper et al. 1983). Here at first, MTX was covalently conjugated to bis(aminopropyl) terminated PEG *via* EDC chemistry using aqueous buffer solution (as shown as *inset* in Scheme 4) and then the MTX conjugate (MP conjugate) was further conjugated onto the surface of Alg-Ccm AuNPs following

the synthetic route shown in Scheme 4. The characteristic SPR absorption of AuNPs shown in Figure 25A proved our hypothesis regarding generation and stabilization of AuNPs by Alg-Ccm conjugate. Figure 25A clearly depicted that the characteristic absorbance of curucmin (at ≈ 427 nm in Alg-Ccm) was masked by the strong SPR band of Alg-Ccm AuNPs. However, the sharp peak at 280 nm evidently indicated the capping of AuNPs by Alg-Ccm conjugate. The XRD pattern of the conjugate in Figure 25B indicated almost amorphous or disordered crystalline phase of Ccm in Alg-Ccm conjugate. However, the XRD pattern of Alg-Ccm AuNPs in Figure 25B showed distinct Bragg reflections corresponding to (111), (200), (220) and (311) Miller indices (at 2θ of 38.3°, 44.3°, 64.7° and 77.6° respectively) confirming face centered cubic (FCC) crystalline geometry of the AuNPs formed by Alg-Ccm conjugate. Formation of water soluble MP conjugate was confirmed by FTIR spectra as shown in Figure 26A. Comparative study of the UV-Vis absorption spectra of bis (aminopropyl) PEG and MP conjugate also established the formation of MP conjugate (Figure 26B). Synthesis of MP@Alg-Ccm AuNPs was further confirmed by SPR absorption, FTIR and ^{1}H NMR spectroscopic analyses as depicted in Figure 27, Figure 28 and Figure 29 respectively. The negative surface charge of Alg-Ccm AuNPs decreased further in MP@Alg-Ccm AuNPs (shown in Table 4). This may be attributed to the presence of PEG on the surface of Alg-Ccm AuNPs upon conjugation with MP conjugate. However, the surface charge was sufficient enough to stabilize the nano-vectors in aqueous dispersion as supported by the TEM images shown in Figure 30.

It is evident from Figure 31 that the cell viability decreased (for both C6 glioma and MCF7 cell lines) with increasing concentration of free Ccm, free MTX and MP@Alg-Ccm AuNPs. However, at each tested concentration, MP@Alg-Ccm AuNPs exhibited significantly higher cytotoxicity than that by each of the free drug. This improved toxicity of MP@Alg-Ccm AuNPs can be attributed to the factors such as (i) synergistic effect of co-administration of two anticancer agents (ii) pleiotropic effect of Ccm and (iii) improved uptake of the nano-sized DDS by both the cells. It can also be reasoned that due to the conjugation of MTX onto the AuNPs through hydrophilic polymer, the efflux of the drug was probably reduced to a large extent resulting in an improved cytotoxic activity.

Figure 32 (A to F) indicated improved uptake of MP@Alg-Ccm AuNPs by both the cells. MTX uptake is known to take place through at least two different carrier systems such as (i) the folate receptors (FR) and (ii) the reduced folate carriers (Kohler et al. 2005). Here both C6 and MCF-7 cells possess FR and MCF-7 cells are also known to be positive for reduced folate carrier (Trippett et al. 2001) (Wang et al. 2004). This can be the reason of improved cellular uptake of MP@Alg-Ccm AuNPs by the cells. In a study by Chen et al. (Chen et al. 2013), it has been shown by microscopic images that a multifunctional fluorescent nanogel based DDS was uptaken in a higher extent by FR positive MDA-MB-231 cells when it was decorated with FA and uptake was lower for the DDS without any FA decoration. Similarly in this study, MCF-7 cells were exposed to MP@Alg-Ccm AuNPs and Alg-Ccm AuNPs both of which was tagged with same density of FITC. Here MCF-7 cell line was chosen for this study as MTX has higher

affinity to reduced folate carriers that are over expressed in MCF-7 cells (Kohler et al. 2005). Comparing the merged fluorescent images in Figure 32G and Figure 32H, it was confirmed that improved uptake of MP@Alg-Ccm AuNPs by MCF-7 cells was due to the targeting efficiency of MTX.

MP@Alg-Ccm AuNPs showed percentage of hemolysis of about 0.11% which is much less than the acceptable limit of 5 % confirming the non-hemolytic nature of the nano-vector. In this study, the AuNPs based DDS contains two cytotoxic drugs but presence of non-immunogenic polymer alginate and biocompatible PEG on the surface of the AuNPs has nullified the hemolytic toxicity of the system.

5.4 Synthesis and Characterization of Glutathione Containing Fluorescent Polymer and Its Curcumin Conjugate for Safer Curcumin Delivery and Label-Free Cellular Imaging

At present, biomaterials with intrinsic photoluminescence are of prime importance. Of late, Yang et al. have developed a family of amino acid based aliphatic, biodegradable, photoluminescent polymers (BPLPs) (Yang et al 2009). In the present study, a water soluble, biodegradable, low molecular weight polymer with inherent fluorescence and containing GSH as one of the monomer was designed. GSH is a natural tripeptide and potential antioxidant that helps in cancer regression. The fluorescent polymer GSHBP was synthesized *via* solvent-free melt poly-condensation reaction as shown in Scheme 5A. Formation of a six-membered cyclic structure (as shown in Scheme 5A) with extensive hyperconjugation was responsible for the auto-fluorescence

in GSHBP (Yang et al. 2009). It was reasoned that the free functional groups (such as –COOH, -SH, -OH) present in GSHBP could be used for essential modification of the polymer without affecting its fluorescence property. Hence, with the aim to develop a fluorescent drug conjugate, GSHBP-Ccm conjugate was synthesized by covalent conjugation of Ccm with the reactive –COOH functionality in GSHBP (Scheme 5B).

GSHBP was thoroughly characterized by UV-Vis absorption and fluorescence emission spectroscopy as shown in Figure 33A and Figure 34A respectively. The water soluble polymer exhibited intense blue fluorescence with a fluorescence Q.Y. of 36 % (Figure 34B). The biodegradation of low molecular weight GSHBP under physiological condition was confirmed by LC and GPC techniques (as depicted in Figure 35A and Figure 35B respectively). The ^{13}C NMR, ^{1}H NMR and FTIR spectra shown in Figure 36, Figure 37A and Figure 38A respectively confirmed the formation of GSHBP. Similarly, Figure 37B and Figure 38B showing the ^{1}H NMR and FTIR spectra of GSHBP-Ccm conjugate respectively, confirmed the covalent conjugation of Ccm to GSHBP. UV-Vis spectra of GSHBP-Ccm exhibited the characteristic absorption band of GSHBP along with the red shifted absorption of Ccm at 428 nm (Figure 39A) indicating covalent conjugation of Ccm to GSHBP (a. Manju and Sreenivasan 2011). In addition; the fluorescence emission of Ccm was blue shifted in the conjugate which is also a validation of the covalent conjugation (*inset* Figure 39B and Figure 40) (Dey and Sreenivasan 2014). The intrinsic fluorescence of GSHBP was retained in the conjugate (Figure 41A).

Here it was hypothesized that the conjugate comprised of hydrophilic polymer GSHBP and hydrophobic drug Ccm, could self-assemble in aqueous medium. It was found that in aqueous medium GSHBP-Ccm self-assembled to form micelles of nano-dimension. It was reasoned that PEG based hydrophilic polymer backbone could form the outer shell and Ccm might occupy the inner core of the micelles as depicted in Scheme 7. Presence of Ccm in the hydrophobic inner core of the conjugate micelles ensured that the drug can be carried safely with the protected outer shell of hydrophilic PEG through the systemic circulation. The conjugate micelles exhibited low negative zeta potential. PEG (possessing stealth potential) constituted the hydrophilic outer shell of the micelles; this might be the reason behind lower surface charge of the GSHBP-Ccm micelles. However, the low negative surface charge was sufficient enough to generate a potentially stable aqueous dispersion of GSHBP-Ccm micelles which was proved by TEM imaging (Figure 41B) of conjugate micelles in aqueous suspension under cryogenic condition. Spherical morphology of the conjugate micelles in aqueous suspension was clearly observed in the cryo-TEM image in Figure 41B.

The hydrodynamic diameter of GSHBP-Ccm conjugate micelles in aqueous dispersion was found to be 140.8 ± 0.77 nm (Figure 42A). The conjugate micelles also exhibited low CMC value of 0.17 mg/mL (Figure 42B). In addition, aqueous solubility of Ccm was also increased upon conjugation with GSHBP polymer. In this study, GSHBP-Ccm conjugate exhibited a slow drug release profile (Figure 43) at physiological condition (*i.e.* in PBS at pH 7.4 and 37 °C temperature). This can be attributed to the fact that the ester linkage between the drug and polymer was fairly

stable at pH 7.4 (physiological condition). In GSHBP-Ccm the drug was residing at the hydrophobic interior of the micelles. Hence, the drug can be safely carried under physiological condition through blood stream.

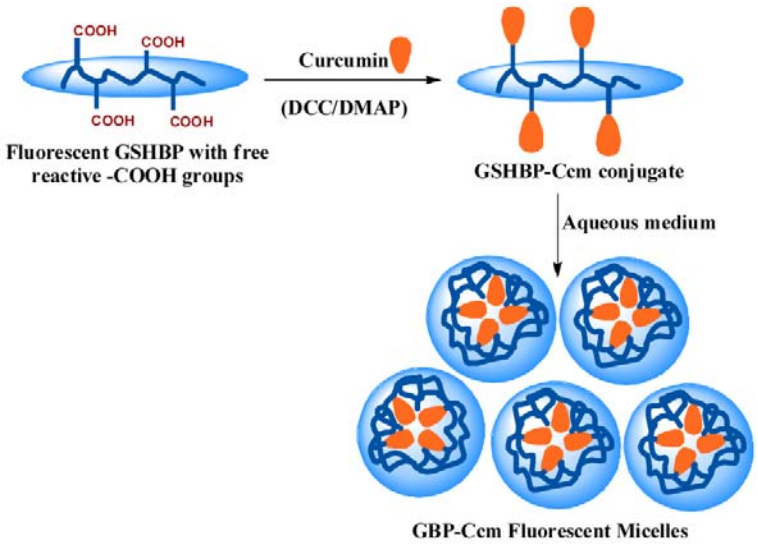

Scheme 7: Schematic representation of micellization of GSHBP-Ccm conjugate in aqueous medium.

GSHBP showed no toxicity (against C6 cancer cells) upto a concentration of 1600 µg/mL (Figure 44A) confirming that GSHBP possessed almost no or very less intrinsic toxicity. Thus the polymer was found to be a good candidate for the fabrication of drug delivery vehicles. The cytotoxic potential of GSHBP-Ccm conjugate was also evaluated by MTT assay against C6 cancer cells and a concentration dependent toxic response of the drug conjugate (Figure 44B) was noted. Interestingly, Ccm in the conjugate showed better toxic response than in the bare form. This observation may be attributed to the better internalization of nano-sized GSHBP-Ccm micelles along with

augmented solubility and stability of Ccm in the conjugate. The drug in GSHBP-Ccm probably experienced a longer exposure time to the cells owing to its enhanced solubility and stability in aqueous medium resulting in improved toxic potential. In the present study, it was also hypothesized that the nano-sized fluorescent micelles could effectively be internalized by cancer cells and might be employed in label-free cellular imaging. Our hypothesis was successfully proved by imaging the C6 cancer cells utilizing the inherent intense blue fluorescence of the polymer (as shown in Figure 45A). This observation clearly indicated that the water soluble, fluorescent polymer with almost no intrinsic toxicity might be a promising candidate for label-free cellular imaging. Fortunately, in this study Ccm was used as the hydrophobic drug that has inherent fluorescence. The characteristic green fluorescence of Ccm was also exploited to prove the internalization of GSHBP-Ccm micelles by C6 cancer cells (Figure 45C).

The hemolytic potential of GSHBP and GSHBP-Ccm conjugate was assessed by determining the percentage of hemolysis. Both the polymer and its Ccm conjugate were found to be non-hemolytic (as the % hemolysis was < 0.1 % for both). Presence of CA, a well-known anticoagulant, in the polymer backbone may have some influence in making the systems non-hemolytic in nature.

CHAPTER 6
SUMMARY AND CONCLUSION

6 Summary and Conclusion

It is now well documented that, although cancer is a disease of old age yet lifestyle plays a prime role in the development of most of the cancers. Studies revealed that only 5 to 10% of all human cancers are caused by genetic factors, whereas lifestyle is responsible for the remaining percentage of cancers in human beings (Anand et al. 2008). It is further supported by the fact that certain types of cancers are more common only in some countries. Dietary habit is an important part of lifestyle that may have certain relation with cancer. For example, Southeast Asia is a continent with low incidence of most of the cancers and people from this continent very often consume turmeric (*curcuma longa*) as one of the spices (Ravindran et al. 2009). Turmeric contains a polyphenolic compound "curcumin" which has chemopreventive and chemotherapeutic activity (Duvoix et al. 2005). Ccm has the potential to be used as a chemotherapeutic agent for the treatment of cancer. But extremely low aqueous solubility, instability and resulting poor bioavailability of Ccm is a barrier to its application as a therapeutic agent for cancer. Considering all these aspects, in this study, nano-sized delivery vehicles were developed based on polymer-drug conjugates and polymer stabilized AuNPs for augmentation of aqueous solubility and stability of Ccm along with safer Ccm delivery to cancer cells.

In order to augment the aqueous solubility and stability of Ccm, the hydrophobic drug was covalently conjugated to non-immunogenic biopolymer Alg. Result showed that 100 mg of Alg-Ccm conjugate contained ~ 1.09 mg of Ccm and the solubility of the

conjugate was more than 10 mg/mL. Thus the aqueous solubility of Ccm in conjugated state was ~ 109 µg/ mL and it was sufficiently higher than that of free Ccm. Results also revealed that Alg-Ccm self-assembled in aqueous medium giving rise to nano-sized spherical micelles. Ccm, being hydrophobic, occupied the inner core of the conjugate micelles and hydrophilic Alg made the outer shell. Such an architecture prevented Ccm from hydrolytic degradation resulting in enhanced stability of the drug under physiological condition. The cytotoxicity evaluations (by both tests on extract method and MTT assay) showed that Alg-Ccm was potentially cytotoxic and covalent conjugation of Ccm had no adverse effect on the intrinsic cytotoxic effect of Ccm. On the contrary, Ccm in conjugated state exhibited improved cytotoxic response against L-929 cells due to augmented solubility of the hydrophobic drug and better cellular internalization of the nano-sized Alg-Ccm conjugate micelles. In conclusion, the non-immunogenic, biopolymer based Alg-Ccm conjugate can be considered as a useful drug conjugate. In Alg-Ccm conjugate, other functional groups are still present for further modifications to make a targeted multifunctional DDS. In addition, the conjugate micelles can encapsulate other hydrophobic drug molecules inside the hydrophobic inner core and can also be used as a nano-structured dual drug delivery vehicle.

In chemotherapeutic treatment, suitably designed drug delivery vectors are required for improved efficacy and reduced side effects. Nano-structured DDS are excellent candidates for delivering chemotherapeutics to the desired site exploiting the leaky tumor vasculature (*i.e.* EPR effect). In the present study, a hybrid nano-structured DDS based on polymer stabilized AuNPs was developed for pH responsive Ccm

delivery. To design the nano-vector, an aliphatic, low molecular weight, water soluble polymer (P1) was synthesized using PEG, CA and L-Cys as the monomers. P1 bearing free thiol functionality was utilized to generate P1-AuNPs from citrate reduced AuNPs through ligand replacement reaction. P1 with free –SH group stabilized the AuNPs which was then succinylated followed by Ccm conjugation to generate Ccm-SA-P1-AuNPs. Ccm-SA-P1-AuNPs was readily dispersible in water and 10 mg of the sample contained 67.5 ± 0.08 μg of Ccm. Thus conjugation of Ccm to AuNPs *via* hydrophilic P1 was aided in enhancing the water solubility of Ccm. The small sized (hydrodynamic size ≈ 43 nm) Ccm-SA-P1-AuNPs with negative surface charge can be easily taken up by cancer cells (by EPR effect). The succinate ester linkage between P1-AuNPs and Ccm being pretty stable at physiological pH (pH = 7.4), very little amount of Ccm was released under physiological condition. However, the acid cleavable succinate ester bond resulted in faster Ccm release at pH 5.3. This indicated that the pH responsive DDS can carry Ccm safely through systemic circulation and release the pay load in cancer tissues (where the pH is low). MTT assay analysis proved that Ccm in Ccm-SA-P1-AuNPs exhibited improved cytotoxic potential than that of free Ccm. This can be attributed to several factors such as improved solubility of the drug, better uptake of the nano-sized DDS by cancer cells and facile release of the drug at lower pH range in cancer cells. Hence, it can be concluded that Ccm-SA-P1-AuNPs can serve as a potential nano-vector for pH responsive Ccm delivery to cancer cells.

In this study, another hybrid nano-structured DDS based on polymer stabilized AuNPs containing two anticancer agents (Ccm and MTX) was also developed. Alg-Ccm

conjugate was used for the simultaneous generation and stabilization of Ccm conjugated biopolymer stabilized AuNPs in aqueous medium. Anticancer drug MTX was conjugated to Alg-Ccm AuNPs system to generate the dual drug conjugated biopolymer stabilized AuNPs. Basically MTX conjugate of bis(aminopropyl) terminated PEG (MP conjugate) was synthesized (in aqueous buffer solution) to conjugate with Alg-Ccm AuNPs through "EDC" chemistry. Thus, dual drug conjugated biopolymer stabilized DDS (MP@Alg-Ccm AuNPs) was fabricated by two simple reaction steps without using any organic solvent. The DDS was designed by utilizing "green chemical" Alg (Yang et al. 2011) in presence of "green solvent" water. It was found that 100 mg of MP@Alg-Ccm AuNPs contained 1.05 ± 0.01 mg of Ccm and 1.26 ± 0.05 mg of MTX. The dual drug conjugated AuNPs were small enough with negative surface charge. Here the AuNPs, being stabilized by Alg and PEG, can easily evade unwanted protein adsorption while circulating through the blood stream. Thus the DDS may have longevity in systemic circulation resulting in augmented EPR effect and improved uptake by cancer cells. MP@Alg-Ccm AuNPs exhibited excellent cytotoxic activity against both C6 and MCF-7 cancer cell lines. This improved ability to kill cancer cells can be attributed to the synergistic effect of two anticancer drugs along with the pleiotropic effect of Ccm and enhanced uptake of the DDS by cancer cells. In addition, conjugation of MTX to hydrophilic polymer could probably redress the problem of drug efflux from the cancer cells. In the present study, fluorescence microscopic images proved the active targeting efficiency of MTX in MCF-7 cells possessing both folate receptors and reduced folate carriers that are required for MTX uptake (Kohler et al.2005). The percentage of

hemolysis of MP@Alg-Ccm AuNPs was found to be much lower than the acceptable limit (5 %) indicating the DDS to be non-hemolytic. In conclusion, MP@Alg-Ccm AuNPs being fabricated by two simple reaction steps *via* "green synthetic route" is pretty interesting from synthetic point of view. In addition, the small sized, negatively charged, biopolymer stabilized AuNPs based DDS may be a promising candidate for targeted combination chemotherapy in cancer treatment.

Of late, Biomaterials with inherent photoluminescence are of leading importance in biomedical field. In this study, with the aim to develop a fluorescent drug conjugate, at first a water soluble, aliphatic, biodegradable, non-toxic polymer (GSHBP) with intrinsic blue fluorescence was synthesized and thoroughly characterized. GSHBP was made of natural tripeptide GSH that is extremely important for its antioxidant property and useful for cancer regression. GSHBP contained free reactive sites like –SH, –OH and –COOH. The free –COOH reactive site of GSHBP was utilized to conjugate Ccm to design fluorescent GSHBP-Ccm conjugate. Each 100 mg of GSHBP-Ccm contained ~ 178 µg Ccm and the solubility of the conjugate was more than 30 mg/mL. Thus GSHBP-Ccm conjugate also augmented the aqueous solubility of Ccm significantly. GSHBP-Ccm conjugate formed nano-structured conjugate micelles in aqueous medium with hydrophobic Ccm occupying the inner core. GSHBP-Ccm conjugate micelles with an outer shell of hydrophilic GSHBP polymer, safely carried Ccm through systemic circulation (at pH = 7.4). The spherical morphology of the conjugate micelles in aqueous dispersion was captured by TEM imaging under cryogenic condition. MTT assay unveiled that GSHBP had almost no intrinsic toxicity whereas, GSHBP-Ccm not only

retained the intrinsic cytotoxic effect of Ccm but also exhibited improved cytotoxic potential than that of the free drug. The reason of improved cytotoxic potential of Ccm in the conjugate can be two-fold, (i) enhanced water solubility due to conjugation with a hydrophilic polymer and (ii) enhanced cellular uptake of the nano-structured Ccm conjugate. However, the most interesting part of the present study was the ability of the fluorescent GSHBP-Ccm conjugate to image cancer cells. The characteristic blue fluorescence of the polymer was retained in the conjugate. C6 cancer cells were imaged exploiting the intrinsic blue fluorescence of GSHBP-Ccm conjugate micelles. Besides, both GSHBP polymer and GSHBP-Ccm conjugate were found to be non-hemolytic in nature. Hence, in conclusion, GSHBP may be used as a safe fluorescent polymer for designing fluorescent biomaterials. GSHBP-Ccm conjugate can be helpful for safer Ccm delivery along with label-free cellular imaging. Thus GSHBP-Ccm conjugate can be considered as a biomaterial with theranostic potential. In addition, the other free reactive functional groups in GSHBP-Ccm can be utilized to design a multifunctional targeted nano-structured DDS. Moreover, the hydrophobic inner core of GSHBP-Ccm conjugate micelles can be useful to encapsulate other hydrophobic drugs to generate dual drug containing polymeric micelles.

Thus all the DDS designed in the present work are promising candidates for chemotherapy. Future study will be focused on (i) Development of multifunctional drug delivery vectors with intrinsic fluorescence based on fluorescent polymers, (ii) Studying the effect of combination of chemotherapeutics on multidrug resistant cancer cell lines and (iii) *in vivo* study to choose the better platform for anticancer drug delivery.

References

Agarwal BB, Shishodia S (2006) Molecular targets of dietary agents for prevention and therapy of cancer. *Biochem Pharmacol* 71: 1397–1421.

Aggarwal BB (2004) Nuclear factor-kappa B: the enemy within. *Cancer Cell* 6: 203-208.

Aggarwal BB, Kumar A, Bharti AC (2003) Anticancer potential of curcumin: preclinical and clinical studies. *Anticancer Res* 23: 363-398.

Aggarwal BB, Sung B (2009) Pharmacological basis for the role of curcumin in chronic diseases: an age-old spice with modern targets. *Trends Pharmacol Sci* 30: 85-94.

Aggarwal S, Takada Y, Singh S, Myers JN, Aggarwal BB (2004) Inhibition of growth and survival of human head and neck squamous cell carcinoma cells by curcumin via modulation of nuclear factor-kappaB signaling. *Int J Cancer* 111: 679-692.

Alexis F, Pridgen E, Molnar LK, Farokhzad OC (2008) Factors affecting the clearance and biodistribution of polymeric nanoparticles. *Mol Pharm* 5: 505–515.

Allen TM (2002) Ligand-targeted therapeutics in anticancer therapy. *Nat Rev Cancer* 2: 750-763.

Allen TM, Cullis PR (2004) Drug delivery systems: entering the mainstream. *Science* 303: 1818-1822.

Anand P, Kunnumakkara AB, Newman RA, Aggarwal BB (2007) Bioavailability of curcumin: problems and promises. *Mol Pharm* 4: 807-818.

Anand P, Sundaram C, Jhurani S, Kunnumakkara AB, Aggarwal BB (2008) Curcumin and cancer: An ‘‘old-age” disease with an ‘‘age-old” solution. *Cancer Lett* 267: 133–164.

Anitha A, Deepagan VG, Rani VVD, Menon D, Nair SV, Jayakumar R (2011) Preparation, characterization, in vitro drug release and biological studies of curcumin loaded dextran sulphate–chitosan nanoparticles. *Carbohydr Polym* 84: 1158-1164.

Aryal S, Grailer JJ, Pilla S, Steeber DA, Gong S (2009) Doxorubicin conjugated gold nanoparticles as water-soluble and pH-responsive anticancer drug nanocarriers. *J Mater Chem* 19: 7879-7884.

Bae YH, Park K (2011) Targeted drug delivery to tumors: myths, reality and possibility. *J Control Release* 153: 198-205.

Baek SH, Chang WJ, Baek JY, Yoon DS, Bashir R, Lee SW (2009) Dielectrophoretic technique for measurement of chemical and biological interactions. *Anal Chem* 81: 7737-7742.

Balasubramanian SK, Yang L, Yung LY, Ong CN, Ong WY, Yu LE (2010) Characterization, purification, and stability of gold nanoparticles. *Biomaterials* 31: 9023-9030.

Banerjee D, Mayer-Kuckuk P, Capiaux G, Budak-Alpdogan T, Gorlick R, Bertino JR (2002) Novel aspects of resistance to drugs targeted to dihydrofolate reductase and thymidylate synthase. *Biochim Biophys Acta* 1587: 164-173.

Boyer C, Bulmus V, Davis TP, Ladmiral V, Liu J, Perrier S (2009) Bioapplications of RAFT polymerization. *Chem Rev* 109: 5402-5436**.**

Brust M, Walker M, Bethell D, Schiffrin DJ, Whyman R (1994) Synthesis of thiol-derivatised gold nanoparticles in a two-phase liquid-liquid system. *J Chem Soc Chem Commun* 801-802.

Byrne JD, Betancourt T, Brannon-Peppas L (2008) Active targeting schemes for nanoparticle systems in cancer therapeutics. *Adv Drug Deliv Rev* 60: 1615-1626.

Cairns J (1975) Mutation selection and the natural history of cancer. *Nature* 255: 197-200.

Chen C, Liu G, Liu X, Pang S, Zhu C, Lv L, Ji J (2011) Photo-responsive, biocompatible polymeric micelles self-assembled from hyperbranched polyphosphate-based polymers. *Polym Chem* 2: 1389–1397.

Chen WC, Lai YA, Lin YC, Ma JW, Huang LF, Yang NS, Ho CT, Kuo SC, Way TD (2013) Curcumin suppresses doxorubicin-induced epithelial-mesenchymal transition via the inhibition of TGF-β and PI3K/AKT signaling pathways in triple-negative breast cancer cells. *J Agric Food Chem* 61: 11817-11824.

Chen Y, Wilbon PA, Zhou J, Nagarkatti M, Wang C, Chu F, Tang C (2013) Multifunctional self-fluorescent polymer nanogels for label-free imaging and drug delivery. *Chem Commun* 49: 297-299.

Chen YH, Tsai CY, Huang PY, Chang MY, Cheng PC, Chou CH, Chen DH, Wang CR, Shiau AL, Wu CL (2007) Methotrexate conjugated to gold nanoparticles inhibits tumor growth in a syngeneic lung tumor model. *Mol Pharm* 4: 713–722.

Cheng Y, Samia CA, Meyers JD, Panagopoulos I, Fei B, Burda C (2008) Highly efficient drug delivery with gold nanoparticle vectors for *in vivo* photodynamic therapy of cancer. *J Am Chem Soc* 130: 10643-10647.

Chi H, Xu K, Xue D, Song C, Zhang W, Wang P (2007) Synthesis of dodecenyl succinic anhydride (DDSA) corn starch. *Food Res Int* 40: 232–238.

Chidambaram M, Manavalan R, Kathiresan K (2011) Nanotherapeutics to overcome conventional cancer chemotherapy limitations. *J Pharm Pharm Sci* 14: 67-77.

Cho EC, Xie J, Wurm PA, Xia Y (2009) Understanding the role of surface charges in cellular adsorption versus internalization by selectively removing gold nanoparticles on the cell surface with a I2/KI etchant. *Nano Lett* 9:1080-1084.

Choi BH, Kim CG, Lim Y, Shin SY, Lee YH (2008) Curcumin down-regulates the multidrug-resistance mdr1b gene by inhibiting the PI3K/Akt/NF kappa B pathway. *Cancer Lett* 259: 111-118.

Clawson C, Ton L, Aryal S, Fu V, Esener S, Zhang L (2011) Synthesis and characterization of lipid-polymer hybrid nanoparticles with pH-triggered PEG shedding. *Langmuir* 27: 10556–10561.

Danhier F, Feron O, Préat V (2010) To exploit the tumor microenvironment: Passive and active tumor targeting of nanocarriers for anti-cancer drug delivery *J Control Release* 148: 135-146.

Daniel MC, Astruc D (2004), Gold nanoparticles: assembly, supramolecular chemistry, quantum-size-related properties, and applications toward biology, catalysis, and nanotechnology. *Chem Rev* 104: 293-346.

Dey S, Sreenivasan K (2014) Conjugation of curcumin onto alginate enhances aqueous solubility and stability of curcumin. *Carbohydr Polym* 99: 499-507.

Dhanasekaran S, Biswal BK, Sumantran VN, Verma RS (2013) Augmented sensitivity to methotrexate by curcumin induced overexpression of folate receptor in KG-1 cells. *Biochimie* 95: 1567-1573.

Duncan B, Kim C, Rotello VM (2010) Gold nanoparticle platforms as drug and biomacromolecule delivery systems. *J Control Release* 148: 122-127.

Duncan R (2003) The Dawning Era of polymer therapeutics. *Nat Rev Drug Discov* 2: 347-360.

Duncan R (2006) Polymer conjugates as anticancer nanomedicines. *Nat Rev Cancer* 6: 688-701.

Durgadas CV, Sharma CP, Paul W, Rekha MR, Sreenivasan K (2012) Aggregation of gold nanoparticles followed by methotrexate release enables Raman imaging of drug delivery into cancer cells. *J Nanopart Res* 14: 1127-1138.

Duthie SJ (2001) Folic-acid-mediated inhibition of human colon-cancer cell growth. *Nutrition* 17: 736-737.

Duve CD, Barsy TD, Poole B, Trouet A, Tulkens P, Hoof FV (1974) Lysosomotropic agents. *Biochem Pharmacol* 23: 2495–2531.

Duvoix A, Blasius R, Delhalle S, Schnekenburger M, Morceau F, Henry E, Dicato M, Diederich M (2005) Chemopreventive and therapeutic effects of curcumin. *Cancer Lett* 223: 181-190.

Ejendal KF, Hrycyna CA (2002) Multidrug resistance and cancer: the role of the human ABC transporter ABCG2. *Curr Protein Pept Sci* 3: 503–511.

Espinosa E, Zamora P, Feliu J, González BM (2003) Classification of anticancer drugs--a new system based on therapeutic targets. *Cancer Treat Rev* 29: 515-523.

Farokhzad OC, Langer R (2009) Impact of nanotechnology on drug delivery. *ACS Nano* 3: 16–20.

Feinberg AP, Ohlsson R, Henikoff S (2006) The epigenetic progenitor origin of human cancer. *Nat Rev Genet* 7: 21–33.

Ferrari M (2005) Cancer nanotechnology: opportunities and challenges. *Nat Rev Cancer* 5: 161-171.

Frens G (1973) Controlled nucleation for the regulation of the particle size in monodisperse gold suspensions. *Nat Phys Sci* 241: 20-22.

Futreal PA, Coin L, Marshall M, Down T, Hubbard T, Wooster R, Rahman N, Stratton MR (2004) A census of human cancer genes. *Nat Rev Cancer* 4: 177–183.

Ganta S, Amiji M (2009) Coadministration of Paclitaxel and curcumin in nanoemulsion formulations to overcome multidrug resistance in tumor cells. *Mol Pharm* 6: 928-939.

Ghosh SK, Pal T (2007) Interparticle coupling effect on the surface plasmon resonance of gold nanoparticles: from theory to applications. *Chem Rev* 107: 4797-4862.

Giljohann DA, Seferos DS, Daniel WL, Massich MD, Patel PC, Mirkin CA (2010) Gold nanoparticles for biology and medicine. *Angew Chem Int Ed Engl* 49: 3280-3294.

GLOBOCAN 2012: Estimated Cancer Incidence, Mortality and Prevalence Worldwide in 2012. [Online]. Available: http://globocan.iarc.fr/Pages/fact_sheets_cancer.aspx [Accessed on 7th November 2014].

Gref R, Minamitake Y, Peracchia MT, Trubetskoy V, Torchilin V, Langer R (1994) Biodegradable long-circulating polymeric nanospheres. *Science* 263:1600-1603.

Guo O, Li X, Yang Y, Wei J, Zhao Q, Luo F, Qian Z (2014) Enhanced 4T1 breast carcinoma anticancer activity by co-delivery of doxorubicin and curcumin with core-shell drug-carrier based on heparin modified poly(L-lactide) grafted polyethylenimine cationic nanoparticles. *J Biomed Nanotechnol* 10: 227-237.

Gyawali D, Zhou S, Tran RT, Zhang Y, Liu C, Bai X, Yang J (2013) Fluorescence imaging enabled biodegradable photostable polymeric micelle. *Adv Healthc Mater* 3: 182-186.

Hanahan D, Weinberg RA (2000) The hallmarks of cancer. *Cell* 100: 57–70.

Hans ML, Lowman AM (2002) Biodegradable nanoparticles for drug delivery and targeting. *Curr Opin Solid State Mater Sci* 6: 319–327.

Hong R, Han G, Fernández JM, Kim BJ, Forbes NS, Rotello VM (2006) Glutathione-mediated delivery and release using monolayer protected nanoparticle carriers. *J Am Chem Soc* 128: 1078-1079.

Hu CM, Aryal S, Zhang L (2010) Nanoparticle-assisted combination therapies for effective cancer treatment. *Ther Deliv* 1: 323–334.

Huang SP, Huang GS, Chen SA (2007) Deep blue electroluminescent phenylene-based polymers. *Synth Met* 157: 863-871.

Huang X, Qian W, El-Sayed IH, El-Sayed MA (2007) The potential use of the enhanced nonlinear properties of gold nanospheres in photothermal cancer therapy. *Lasers Surg Med* 39: 747-753.

Jain PK, El-Sayed IH, El-Sayed MA (2007) Au nanoparticles target cancer. *Nano Today* 2: 18-29.

Jain RK, Stylianopoulos T (2010) Delivering nanomedicine to solid tumors. *Nat Rev Clin Oncol* 7: 653-664.

Jamieson T, Bakhshi R, Petrova D, Pocock R, Imani M, Seifalian AM (2007) Biological applications of quantum dots. *Biomaterials* 28:4717-4732.

Jemal A, Bray F, Center MM, Ferlay J, Ward E, Forman D (2011) Global cancer statistics. *CA Cancer J Clin* 61: 69–90.

Karnofsky DA (1968) Mechanism of action of anticancer drugs at a cellular level. *CA Cancer J Clin* 18: 232-234.

Kim CY, Bordenave N, Ferruzzi MG, Safavy A, Kim KH (2011) Modification of curcumin with polyethylene glycol enhances the delivery of curcumin in preadipocytes and its antiadipogenic property. *J Agric Food Chem* 59: 1012-1019.

Knop K, Hoogenboom R, Fischer D, Schubert US (2010) Poly(ethylene glycol) in drug delivery: pros and cons as well as potential alternatives. *Angew Chem Int Ed Engl* 49: 6288-6308.

Kohler N, Sun C, Wang J, Zhang M (2005) Methotrexate-modified superparamagnetic nanoparticles and their intracellular uptake into human cancer cells. *Langmuir* 21: 8858-8864.

Kumar A, Huo S, Zhang X, Liu J, Tan A, Li S, Jin S, Xue X, Zhao YY, Ji T, Han L, Liu H, Zhang XN, Zhang J, Zou G, Wang T, Tang S, Liang XJ (2014) Neuropilin-1-targeted gold nanoparticles enhance therapeutic efficacy of platinum(iv) drug for prostate cancer treatment. *ACS Nano* 8: 4205-4220.

Lammers T, Kiessling F, Hennink WE, Storm G (2012) Drug targeting to tumors: principles, pitfalls and (pre-) clinical progress. *J Control Release* 161: 175–187.

Lantz RC, Chen GJ, Solyom AM, Jolad SD, Timmermann BN (2005) The effect of turmeric extracts on inflammatory mediator production. *Phytomedicine* 12: 445-452.

Lao CD, Ruffin MT 4th, Normolle D, Heath DD, Murray SI, Bailey JM, Boggs ME, Crowell J, Rock CL, Brenner DE (2006) Dose escalation of a curcuminoid formulation. *BMC Complement Altern Med* 6: 10.

Larson N, Ghandehari H (2012) Polymeric conjugates for drug delivery. *Chem Mater* 24: 840-853.

Lee K, Lee H, Bae KH, Park TG (2010) Heparin immobilized gold nanoparticles for targeted detection and apoptotic death of metastatic cancer cells. *Biomaterials* 31: 6530–6536.

Lee WI, Bae Y, Bard AJ (2004) Strong blue photoluminescence and ECL from OH-terminated PAMAM dendrimers in the absence of gold nanoparticles. *J Am Chem Soc* 126: 8358-8359.

Lehár J, Krueger AS, Avery W, Heilbut AM, Johansen LM, Price ER, Rickles RJ, Short GF 3rd, Staunton JE, Jin X, Lee MS, Zimmermann GR, Borisy AA (2009) Synergistic drug combinations tend to improve therapeutically relevant selectivity. *Nat Biotechnol* 27: 659–666.

Li J, Wang Y, Yang C, Wang P, Oelschlager DK, Zheng Y, Tian DA, Grizzle WE, Buchsbaum DJ, Wan M (2009) Polyethylene glycosylated curcumin conjugate inhibits pancreatic cancer cell growth through inactivation of jab1. *Mol Pharmcol* 76: 81-90.

Li L, Braiteh FS, Kurzrock R (2005) Liposome-encapsulated curcumin: *in vitro* and *in vivo* effects on proliferation, apoptosis, signaling, and angiogenesis. *Cancer* 104: 1322-1331.

Li Q, Liu CG, Huang ZH, Xue FF (2011) Preparation and characterization of nanoparticles based on hydrophobic alginate derivative as carriers for sustained release of vitamin D3. *J Agric Food Chem* 59: 1962–1967.

Li SD, Huang L (2008) Pharmacokinetics and biodistribution of nanoparticles. *Mol Pharm* 5: 496-504.

Liang M, Lin IC, Whittaker MR, Minchin RF, Monteiro MJ, Toth I (2010) Cellular uptake of densely packed polymer coatings on gold nanoparticles. *ACS Nano* 4: 403-413.

Lu J, Owen SC, Shoichet MS (2011) Stability of self-assembled polymeric micelles in serum. *Macromolecules* 44: 6002-6008.

Maeda H, Sawa T, Konno T (2001) Mechanism of tumor-targeted delivery of macromolecular drugs, including the EPR effect in solid tumor and clinical overview of the prototype polymeric drug SMANCS. *J Control Release* 74: 47-61.

Maeda H, Wu J, Sawa T, Matsumura Y, Hori K (2000) Tumor vascular permeability and the EPR effect in macromolecular therapeutics: a review. *J Control Release* 65: 271–284.

Mahmoudi M, Lynch I, Ejtehadi MR, Monopoli MP, Bombelli FB, Laurent S (2011) Protein-nanoparticle interactions: opportunities and challenges. *Chem Rev* 111: 5610-5637.

Maiti K, Mukherjee K, Gantait A, Saha BP, Mukherjee PK (2007) Curcumin–phospholipid complex: Preparation, therapeutic evaluation and pharmacokinetic study in rats. *Int J Pharm* 330: 155-163.

Mancini MC, Kairdolf BA, Smith AM, Nie S (2008) Oxidative quenching and degradation of polymer-encapsulated quantum dots: new insights into the long-term fate and toxicity of nanocrystals in vivo. *J Am Chem Soc* 130: 10836-10837.

Manju S, Sharma CP, Sreenivasan K (2011) Targeted coadministration of sparingly soluble paclitaxel and curcumin into cancer cells by surface engineered magnetic nanoparticles. *J Mater Chem* 21: 15708-15717.

a. Manju S, Sreenivasan K (2011) Conjugation of curcumin onto hyaluronic acid enhances its aqueous solubility and stability. *J Colloid Interface Sci* 359: 318-325.

b. Manju S, Sreenivasan K (2011) Enhanced drug loading on magnetic nanoparticles by layer-by-layer assembly using drug conjugates: blood compatibility evaluation and targeted drug delivery into cancer cells. *Lanagmuir* 27: 14489-14496.

c. Manju S, Sreenivasan K (2011) Synthesis and characterization of a cytotoxic cationic polyvinylpyrrolidone-curcumin conjugate. *J Pharm Sci* 100: 504-511.

Manju S, Sreenivasan K (2012) Gold nanoparticles generated and stabilized by water soluble curcumin-polymer conjugate: blood compatibility evaluation and targeted drug delivery onto cancer cells. *J Colloid Interface Sci* 368: 144-151.

Manson J, Kumar D, Meenan BJ, Dixon D (2011) Polyethylene glycol functionalized gold nanoparticles: the influence of capping density on stability in various media *Gold bull* 44: 99-105.

Matsumura Y, Maeda H (1986) A new concept for macromolecular therapeutics in cancer chemotherapy: Mechanism of tumoritropic accumulation of proteins and the antitumor agent smancs. *Cancer Res* 46: 6387–6392.

Matyjaszewski K, Xia J (2001) Atom transfer radical polymerization. *Chem Rev* 101: 2921-2990.

Mauring K, Krasnenko V, Miller S (2007) Photophysics of the blue fluorescent protein. *J Lumin* 122: 291-293.

Moorthi C, Manavalan R, Kathiresan K (2011) Nanotherapeutics to overcome conventional cancer chemotherapy limitations. *J Pharm Pharm Sci*14: 67–77.

Motterlini R, Foresti R, Bassi R, Green CJ (2000) Curcumin, an antioxidant and anti-inflammatory agent, induces heme oxygenase-1 and protects endothelial cells against oxidative stress. *Free Radic Biol Med* 28: 1303-1312.

Mukherjee S (2010) *The Emperor of All Maladies: A Biography of Cancer*. Scribner, United States.

Mythri RB, Bharath MM (2012) Curcumin: a potential neuroprotective agent in Parkinson's disease. *Curr Pharm Des* 18: 91-99.

Nogueira DR, Tavano L, Mitjans M, Pérez L, Infante MR, Vinardell MP (2013) *In vitro* antitumor activity of methotrexate via pH-sensitive chitosan nanoparticles. *Biomaterials* 34: 2758-2772.

Paciotti GF, Kingston DGI, Tamarkin L (2006) Colloidal gold nanoparticles: a novel nanoparticle platform for developing multifunctional tumor-targeted drug delivery vectors. *Drug Dev Res* 67: 47–54.

Paciotti GF, Myer L, Weinreich D, Goia D, Pavel N, McLaughlin RE, Tamarkin L (2004) Colloidal gold: a novel nanoparticle vector for tumor directed drug delivery. *Drug Deliv* 11: 169-183.

Pan MH, Huang TM, Lin JK (1999) Biotransformation of curcumin through reduction and glucuronidation in mice. *Drug Metab Dispos* 27: 486-494.

Pandey MK, Kumar S, Thimmulappa RK, Parmar VS, Biswal S, Watterson AC (2011) Design, synthesis and evaluation of novel PEGylated curcumin analogs as potent Nrf2 activators in human bronchial epithelial cells. *Eur J Pharm Sci* 43: 16 – 24.

Pawar SN, Edgar KJ (2011) Chemical modification of alginates in organic solvent systems. *Biomacromolecules* 12: 4095−4103.

Piper JR, McCaleb GS, Montgomery JA (1983) A synthetic approach to poly(gamma-glutamyl) congugates of methotrexate. *J Med Chem* 26: 291-294.

Piper JR, McCaleb GS, Montgomery JA (1983) A synthetic approach to poly(gamma-glutamyl) congugates of methotrexate. *J Med Chem* 26: 291-294.

Ravindran J, Prasad S, Aggarwal BB (2009) Curcumin and cancer cells: how many ways can curry kill tumor cells selectively? *AAPS J* 11: 495-510.

Ravindranath V, Chandrasekhara N (1980) Absorption and tissue distribution of curcumin in rats. *Toxicology* 16: 259-265.

Riebeseel K, Biedermann E, Löser R, Breiter N, Hanselmann R, Mülhaupt R, Unger C, Kratz F (2002) Poly(ethylene glycol) conjugates of methotrexate varying in their molecular weight from MW 750 to MW 40000: synthesis, characterization, and structure-activity relationships *in vitro* and *in vivo*. *Bioconjug Chem* 13**:** 773-785.

Ringsdorf H (1975) Structure and properties of pharmacologically active polymers. *J Polym Sci Polym Symp* 51:135-153.

Safavy A, Raisch KP, Mantena S, Sanford LL, Sham SW, Krishna NR, Bonner JA (2007) Design and development of water-soluble curcumin conjugates as potential anticancer agents. *J Med Chem* 50: 6284–6288.

Schneider G, Decher G, Nerambourg N, Praho R, Werts MH, Blanchard-Desce M (2006) Distance-dependent fluorescence quenching on gold nanoparticles ensheathed with layer-by-layer assembled polyelectrolytes. *Nano Lett* 6: 530-536.

Serrano CA, Zhang Y, Yang J, Schug KA (2011) Matrix-assisted laser desorption/ionization mass spectrometric analysis of aliphatic biodegradable photoluminescent polymers using new ionic liquid matrices. *Rapid Commun Mass Spectrom* 25: 1152–1158.

Shan J, Tenhu H (2007) Recent advances in polymer protected gold nanoparticles: synthesis, properties and applications. *Chem Commun* 4580–4598.

Sharma RA, Gescher AJ, Steward WP (2005) Curcumin: the story so far. *Eur J Cancer* 41: 1955–1968.

Shi M, Cai Q, Yao L, Mao Y, Ming Y, Ouyang G (2006) Antiproliferation and apoptosis induced by curcumin in human ovarian cancer cells. *Cell Biol Int* 30: 221-226.

Shishodia S, Amin HM, Lai R, Aggarwal BB (2005) Curcumin (diferuloylmethane) inhibits constitutive NF-kappaB activation, induces G1/S arrest, suppresses proliferation, and induces apoptosis in mantle cell lymphoma. *Biochem Pharmacol* 70: 700–713.

Shoba G, Joy D, Joseph T, Majeed M, Rajendran R, Srinivas PS (1998) Influence of piperine on the pharmacokinetics of curcumin in animals and human volunteers. *Planta Med* 64: 353-356.

Sindhu K, Rajaram A, Sreeram KJ, Rajaram R (2014) Curcumin conjugated gold nanoparticle synthesis and its biocompatibility. *RSC Adv* 4: 1808-1818.

Singh DK, Jagannathan R, Khandelwal P, Abraham PM, Poddar P (2013) In situ synthesis and surface functionalization of gold nanoparticles with curcumin and their antioxidant properties: an experimental and density functional theory investigation. *Nanoscale* 5: 1882-1893.

Song S, Wang Z, Qian Y, Zhang L, Luo E (2012) The release rate of curcumin from calcium alginate beads regulated by food emulsifiers. *J Agric Food Chem* 60: 4388−4395.

Sumer B, Gao J (2008) Theranostic nanomedicine for cancer. *Nanomedicine (Lond)* 3: 137-140.

Szakács G, Paterson JK, Ludwig JA, Booth-Genthe C, Gottesman MM. (2006) Targeting multidrug resistance in cancer. *Nat Rev Drug Discov* 5: 219-234.

a. Tang H, Murphy CJ, Zhang B, Shen Y, Sui M, Van KEA, Feng X, Murdoch WJ (2010) Amphiphilic curcumin conjugate-forming nanoparticles as anticancer prodrug and drug carriers: in vitro and in vivo effects. *Nanomedicine (Lond)* 5: 855-865.

b. Tang H, Murphy CJ, Zhang B, Shen Y, Van KEA, Murdoch WJ, Radosz M (2010) Curcumin polymers as anticancer conjugates. *Biomaterials* 31: 7139-7149.

Torchilin VP (2012) Multifunctional nanocarriers. *Adv Drug Deliv Rev* 64: 302-315.

Torchilin VP, Trubetskoy VS (1995) Which polymers can make nanoparticulate drug carriers long-circulating? *Adv Drug Deliv Rev* 16: 141-155.

Trippett TM, Garcia S, Manova K, Mody R, Cohen-Gould L, Flintoff W, Bertino JR (2001) Localization of a human reduced folate carrier protein in the mitochondrial as well as the cell membrane of leukemia cells. *Cancer Res* 61: 1941-1947.

Turkevitch J, Stevenson PC, Hillier J (1951) A study of the nucleation and growth processes in the synthesis of colloidal gold. *Discuss Faraday Soc* 11: 55-75.

Wadajkar AS, Kadapure T, Zhang Y, Cui W, Nguyen KT, Yang J (2012) Dual-imaging enabled cancer-targeting nanoparticles. *Adv Healthc Mater* 1: 450-456.

Wang D, Imae T (2004) Fluorescence emission from dendrimers and its pH dependence. *J Am Chem Soc* 126: 13204-13205.

Wang F, Wang YC, Dou S, Xiong MH, Sun TM, Wang J (2011) Doxorubicin-tethered responsive gold nanoparticles facilitate intracellular drug delivery for overcoming multidrug resistance in cancer cells. *ACS Nano* 5: 3679-3692.

Wang S, Chen KJ, Wu TH, Wang H, Lin WY, Ohashi M, Chiou PY, Tseng HR (2010) Photothermal effects of supramolecularly assembled gold nanoparticles for the targeted treatment of cancer cells. *Angew Chem Int Ed Engl* 49: 3777-3781.

Wang Y, Yin H, Wang L, Shuboy A, Lou J, Han B, Zhang X, Li J (2013) Curcumin as a potential treatment for Alzheimer's disease: a study of the effects of curcumin on hippocampal expression of glial fibrillary acidic protein. *Am J Chin Med* 41: 59-70.

Wang Y, Zhao R, Goldman ID (2004) Characterization of a folate transporter in HeLa cells with a low pH optimum and high affinity for pemetrexed distinct from the reduced folate carrier. *Clin Cancer Res*10: 6256-6264.

Wang YJ, Pan MH, Cheng AL, Lin LI, Ho YS, Hsieh CY, Lin JK (1997) Stability of curcumin in buffer solutions and characterization of its degradation products. *J Pharm Biomed Anal* 15: 1867-1876.

Williams ATR, Winfield SA, Miller JN (1983) Relative Fluorescence Quantum Yields Using a Computer-controlled Luminescence Spectrometer. *Analyst* 108: 1067-1071.

Wu D, Liu Y, He C, Goh SH (2005) Blue Photoluminescence from Hyperbranched Poly(amino esters). *Macromolecules* 38: 9906-9909.

Wu W, Shen J, Banerjee P, Zhou S (2011) Water-dispersible multifunctional hybrid nanogels for combined curcumin and photothermal therapy. *Biomaterials* 32: 598-609.

Yang J, Gautam S (2013) *Biodegradable photoluminescent polymers*, US Patent US2013/0345369A1.

Yang J, Zhang Y, Gautam S, Liu L, Dey J, Chen W, Mason RP, Serrano CA, Schug KA, Tang L (2009) Development of aliphatic biodegradable photoluminescent polymers. *Proc Natl Acad Sci U S A* 106: 10086-10091.

Yang JS, Ren HB, Xie YJ (2011) Synthesis of amidic alginate derivatives and their application in microencapsulation of λ-cyhalothrin. *Biomacromolecules* 12: 2982-2987.

Yang KY, Lin LC, Tseng TY, Wang SC, Tsai TH (2007) Oral bioavailability of curcumin in rat and the herbal analysis from Curcuma longa by LC-MS/MS. *J. Chromatogr B Analyt Technol Biomed Life Sci* 853: 183–189.

Yang L, Zhang B, Wen L, Liang Q, Zhang LM (2007) Amphiphilic cholesteryl grafted sodium alginate derivative: Synthesis and self-assembly in aqueous solution. *Carbohydr Polym* 68: 218–225.

Yang R, Zhang S, Kong D, Gao X, Zhao Y, Wang Z (2012) Biodegradable polymer-curcumin conjugate micelles enhance the loading and delivery of low-potency curcumin. *Pharm Res* 29: 3512-3525.

Yoon SA, Choi JR, Kim JO, Shin JY, Zhang X, Kang JH (2010) Influence of reduced folate carrier and dihydrofolate reductase genes on methotrexate-induced cytotoxicity. *Cancer Res Treat* 42: 163-171.

Zhang X, Chibli H, Mielke R, Nadeau J (2011) Ultrasmall gold-doxorubicin conjugates rapidly kill apoptosis-resistant cancer cells. *Bioconjug Chem* 22: 235-243.

Zhang Y, Tran RT, Qattan IS, Tsai YT, Tang L, Liu C, Yang J (2013) Fluorescence imaging enabled urethane-doped citrate-based biodegradable elastomers. *Biomaterials* 34: 4048-4056.

Zhang Y, Yang J (2013) Design strategies for fluorescent biodegradable polymeric biomaterials. *J Mater Chem B Mater Biol Med* 1: 132-148.

Zhang Z, Jia J, Lai Y, Ma Y, Weng J, Sun L (2010) Conjugating folic acid to gold nanoparticles through glutathione for targeting and detecting cancer cells. *Bioorg Med Chem* 18: 5528-5534

List of Publications

Publications arising from the thesis

1. **S. Dey** and K. Sreenivasan, 'Conjugation of Curcumin onto Alginate Enhances Aqueous Solubility and Stability of Curcumin', *Carbohydr. Polym.*, 2014, **99**, 499– 507.
2. **S. Dey** and K. Sreenivasan, 'Conjugating Curcumin to Water Soluble Polymer Stabilized Gold Nanoparticles via pH Responsive Succinate Linker', *J. Mater. Chem. B*, 2015, **3**, 824 – 833.
3. **S. Dey**, M. C. D. Sherly, M. R. Rekha and K. Sreenivasan, 'Alginate Stabilized Gold Nanoparticle as Multidrug Carrier: Evaluation of Cellular Interactions and Hemolytic Potential', *Carbohydr. Polym.*, 2016, **136**, 71–80.
4. **S. Dey**, L. A. Ambattu, P. R. Hari, M. R. Rekha and K. Sreenivasan, 'Glutathione-Bearing Fluorescent Polymer-Curcumin Conjugate Enables Simultaneous Drug Delivery and Label-free Cellular Imaging', *Polymer,* 2015, **75**, 25 – 33.

Conference Proceedings

1. **S. Dey** and K. Sreenivasan, 'Synthesis and Characetrizationn of Alginate-Curcumin Conjugate', in 3rd FAPS Polymer Congress and MACRO 2013, 15th to 18th May 2013, IISC Bangalore, Karnataka, India. (Poster presentation).

2. **S. Dey** and K. Sreenivasan, 'Synthesis and Stabilization of Gold Nanoparticles Using Alginate-Curcumin Conjugate: Physicochemical Characterizations and Blood Compatibility Evaluation', in International Conference on Functional Materials (ICFM) 2014, 5th to 7th February 2014, Materials Science Centre, IIT Kharapur, West Bengal, India. (Oral presentation).
3. **S. Dey** and K. Sreenivasan, 'pH Induced Aggregation-Disaggregation of Amino Acid Based Water Soluble Oligomer Capped Gold Nanoparticles', International Conference on Advanced Functional Materials (ICAFM) 2014, 19th to 21st February 2014, NIIST, Trivandrum, Kerala, India. (Poster presentation).

Curriculum Vitae

Present Address

Karthik Niwas,
PURA – 135C,
Poojappura,
Trivandrum – 695012
Kerala,
India

Permanent Address

Naboday Pally,
P.O – Belda,
West Midnapore,
PIN – 721424,
West Bengal,
India

Contacts

Mobile: +919645540784
E-Mail: deysoma1@gmail.com

Personal

Name: Soma Dey
Sex: Female
Nationality: Indian
Marital status: Married

Education

After graduating from **Midnapore College**, **Vidyasagar University** joined **IIT Guwahati** in 2007 for M.Sc. studies. After successful completion of M.Sc. in Chemistry, joined the research group of **Dr. K. Sreenivasan** in **SCTIMST** as a research scholar in 2010 with CSIR Fellowship (JRF) and was successfully upgraded to CSIR-SRF in 2012.

Research Experience

A project work entitled **"Synthesis, Characterization and Self-aggregation of Amino Acid Based Amphiphiles"** under the supervision of **Dr. Gopal Das**, Associate Professor, Department of Chemistry, **IIT Guwahati** was done as a part of M.Sc. project in 2009.

National Level Examinations and Awards

1. Received **NATIONAL SCHOLARSHIP** in 1998.
2. **GATE** qualified, in 2008 (PERCENTILE = 94.42, AIR=356).
3. Qualified CSIR-UGC NET held in 2008 December (**CSIR-JRF**).
4. Qualified in the assessment for **CSIR-SRF** in 2012.

APPENDICES

LIST OF THE "PhD COURSE WORK" COMPLETED AS A PART OF PhD PROGRAM

❖ ***Compulsory courses***

1. Biostatistics
2. Ethics in Research
3. Research Methodology
4. Work Culture Development
5. Small Animal Handling
6. Computer Application

❖ ***Optional courses***

1. Toxicology
2. Introduction to Biomaterials
3. Nanomaterials for Drug Delivery

LIST OF "PhD SEMINARS" CONDUCTED AS A PART OF PhD PROGRAM

❖ ***Titles of the six seminars conducted***

1. Biodegradable and Photoluminescent Polymers
2. Polymeric Micelles in therapeutic Applications
3. Chemistry behind the Synthesis of Polymer stabilized Gold Nanoparticles
4. Characterization of Nanoparticles Intended for Medical Applications
5. Stimuli Responsive Polymers in Development of Smart Nano-structures
6. Functionalized Gold Nanoparticles as Nanomedicine

FTIR AND ^{1}H NMR SPECTRA OF FREE CURCUMIN

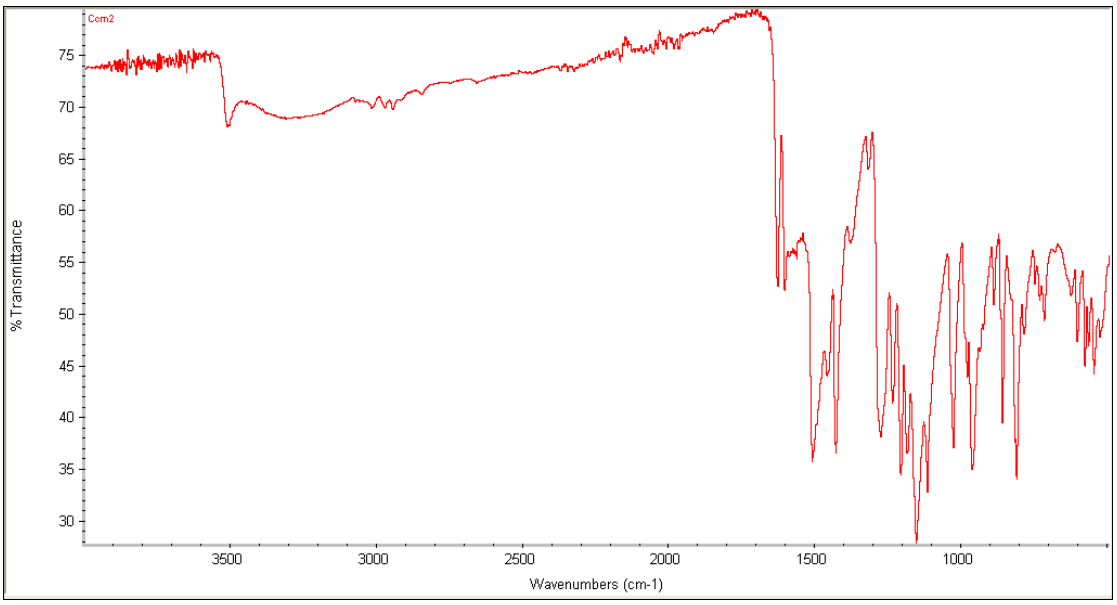

Figure A1: FTIR spectrum of free curcumin.

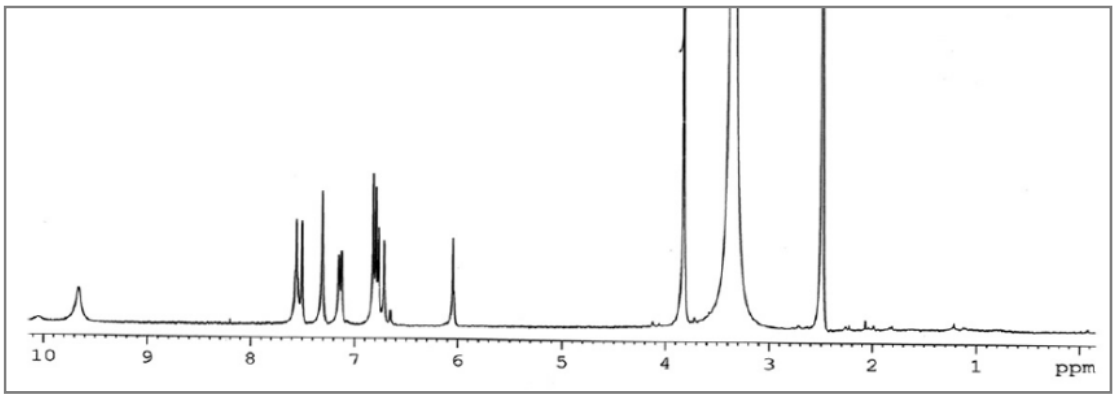

Figure A2: ^{1}H NMR spectrum of free curcumin.

CONFOCAL LASER SCANNING MICROSCOPIC IMAGES CONFIRMING THE FACILE CELLULAR UPTAKE OF FITC LABELLED MP@Alg-Ccm AuNPs BY CANCER CELL LINES

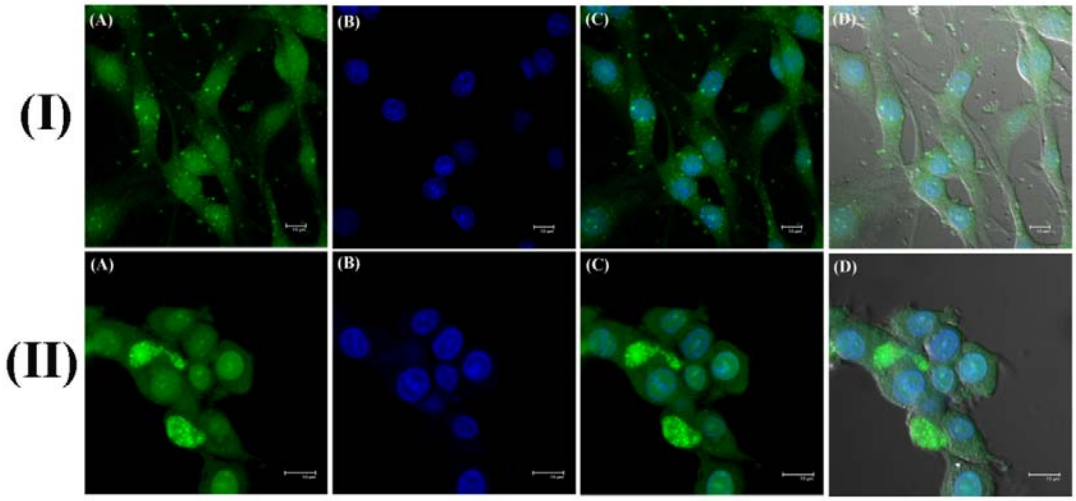

Figure A3: Confocal laser scanning microscopic images after incubation with FITC labeled MP@Alg–Ccm AuNPs for 3 h; (I) C6 glioma cells and (II) MCF-7 cells: (A) fluorescent image, (B) Hoechst 33342 stained nucleus, (C) merged fluorescent image in dark field and (D) merged fluorescent image in bright field. The confocal laser scanning microscopic images were recorded in Nicon A1R.

CONFOCAL LASER SCANNING MICROSCOPIC IMAGES CONFIRMING THE FACILE CELLULAR UPTAKE OF FLUORESCENT GSHBP-Ccm CONJUGATE MICELLES BY CANCER CELL LINE

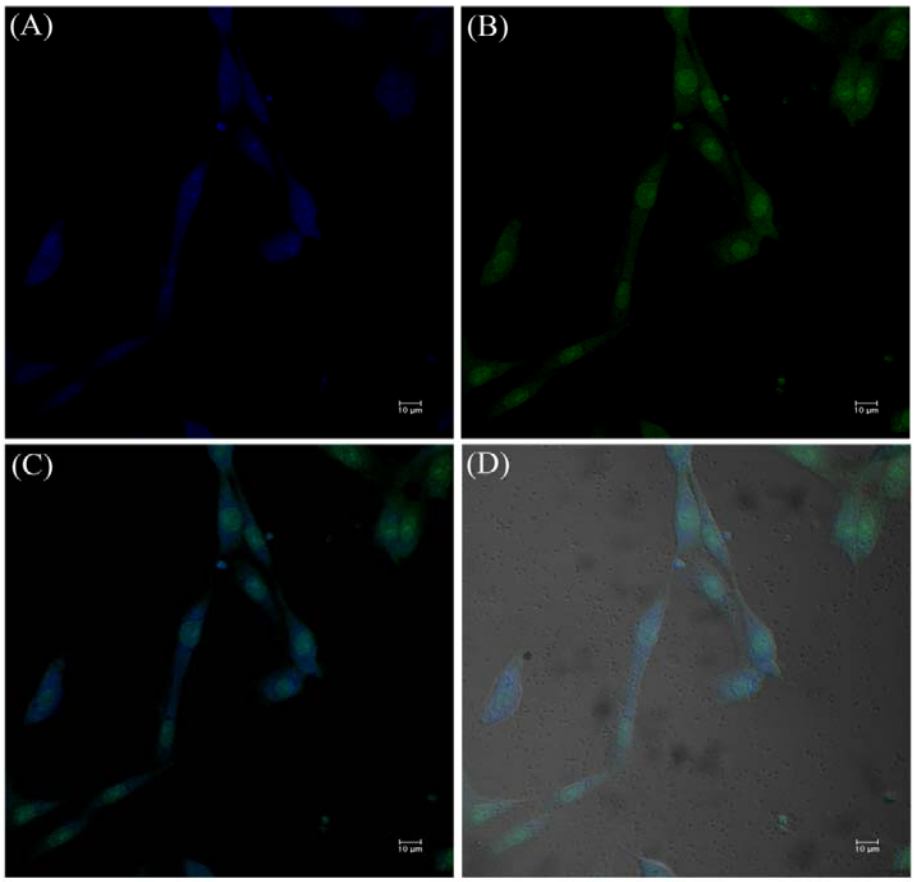

Figure A4: Confocal laser scanning microscopic images of C6 cells incubated with fluorescent GSHBP-Ccm micelles for 3 h: (A) blue fluorescent image (from self-fluorescent GSHBP) in dark field, (B) green fluorescent image of Ccm in dark field; merged fluorescent images of both blue and green fluorescence (C) in dark field and (D) in bright field. The confocal laser scanning microscopic images were recorded in Nicon A1R.